

ANA FRANCISCA TIBÚRCIA AMORIM FERREIRA E FERREIRA

**ANALYSES AT THE COMMUNITY, POPULATION, AND INDIVIDUAL  
LEVELS FOR BETTER UNDERSTANDING OF SOUTH AMERICAN LEAF  
BLIGHT AND OF ITS ETIOLOGICAL AGENT, *Pseudocercospora ulei***

Tese apresentada à Universidade Federal de Viçosa, como parte das exigências do Programa de Pós-Graduação em Fitopatologia, para obtenção do título de *Doctor Scientiae*.

VIÇOSA  
MINAS GERAIS – BRASIL  
2018

Ficha catalográfica preparada pela Biblioteca Central da Universidade  
Federal de Viçosa - Câmpus Viçosa

T

F383a  
2018  
Ferreira, Ana Francisca Tibúrcia Amorim Ferreira e, 1989-  
Analyses at the community, population, and individual  
levels for better understanding of South American Leaf Blight  
and of its etiologial agent, *Pseudocercospora ulei* / Ana  
Francisca Tibúrcia Amorim Ferreira e Ferreira. – Viçosa, MG,  
2018.

ix, 168 f. : il. (algumas color.) ; 29 cm.

Texto em inglês.

Inclui anexos.

Orientador: Eduardo Seiti Gomide Mizubuti.

Tese (doutorado) - Universidade Federal de Viçosa.

Inclui bibliografia.

1. Mal das folhas da seringueira. 2. Seringueira - Doenças e  
pragas. 3. Melanina. I. Universidade Federal de Viçosa.  
Departamento de Fitopatologia. Programa de Pós-Graduação em  
Fitopatologia. II. Título.


CDD 22. ed. 633.895294

ANA FRANCISCA TIBÚRCIA AMORIM FERREIRA E FERREIRA

**ANALYSES AT THE COMMUNITY, POPULATION, AND INDIVIDUAL  
LEVELS FOR BETTER UNDERSTANDING OF SOUTH AMERICAN LEAF  
BLIGHT AND OF ITS ETIOLOGICAL AGENT, *Pseudocercospora ulei***

Tese apresentada à Universidade Federal de Viçosa, como parte das exigências do Programa de Pós-Graduação em Fitopatologia, para obtenção do título de *Doctor Scientiae*.

APROVADA: 15 de junho de 2018

  
Braz Tavares da Hora Júnior

  
Hilário Cuquetto Mantovani

  
Luiz Orlando de Oliveira

  
Marisa Vieira De Queiroz

  
Eduardo Seiti Gomide Mizubuti  
(Orientador)

## ACKNOWLEDGEMENTS

À Universidade Federal de Viçosa, em especial ao Programa de Pós-Graduação em Fitopatologia, por todo o suporte e infraestrutura disponibilizados na condução dos experimentos.

Ao Prof. Eduardo Mizubuti, por toda a dedicação, suporte e ensinamentos.

Aos professores e técnicos do Departamento de Fitopatologia (DFP), pelo suporte, ensinamentos e pelo convívio.

Aos colegas e amigos do DFP e da Microbiologia, em especial Amarildo Junior, Carmem Herrera, Leticia Monteiro, Luciano Nunes, Orlando, Rita, Sérgio e Josenilda, pela amizade e momentos de descontração.

Aos colegas do Laboratório de Biologia de População de Fitopatógenos, em especial a Cristhian, Izabel e Taciana pela amizade, auxílio e convívio.

Ao Pablo Alvarez, pela amizade, convívio e desafios enfrentados juntos durante o doutorado.

Ao Braz Tavares, pelas colaborações e suporte.

Ao Lucas Magalhães, pelo incentivo e amizade.

À Anna Carolina, Laís Bentes, Lays Helena e Elisângela Farias, pela amizade e incentivo durante o doutorado.

Aos meus familiares, pelo amor, incentivo e compreensão.

À CAPES pela concessão da bolsa de estudos.

Aos meu pais, Graça e Humberto (*in memoriam*), **dedico.**

“Aos índios e aos caboclos que enfrentam(ram) a solidão, as doenças e todas as dificuldades da selva Amazônica, na exploração da seringueira e de outras riquezas, e mantendo nossas fronteiras para o bem de outros e que raramente são (foram) lembrados.”

**Luadir Gasparotto**

## SUMMARY

<b>ABSTRACT</b> .....	vi
<b>RESUMO</b> .....	viii
<b>GENERAL INTRODUCTION</b> .....	1
<b>REFERENCES</b> .....	4
<b>CHAPTER 1</b> .....	6
<b>Microbiome of <i>Hevea brasiliensis</i></b> .....	6
<b>ABSTRACT</b> .....	7
<b>INTRODUCTION</b> .....	9
<b>MATERIAL AND METHODS</b> .....	13
<b>Sampling site of <i>Hevea brasiliensis</i></b> .....	13
<b>Sample processing and DNA extraction</b> .....	13
<b>Illumina high-throughput sequencing</b> .....	14
<b>Sequence processing</b> .....	15
<b>Data Analysis</b> .....	16
<b>RESULTS</b> .....	18
<b>DISCUSSION</b> .....	27
<b>ACKNOWLEDGEMENT</b> .....	34
<b>REFERENCES</b> .....	35
<b>FIGURE LEGENDS</b> .....	44
<b>FIGURES AND TABLES</b> .....	46
<b>SUPPORTING INFORMATION</b> .....	62
<b>CHAPTER 2</b> .....	72
<b>Genetic variability and evolution of putative effector genes of <i>Pseudocercospora ulei</i> in Amazonian and Non-Amazonian populations of the pathogen</b> .....	72
<b>ABSTRACT</b> .....	73
<b>INTRODUCTION</b> .....	75
<b>MATERIAL AND METHODS</b> .....	78
<b>Sampling and isolation of <i>P. ulei</i></b> .....	78
<b>DNA extraction and sequencing</b> .....	78
<b>DNA polymorphism</b> .....	81
<b>Recombination and mutation analysis</b> .....	81
<b>Selection analysis</b> .....	82
<b>RESULTS</b> .....	83
<b>DISCUSSION</b> .....	87

<b>ACKNOWLEDGMENTS .....</b>	<b>92</b>
<b>REFERENCES.....</b>	<b>93</b>
<b>FIGURE LEGEND.....</b>	<b>98</b>
<b>FIGURES AND TABLES .....</b>	<b>99</b>
<b>CHAPTER 3.....</b>	<b>120</b>
<b>The dark side of <i>Pseudocercospora ulei</i> .....</b>	<b>120</b>
<b>ABSTRACT.....</b>	<b>121</b>
<b>INTRODUCTION.....</b>	<b>123</b>
<b>MATERIAL AND METHODS .....</b>	<b>127</b>
<b>Selection of isolate and cultivation .....</b>	<b>127</b>
<b>Melanin extraction.....</b>	<b>127</b>
<b>Mass spectrometry .....</b>	<b>128</b>
<b>FT-IR spectroscopy.....</b>	<b>128</b>
<b>Histochemical assay of carbohydrates on <i>P. ulei</i> stromata.....</b>	<b>129</b>
<b>Inhibition of melanization.....</b>	<b>129</b>
<b>Genes involved with 1,8-DHN biosynthesis in <i>P. ulei</i>.....</b>	<b>130</b>
<b>RESULTS.....</b>	<b>131</b>
<b>DISCUSSION.....</b>	<b>136</b>
<b>ACKNOWLEDGMENTS .....</b>	<b>142</b>
<b>REFERENCES.....</b>	<b>143</b>
<b>FIGURE LEGENDS .....</b>	<b>150</b>
<b>FIGURES AND TABLES .....</b>	<b>153</b>
<b>GENERAL CONCLUSIONS .....</b>	<b>168</b>

## ABSTRACT

FERREIRA, Ana Francisca Tibúrcia Amorim Ferreira e, D.Sc., Universidade Federal de Viçosa, June, 2018. **Analyses at the community, population, and individual levels for better understanding of South American Leaf Blight and of its etiological agent, *Pseudocercospora ulei***. Adviser: Eduardo Seiti Gomide Mizubuti.

*Pseudocercospora ulei* causes the most devastating disease of the rubber tree (*Hevea brasiliensis*), South American leaf blight (SALB). Wild populations of *H. brasiliensis* from different river basins in the Amazon region have variable resistance levels to SALB, and the most resistant genotypes were found in the western Amazon, including the Brazilian state of Acre. Based on the premise that the plant microbiome can directly influence the plant-pathogen interactions and contribute to disease-resistance, we studied the endophytic microbiome of wild *H. brasiliensis* from three Amazonian states in Brazil. The diversity of fungal and prokaryotic endophytes was shaped by plant organ (leaf, sapwood or root) and there is strong evidence that the microbial communities from trees collected in Acre are markedly distinct and more diverse than those from the states of Amazonas and Pará. This pattern may be a function of geographic isolation influenced by differences in the geological history of eastern and western Amazon. Functional prediction revealed important roles of endophytes associated with disease suppressiveness, biological control, but also with pathogenesis. We also studied the allelic variation in five effector proteins genes conserved in Dothideomycetes between pathogen populations from Amazon region (AM) and commercial plantations located in the Northeast and Southeast regions in Brazil (N-AM). The analyzes showed the highest polymorphism in three effector genes (PuAve1, PuEcp2 and PuEcp6) and a pattern of division between groups of haplotypes of the AM and N-AM populations. The diversification in *P. ulei* effector genes is driven for intragenic recombination and selection, and two different mechanisms to avoid the recognition by rubber tree were detected in *P. ulei* populations. Characterization of melanin pigment with mass spectrometry (MALDI-TOF) and infrared (IR) have failed but revealed that data on beta-glucans have apparently been mistakenly assigned to melanin in recent reports in the literature. Using a specific inhibitor of melanization, we have found that the melanin present in *P. ulei* is made from 1,8-dihydroxynaphthalene (1,8-DHN) and



the genes involved in this biosynthetic pathway were mapped into the fungus genome. Taken together, our results provide new and important information about the microbial components (pathogen and whole microbiota) of the yet neglected SALB pathosystem.

## RESUMO

FERREIRA, Ana Francisca Tibúrcia Amorim Ferreira e, D.Sc., Universidade Federal de Viçosa, Junho de 2018. **Análises em nível de comunidade, populacional e indivíduo para melhor compreensão do Mal-das-folhas da seringueira e de seu agente etiológico, *Pseudocercospora ulei*.** Orientador: Eduardo Seiti Gomide Mizubuti.

*Pseudocercospora ulei* causa a doença conhecida como Mal-das-Folhas (em inglês, *South American Leaf Blight* - SALB) da seringueira (*Hevea brasiliensis*). Populações nativas de *H. brasiliensis* de diferentes bacias hidrográficas da Amazônia apresentam níveis de resistência variáveis a SALB, e os genótipos mais resistentes foram encontrados na Amazônia Ocidental, incluindo o estado do Acre. Baseado na premissa de que o microbioma da planta pode influenciar diretamente as interações planta-patógeno e contribuir para a resistência a doenças, realizou-se um estudo com *DNA metabarcoding* de endófitos de *H. brasiliensis* nativas de três estados da Amazônia brasileira. A diversidade de endófitos fúngicos e procarióticos foi modelada por órgão da planta (folha, alburno ou raiz trófica). As comunidades microbianas das árvores coletadas no Acre foram distintas e mais diversificadas que as dos estados do Amazonas e Pará. Este resultado pode ser consequência do isolamento geográfico influenciado por diferenças na história geológica da Amazônia Oriental e Ocidental. A predição funcional revelou importantes papéis dos endófitos, associados à supressividade da doença, controle biológico, mas também à patogênese. Estudou-se também a variação alélica de cinco genes que codificam proteínas efetoras conservadas em Dotideomicetos em populações do patógeno da região amazônica (AM) e plantios comerciais localizados nas regiões Nordeste e Sudeste do Brasil (N-AM). As análises mostraram um maior polimorfismo em três genes efetores (PuAve1, PuEcp2 e PuEcp6) e um padrão de divisão entre grupos de haplótipos das populações AM e N-AM. A diversificação em genes efetores de *P. ulei* é dirigida por recombinação intragênica e seleção, e dois mecanismos para evitar o reconhecimento pela seringueira foram detectados em populações de *P. ulei*. Por fim, investigamos o processo de melanização do patógeno. A caracterização da melanina utilizando espectrometria de massa (MALDI-TOF) e Infravermelho (IR) falhou, mas revelou que os dados sobre beta-glucanas aparentemente foram erroneamente

atribuídos à melanina em relatos recentes da literatura. Usando um inibidor específico de melanização (Triciclazol), verificou-se que a melanina presente em *P. ulei* é produzida a partir de 1,8-di-hidroxi-naftaleno (1,8-DHN) e os genes envolvidos nesta via biossintética foram mapeados no genoma do fungo. Assim, nossos resultados fornecem informações novas e importantes sobre os componentes microbianos (patógeno e microbiota total) deste patossistema negligenciado.

## GENERAL INTRODUCTION

The rubber tree (*Hevea brasiliensis*) is an Amazonian species widely grown for the production of latex and provision of natural rubber for a number of industrial and medical purposes (van Beilen and Poirier 2007; Priyadarshan and Goncalves 2003; Schultes 1956). Brazil pioneered the commercial production of natural rubber and, in the early 20<sup>th</sup> century, the American industrialist Henry Ford implanted large-scale plantations of rubber trees in the state of Pará. The attempt of supplying the demands of the car industry for natural rubber eventually failed, with whole plantations and even cities built around them being abandoned (Guyot and Le Guen 2018). The decline of Brazilian natural rubber production was largely caused by severe epidemics of the destructive fungal disease known as South American leaf blight (SALB) (Lieberei 007). Today, the Asian countries like Thailand, Indonesia, Malaysia, Vietnam, India, and China are responsible for the worldwide supply of natural rubber (Lieberei 2007). Asia is a SALB-free zone since the disease is still restricted to the American continent.

The ascomycete *Pseudocercospora ulei* is the etiological agent of SALB and completes its entire life cycle in association with plants of *Hevea* spp. (Hennings 1904; Hora Júnior et al. 2014). Conidia of *P. ulei* infect young leaves and cause successive cycles of infection. Heavily infected young leaves fall prematurely, leading to intense defoliation, dieback of young stems, reduction of latex yields and general plant decline. On the surface of less infected leaves that reach maturity, the fungus forms black stromata containing pseudothecia that produce ascospores. The ascospores can initiate the disease cycles when new leaves are formed (Garcia et al. 2011; Gasparotto et al. 2012; Hora Júnior et al. 2014).

Planting rubber tree clones with some level of resistance to SALB is the best strategy for controlling epidemics in endemic areas. Breeding programs for resistance to SALB also serve as preventive measures to mitigate the losses derived from an eventual introduction of the pathogen in Asia (Le Guen et al. 2011). Current breeding programs aim to develop clones with high levels of quantitative resistance against SALB and some are already cultivated in the Brazilian states of Bahia, Mato Grosso and São Paulo (Le Guen et al. 2013; Garcia et al. 2004; Le Guen et al. 2007).

There are reports on natural populations of rubber trees exhibiting high levels of resistance to SALB, mainly in the western Amazon (Sethuraj and Mathew 2012; Schultes 1956). In addition to the genetic make-up of the wild rubber tree populations, the composition and functional diversity of the microbial communities closely associated with the plant organs may influence the plant-pathogen interactions and the resulting resistance phenotype observed (Berendsen, Pieterse, and Bakker 2012). The fungal and bacterial endophytic communities of leaves, sapwood and roots of wild rubber trees collected in the basins of Juruá, Purus, Tapajós, Madeira and Amazonas rivers were studied using the Illumina Miseq high throughput sequencing of ITS1 and 16S gene markers. The assembled microbiomes were compared between different plant organs and geographic locations based on alpha and beta diversity estimators, taxonomic composition, functional inferences and distribution patterns of the core microbiomes.

The genetic and phenotypic diversity associated with populations of *P. ulei* is also largely responsible for the outcomes of pathogenic interactions with rubber trees (Le Guen et al. 2011; McDonald and Linde 2002). The population biology of

*P. ulei* isolates from different locations of Brazil is another study performed. A collection of 64 isolates of *P. ulei* was assembled from symptomatic leaves of rubber trees collected in different locations of Brazil. The allelic variation found in the sequences of five putative effector genes was used to distinguish haplotypes, infer evolutionary events such recombination, mutation, selection shaping the populations of *P. ulei*, contrasting the populations found in the Amazon region, considered the center of origin of both the host plant and the pathogen, and those established in commercial rubber tree plantations in Brazil.

*Pseudocercospora ulei* grows very slowly under axenic conditions and requires specific nutrients to grow on culture media (Junqueira et al. 1984). It may take months to grow, producing little or no aerial mycelia, but abundant hard black stromata scattered on the agar surface (Chee 1978). This stromatic and highly melanized form of growth offered challenges to the extraction and purification of nucleic acids from *P. ulei*, hindering our investigations on the population biology of this pathogen. Faced with these challenges, the melanization process of *P. ulei* was investigated using different approaches. The melanin extracted from *P. ulei* was characterized by MALDI-TOF mass spectrometry and Infra-Red spectroscopy. Melanin biosynthesis was also investigated in bioassays using a specific inhibitor of the major melanin type found in ascomycetes, the 1,8-dihydroxynaphthalene (1, 8-DHN) melanin. Additionally, we characterized the genes coding for the main enzymes involved in the biosynthesis of 1, 8-DHN found in the draft genome of one isolate of *P. ulei*.

## REFERENCES

- van Beilen, J. B., and Poirier, Y. 2007. Establishment of new crops for the production of natural rubber. **Trends in Biotechnology**. 25:522–529.
- Berendsen, R. L., Pieterse, C. M. J., and Bakker, P. A. H. M. 2012. The rhizosphere microbiome and plant health. **Trends in Plant Science**. 17:478–486.
- Chee, K. H. 1978. South American leaf blight of *Hevea brasiliensis*: culture of *Microcyclus ulei*. **Transactions of the British Mycological Society**. 70:341–344.
- Garcia, D., Carels, N., Koop, D. M., de Sousa, L. A., Andrade Junior, S. J. de, Pujade-Renaud, V., et al. 2011. EST profiling of resistant and susceptible *Hevea* infected by *Microcyclus ulei*. **Physiological and Molecular Plant Pathology**. 76:126–136.
- Garcia, D., Mattos, C. R. R., Goncalves, P. D. S., and Le Guen, V. 2004. Selection of rubber clones for resistance to South American leaf blight and latex yield in the germplasm of the Michelin plantation of Bahia (Brazil). **Journal of Rubber Research**. 7(3), 188-198.
- Gasparotto, L., & Pereira, J. C. R. 2012. Doenças da seringueira no Brasil. Brasília: **EMBRAPA**, 2.
- Le Guen, V., Garcia, D., Doaré, F., Mattos, C. R. R., Condina, V., Couturier, C., et al. 2011. A rubber tree's durable resistance to *Microcyclus ulei* is conferred by a qualitative gene and a major quantitative resistance factor. **Tree Genetics & Genomes**. 7:877–889.
- Le Guen, V., Garcia, D., Mattos, C., Fouet, O., Doaré, F., Condina, V., et al. 2013. A newly identified locus controls complete resistance to *Microcyclus ulei* in the Fx2784 rubber clone. **Tree Genetics & Genomes**. 9:805–812.
- Le Guen, V., Garcia, D., Mattos, C. R. R., Doaré, F., Lespinasse, D., and Seguin, M. 2007. Bypassing of a polygenic *Microcyclus ulei* resistance in rubber tree, analyzed by QTL detection. **New Phytologist**. 173:335–345.
- Guyot, J., and Le Guen, V. 2018. A Review of a century of studies on South American leaf blight of the rubber tree. **Plant Disease**. 102:1052–1065.
- Hennings, P. 1904. Über die auf *Hevea*-Arten bisher beobachteten parasitischen Pilze. **Notizblatt des Königl. botanischen Gartens und Museums zu Berlin**. 4:133.
- Hora Júnior, B. T. da, de Macedo, D. M., Barreto, R. W., Evans, H. C., Mattos, C. R. R., Maffia, L. A., et al. 2014. Erasing the Past: A new identity for the damoclean pathogen causing South American leaf blight of rubber. **PLoS one**. 9(8), e104750.
- Junqueira, N. T. V., Chavees, G. M., Zambolim, L., Romeiro, R. da S., and Gasparotto, L. 1984. Isolamento, cultivo e esporulação de *Microcyclus ulei*,

- agente etiológico do mal-das-folhas da seringueira. **Revista Ceres**. 31:322–331.
- Lieberei, R. 2007. South American leaf blight of the rubber tree (*Hevea* spp.): new steps in plant domestication using physiological features and molecular markers. **Annals of botany**. 100:1125–42
- McDonald, B. A., and Linde, C. 2002. Pathogen population genetics , evolutionary potential, and durable resistance. **Annual Review of Phytopathology**. 40:349–379.
- Priyadarshan, P. M., and Goncalves, P. de S. 2003. *Hevea* gene pool for breeding. **Genetic Resources and Crop Evolution**. 50:101–114.
- Schultes, R. E. (1956). The Amazon Indian and evolution in *Hevea* and related genera. **Journal of the Arnold Arboretum**. 37(2), 123-152.
- Sethuraj, M. R., & Mathew, N. T. (Eds.). (2012). Natural rubber: biology, cultivation and technology. **Elsevier**. 23.



## **CHAPTER 1**

### **Microbiome of *Hevea brasiliensis***

## ABSTRACT

The diversity of the bacterial and fungal endophytic communities associated with leaves, sapwood and roots of rubber trees collected in the basins of Juruá, Purus, Tapajós, Madeira and Amazonas rivers of the Northern region of Brazil was assessed using DNA metabarcoding approach. Illumina MiSeq sequencing generated 4,272,256 sequences of fungi classified into 2381 OTUs, and 2,250,106 sequences of bacteria belonging to 3414 OTUs. Higher levels of fungal  $\alpha$ -diversity were found in leaf samples, while bacteria were more diverse in sapwood tissues. Beta diversity measures across basins showed strong evidence of differentiation among microbial communities as a function of biogeography, with the microbiome of plants from Juruá and Purus being markedly more diverse than other basins. The fungal endophyte community was dominated by Ascomycota (59.8%), followed by Basidiomycota (21.7%), with small abundance of other phyla. The bacterial endophyte community was dominated by Proteobacteria (29.8%) and Firmicutes (18%). Our culture-independent approach allowed the detection of uncultured microorganisms belonging to the phylum Rozellomycota in fungi, and the bacterial groups Candidate division WPS-1, WPS-2, SR1, together with Candidate Solibacter and Pelagibacter. Functional predictions based on taxonomic information showed that the microbiome of the rubber tree is composed by a large number of organisms with yet unknown modes of interactions with plants, and significant numbers of putative and actual plant pathogens (including 34 sequences assigned to *P. ulmi*) and organisms with known functions in plant growth promotion and biocontrol of diseases. In addition to plant genetics, the levels of resistance to SALB in the

Acre populations of the rubber tree may be largely influenced by the composition and balanced interactions with the associated microbiome.

**Key words:** metabarcoding, plant microbiome, endophytes, rubber tree, SALB, Amazon.

## INTRODUCTION

The rubber tree or Pará rubber tree, *Hevea brasiliensis* (Willd. ex A. Juss.) Müll. Arg., is a native species to the Amazon basin in South America and the main source of latex for the production of natural rubber (Priyadarshan and Gonçalves 2003; Schultes 1956). Brazil pioneered the production and export of natural rubber and dominated the international market during the 19<sup>th</sup> and early 20<sup>th</sup> centuries. The decline of Brazilian natural rubber production began after the implementation of the Asian rubber tree plantations from 80000 seeds collected in the Tapajos basin by Wickham in the 1876 (Serier 1993). Concurrently, severe epidemics of South American leaf blight (SALB), a highly destructive disease caused by the fungus *Pseudocercospora ulei* (Henn.) Hora Júnior & Mizubuti (Hora Júnior et al. 2014; Hennings 1904), affected the rubber tree plantations in Brazil. SALB epidemics were responsible for the historical catastrophe of Fordlândia, a city established by Henry Ford in Pará State, Brazil, built to support large plantations of rubber trees as monocrop. The disease disrupted the rubber industry in Brazil and caused major financial losses to the economy of the country (Guyot and Le Guen 2018).

Currently, the natural rubber production is mainly concentrated in Thailand, Indonesia, Malaysia, Vietnam, India, and China, which are responsible for the worldwide supply of rubber (Lieberei 2007). The genotypes planted in these areas are based on the "Wickham clones", which are highly productive, but susceptible to SALB. Fortunately, *P. ulei* is not present in Asia and the continent is considered free of SALB (Guyot and Le Guen 2018).

The pathogen, *P. ulei*, infects young stems, fruit and leaves, causing defoliation, followed by dieback of terminal twigs and branches and, depending

on the susceptibility of the clones, tree death (Garcia et al. 2011). Deployment of resistant clones is the best strategy to control SALB in endemic areas, and it is an important preventive measure to mitigate the risks of a possible introduction of the pathogen in Asia (Le Guen et al. 2011; Chee and Holliday 1986). Breeding programs for SALB resistance began in 1928, with the aim of producing clones with monogenic resistance, but the high genetic variability of *P. ulei* populations led to the overcome of the resistance shortly after the deployment of resistant clones. Currently, the breeding programs focus on quantitative resistance and some clones with partial resistance to SALB are already being cultivated in Bahia, Mato Grosso and São Paulo states in Brazil (Garcia et al. 2004; Le Guen et al. 2007).

Natural populations of rubber trees seem to be structured along the basins of the affluents of the Amazon river (Le Guen et al. 2009). Among these, there are reports of populations with high levels of resistance to SALB in the Brazilian state of Acre and in Madre de Dios, Peru (Sethuraj and Mathew 1992; Schultes 1956). One may commonly regard resistance to SALB in these native populations as the result of their genetic determinants alone. However, this somewhat simplified paradigm is now challenged by the ubiquity of microorganisms inhabiting all internal and external parts of plants, and their direct impacts on plant health (Berendsen, Pieterse, and Bakker 2012).

The plant genotype can directly influence the composition of the microbiome of the internal or external parts of the plant (Bálint et al. 2013; Andreote et al. 2010). The active recruitment of microorganisms to distinct niches by the plant has not been elucidated yet, but experimental evidences support the role of plants in shaping rhizosphere communities. The synthesis and export of

amino acids, secondary metabolites and other root exudates alter the rhizosphere chemical composition and influence the composition of microbial communities (Mendes et al. 2011). The plant microbiome in turn, confers beneficial traits against abiotic (temperature, salinity and water stress) and biotics (pathogens and pests) factors, and plant growth leading to a positive effect on fitness. This interaction is called microbiome-associated phenotypes (MAPs). Recognizing these patterns and understanding how they affect different plant physiological processes can be key to exploit the yield potential of a crop plant (Oyserman, Medema, and Raaijmakers 2018).

The genetic background provided by microorganisms to plants opens new horizons for breeding called “cultivation of next-generation crops”, and several strategies are being proposed for the coupling of the plant microbiome in the improvement of cultivated plants (Moissl-Eichinger et al. 2016). Nevertheless, the first step is to investigate what microbes are there. Most efforts of plant microbiome research are currently focused on unrevealing the taxonomic composition of microbial assemblages and making inferences about their ecological functions. This approach is based on large scale sequencing of DNA markers useful as barcodes for species identification and known as metabarcoding (Caporaso et al. 2011; Tedersoo et al. 2014). Metabarcoding allowed inferences about the plant microbiota, species richness and abundance, and community structure on different habitats, with lower costs than metagenomic surveys (Deiner et al. 2017).

Here, we first describe the landscape of diversity of endophytic fungal and bacterial communities that inhabit rubber trees in their center of origin, using high-throughput sequencing platform and metabarcoding. We compared the

composition and distribution patterns of the endophytic communities associated with different plant organs of rubber trees and investigated the relation with the genetic structure of the host according to the river basins.

## MATERIAL AND METHODS

### Sampling site of *Hevea brasiliensis*

Samples were collected from June 2014 to February 2015 in the basins of Purus and Juruá rivers, located in Acre and Amazonas states, Madeira and Amazonas rivers, located in Rondônia and Amazonas states, and Tapajós river, located in Pará and Mato Grosso states (Figure 1). These sites were chosen because they are directly related to the genetic structure of *H. brasiliensis* in their center of origin, while the Tapajós basin, in addition to the genetic relevance, has historical importance, since it was in this basin that Wickham collected the seeds that gave origin to the Asian plantations, world leader in natural rubber production (Le Guen et al. 2009; Guyot and Le Guen 2018). In the study, only healthy plants were sampled. On each basin, samples of asymptomatic leaves, sapwood and root from 30 plants were collected and stored in Falcon tubes with silica. Subsequently, the tubes were kept at -80 °C for processing and DNA extraction (Table 1).

### Sample processing and DNA extraction

Small pieces of healthy organs were submitted to surface disinfestation, using 70% ethanol for 2 min, 2.5% sodium hypochlorite for 5 min, and 70% ethanol for 30 s, followed by four washes in sterile distilled water to eliminate the epiphytic communities of fungi and bacteria. The efficiency of the disinfestation process was verified by plating aliquots (0.1 mL) of the water used in the last wash on Petri dishes with PDA medium (dextrose 20 g, potato 200 g and agar 20 g.L<sup>-1</sup>) and incubated at 25-28 °C for 10 days. After checking the absence of epiphytes on disinfested tissues, 3g of each organ (leaf, sapwood and root) were used to DNA extraction. In our study we used the concept of proposed by Petrini



(1991), which defines endophytes as “all organisms inhabiting plant organs that at some time in their life, can colonize internal plant tissues without causing apparent harm to the host”. Tissues were fragmented and placed in 30 mL of 1 x PBS solution (137 mM NaCl, 2.7 mM KCl, 10 mM Na<sub>2</sub>HPO<sub>4</sub>, 2 mM KH<sub>2</sub>PO<sub>4</sub>) containing 0.1% Tween 80® during 5 h under stirring. The liquid phase obtained was centrifuged at 4000 x g for 5 min at 4 °C to separate the remaining plant material. The supernatant was centrifuged at 28000 x g for 30 minutes to concentrate the pellet of endophytic microbial cells.

Mechanical lysis of tissues using zirconia beads on a TissueLyser LT (Qiagen, UK) for 1 minute was followed by DNA purification using PowerSoil® DNA Isolation Kit (MoBio Laboratories Inc., Carlsbad, CA, USA), according to the manufacturer's recommendations. DNA quality was checked using NanoDrop® 2000 spectrophotometer (Thermo Fisher Scientific) (260/280 nm ratio), and agarose gel electrophoresis (0,8%) with Lambda DNA (PROMEGA). The final DNA concentration was adjusted to 20 ng/uL, and samples were stored at -20 °C until use.

### **Illumina high-throughput sequencing**

A total of 180 DNA samples (including duplicates) were lyophilized and sent to Environmental Sample Preparation and Sequencing Facility (ESPSF) of the Argonne National Laboratory (Lemont, Illinois, USA), for paired-end amplicon sequencing using Illumina MiSeq platform. Samples were processed for sequencing using the Illumina MiSeq® reagent kit v2 following a modified manufacturer's protocol. First, bacterial DNA were amplified with the universal 16S rRNA gene primer set 515F and 806R (Table 2), targeting the V4 region of the 16S SSU rRNA, combined with the sequencer adapter used in the Illumina

flowcell (Caporaso et al. 2011, 2012). The reverse amplification primer also contains a 12 bp barcode sequence that supports pooling of up to 2,167 different samples in each lane. To avoid the plant host plastid and mitochondrial 16S contamination in the sequencing, PNA clamp sequences were included in the amplification (Lundberg et al. 2013). The 16S protocol described by the Earth microbiome project (<http://www.earthmicrobiome.org>) was used in the current study.

The fungal communities were accessed by amplifying the internal transcribed spacer (ITS) region of the rRNA, with the ITS1f and ITS2 primer set. The protocol is described at <http://press.igsb.anl.gov/earthmicrobiome/protocols-and-standards/its/>. The PCR reactions of both libraries were carried out in 25  $\mu$ L volumes, including 1  $\mu$ L of DNA template, 0.5  $\mu$ L of each 10  $\mu$ M primer, 13  $\mu$ L of PCR-grade water (Sigma), 10  $\mu$ L of 2x Platinum™ Hot Start PCR master mix (ThermoFisher Scientific). The PCR conditions for bacterial was initial denaturation at 94 °C for 3 min, followed by 35 cycles of 94 °C for 45 s, 50 °C for 60 s, 72 °C for 90 s and final extension of 10 min at 72 °C. For fungal amplifications, the conditions were 94 °C for 1 min, followed by 35 cycles of 94 °C for 30 s, 52 °C for 30 s, 68 °C for 30 s and final extension of 7 min at 68 °C.

### **Sequence processing**

The sequence reads were demultiplexed using the software CASAVA (Consensus Assessment of Sequence and Variation) version 1.8.2 (Eren et al. 2013). The processing of sequences was done with the software Mothur version 1.39.5 (Schloss et al. 2009) following the standard operating procedures (SOP) pipeline for analyzing amplicon sequence data generated by Illumina MiSeq platform, available in [https://www.mothur.org/wiki/MiSeq\\_SOP](https://www.mothur.org/wiki/MiSeq_SOP). First, paired-end

reads were combined forming a contig using *make.contigs* command. Sequences containing ambiguous bases, homopolymer longer than 8 bases, and those that were not in the range of minimum and maximum length established, were removed with *screen.seqs* command. Sequence duplicates were reduced to unique sequences using *unique.seqs* command, to improve computational performance. Sequences were aligned using the V4 region of the 16S rRNA gene from the SILVA database - release 128 (Quast et al. 2013) with *align.seqs* command, and the flip parameter used was "true". To avoid redundancy of sequences, the *unique.seqs* command was executed again and the sequences were preclustered allowing for up to 2 differences between them (diffs=2) implemented in *pre.cluster* command. Chimeras were detected and removed using the VSEARCH algorithm (Rognes et al. 2016) with the *chimera.vsearch* and *remove.seqs* command. Bacterial sequences were classified using Silva database (Yilmaz et al. 2014) release 128 (Quast et al. 2013) and using 80% confidence with the *classify.seqs* command. Fungal sequences were classified using the UNITE community database for Mothur release (Kõljalg et al. 2013). Undesirable lineages were removed, and sequences were clustered into OTUs (operational taxonomic units) with a threshold of 97% identity using *remove.lineage*, *dist.seqs* and *cluster.split* commands. The rubber tree microbiome database will be deposited in National Center for Biotechnology Information (NCBI).

## **Data Analysis**

The statistical analyses were performed in R version 3.4.3 (R Core Team, 2017) using the OTU abundance table from the Mothur output. Alpha-diversity was estimated for plant, tissues (leaf, sapwood and root), and states (Acre,

Amazonas and Pará) using Hill's numbers (effective number of species) function in the iNEXT package, to calculate species richness ( $q = 0$ ), Shannon diversity ( $q = 1$ ) and Simpson diversity ( $q = 2$ ), as well as rarefaction (interpolation) and extrapolation (prediction) curves (Hsieh, Ma, and Chao 2016). Beta-diversity was calculated between states using Principal Coordinates Analysis (PCoA) weighted Uni-Frac distances in Phyloseq package (McMurdie and Holmes 2013). Venn diagrams were constructed to show the proportions of unique and shared taxa between states and between plant tissues using interactive Venn diagram performed in Jvenn (Bardou et al. 2014). Taxonomic composition plots were made using Phyloseq and ggplot packages, pruning the OTUs not present in at least 1% in the OTU table. Heatmaps were constructed with the more abundant OTUs and the prediction of core microbiome for organ and state was based on the DESeq package in R (Anders and Huber 2010). Functional predictions for bacterial communities was done using the Functional Annotation of Prokaryotic Taxa (FAPROTAX) (Louca, Parfrey, and Doebeli 2016), and fungal ecological guilds were predicted by FUNGuild (Nguyen et al. 2016).

## RESULTS

### Sequencing

The sequencing of the fungal microbiome of *H. brasiliensis* using the ITS1 portion of the internal transcribed spacer (ITS) region from the rRNA cistron generated 4,272,256 sequences, with an average 23,734.75 sequences per sample. The processing of eukaryotic sequences in Mothur generated 15,537 abundant sequences and 1,432 rare sequences. The length of most sequences varied from 244 to 375 base pairs and the Good's coverage parameter for most of them was 1.0. The classification was accomplished using the Unite community reference database and assuming a 97% identity threshold clustered the high-quality sequences into 2,381 operational taxonomic units (OTUs). Sequencing of the V4 region of the 16S small subunit rRNA gene (16S) was used to identify bacterial and members of the prokaryotic microbiome of the rubber tree. A total of 2,250,106 sequences was obtained, with an average of 12,500.58 sequences per sample. After processing, sequence lengths varied from 250 to 253 base pairs, and the Good's coverage parameter ranged from 0.9 to 1.0. The reads were clustered into 3,414 OTUs using the SILVA reference database and an identity threshold of 97%.

### Diversity analysis

The diversity estimates for fungal and bacterial communities associated with different plant organs collected in the basins of Amazonas, Juruá, Madeira, Purus, and Tapajós rivers were done using the Hill numbers modelled by different coefficient values ( $q$ ). These estimates included the species richness ( $q=0$ ), the exponential of the Shannon diversity index ( $q=1$ ), which considers relative abundance of OTUs, and the Simpson diversity index ( $q=2$ ), which places more weight on the abundant OTUs (Chao et al. 2014) (Figures 2 and 3). The highest

values of estimated fungal species richness were found in leaf samples in all basins, and more pronounced in the basin of Madeira river, with values ranging from 1,000 to 302,370 OTUs. Diversity estimates based on Shannon and Simpson indices had similar trends, but differences between organs and the dispersion of data were less pronounced in all basins when more weight was given to common (Shannon) or abundant species (Simpson index) (Figure 2), except in the basin of Madeira river.

For bacterial communities, species richness estimators varied between organs and basins. In the basins of Juruá, Purus and Tapajós, the most species-rich and dispersed samples were those from sapwood, followed by root and leaf. In the basin of Tapajós river, sapwood samples were followed by leaf and root samples. In the Amazonas, similar number of species were obtained for all three organs, and data were less dispersed (Figure 3). Flattening of box plots representing estimators weighted for common (Shannon) and abundant (Simpson) species indicates that most differences in prokaryotic alpha diversity among plant organs and states are due to rare taxa.

Differences in the composition of *H. brasiliensis* microbiome among basins were estimated using the phylogenetic beta-diversity approach implemented in Uni-Frac and distances between samples were simultaneously plotted using Principal Coordinates Analysis (PCoA) (Figure 4). There was not a clear distinction in the composition of fungal and bacterial microbiomes between the basins, although samples from basins of Juruá and Purus rivers, and the basins of Amazonas and Tapajós river tended to split from the remaining samples in the axis of the PCoA (Figure 4A and B). A second phylogenetic beta-diversity analysis of microbial communities was done where fungal and bacterial

microbiomes were compared among plant organs in each basin (Figure 5). Leaf microbial communities tended to cluster and separate from those of sapwood and roots, which formed assemblages that are more homogeneous. This trend was clearer for bacterial communities, especially in the basins of Juruá, Purus and Madeira rivers where leaf samples almost did not overlap with those from sapwood and root organs (Figure 5).

Venn diagrams displaying the numbers of unique and shared OTUs among plant organs and basin were constructed (Figure S1). Plant organ analysis showed that leaf samples had the highest number of unique fungal OTUs (n=1589), and sapwood samples the highest number of unique bacterial OTUs (n=1325). The analysis by basins showed that the highest numbers of unique fungal and bacterial OTUs were found in the basin of Purus river, 490 and 960 OTUs, respectively. The smallest number of unique fungal OTUs was found in Amazonas river (n=196), and the smallest number of unique bacterial OTUs was found in Madeira river (n=181), both located in Amazonas state. The numbers of OTUs shared between all organs and basins were 214 and 119, respectively, for fungi, and 233 and 94, respectively, for bacteria.

### **Fungal taxonomic composition**

The 2,381 fungal OTUs classified by the Unite database were clustered into 7 phyla, 30 classes, 71 orders, 209 families, 352 genera and 853 species. The dominant fungal phyla were Ascomycota (59.2%) and Basidiomycota (21.7%). The abundance of the other phyla was less than 1%: Chytridiomycota (0.04%), Glomeromycota (0.04%), Mortierellomycota (0.5%), Mucoromycota (0.7%) and Rozellomycota (0.08%). The percentage of sequences grouped in OTUs that remained unclassified at the phylum level corresponded to 17.2%.

Some fungal phyla had patterns of occurrence corresponding to the type of plant organ and basin. Three phyla were only found in leaf samples: Mortierellomycota in all basins, Glomeromycota only in Madeira river, and Chytridiomycota found only in the basins of Juruá and Purus river.

Members of the Order Diaporthales (family Diaporthaceae) were dominant in leaf samples in the basin of Purus (50%), followed by those of Pleosporales (family Pleosporaceae) in the basin of Juruá (60%), and Saccharomycetales in the basins of Amazonas (70%), Madeira (65%) and Tapajós river (45%). Sapwood and root samples were dominated by members of the Order Botryosphaeriales (B) in the basins of Purus (90% and 70%) and Juruá (52% and 55%), and Sacccharomycetales in the basins of Amazonas (80%), Madeira (70% and 20%) and Tapajós (70%), followed by Xylariales (family Amphisphaeriaceae) and Hypocreales (family Nectriaceae) (< 20%) (Figure 6A and B).

The 35 most abundant taxons are represented in Figure 7, and were dominated by the Ascomycota, followed by members of the Basidiomycota, Mucoromycota and Mortierellomycota. The genus *Lasiodiplodia* spp. was dominant in samples from sapwood and root in the basins of Juruá, Madeira and Purus, while *Cyberlindnera fabianii* was the most abundant taxon in the basins of Amazonas and Tapajós. The most abundant genera in leaf samples were *Meyerozyma*, *Wickerhamomyces*, *Diaporthe*, *Phyllosticta* and *Alternaria*.

### **Bacterial taxonomic composition**

The 3,414 bacterial OTUs were clustered into 28 phyla, 73 classes, 128 orders, 235 families, and 486 genera. The dominant phyla (>1% of relative abundance) were Proteobacteria (29.8%), Firmicutes (18.0%), Actinobacteria (8.4%), Verrucomicrobia (2.6%), Acidobacteria (6.2%), and Bacteroidetes (4.7%)



(Figure 8A). The other phyla had relative abundance < 1%: Chlamydiae (0,6%), Chloroflexi (0,5%), and Candidate division WPS-1 (0.3%). Approximately 25% of bacterial sequences remained in unclassified OTUs.

Bacteria class composition showed the dominance of two major groups in all samples, the classes of Gammaproteobacteria and Bacilli, while the latter represented 95% in leaf samples from the basins of Juruá and Purus rivers (Figure 8A). Members of Actinobacteria were present in all samples with low abundance (<20%), followed by Acidobacteria Gp1. The highest number of unclassified Bacteria was found in sapwood samples from the basin of Juruá (20%). The composition of bacterial families was similar between the basins of Amazonas, Madeira and Tapajós rivers, with high abundance of Staphylococcaceae and Enterobacteriaceae in leaf and sapwood samples. The basins of Juruá and Purus had a different leaf microbiome composed by Leuconostocaceae and Lactobacillaceae (Figure 8B). Sapwood and root samples from Juruá and Purus had the predominance of Bacillaceae and Enterobacteriaceae.

*Pantoea* was the most abundant genus found in samples from Madeira and Tapajós. This genus dominated the microbial assemblages of sapwood and root samples in the basins of Amazonas and Madeira, and leaf and sapwood samples in the basin of Tapajós. On the other hand, the abundance of *Pantoea* was low in samples from the basins of Juruá and Purus, with a maximum of 7.7% of relative abundance in root samples (Figure 9). Members of the genus *Enterobacter* dominated the endophytic microbiome of roots in all basins, mainly in the basins of Juruá, Madeira and Tapajós rivers. *Bacillus* was the most and second most abundant genus in roots in the basins of Purus and Juruá,

respectively, but it was never detected in leaf samples from the same basins or in the basin of the Madeira river. The genus *Staphylococcus* was the most abundant in leaf samples from the basin of Amazonas and the third most abundant in the Madeira and Tapajós rivers. However, the relative abundance of this genus was low in Juruá and Purus, where it attained a maximum of 4.9% in sapwood samples. The genus *Weissella* was the single most abundant genus in leaf samples from the basins of Juruá and Purus. In contrast, the relative abundance of this genus was low to very low, or even absent, in the remaining samples of this study.

### **Uncultured organisms**

The metabarcoding used for accessing bacterial communities detected uncultured microorganisms and these occurred in low abundance in the samples. The phylum Candidate division WPS-1 was detected in all samples and was more abundant in the basins of Juruá and Purus rivers. The Candidate division WPS-2 was detected in root samples of Purus in Acre, and sapwood from Acre and Tapajós. *Candidatus* Solibacter was found in sapwood samples, *Candidatus* Saccharibacteria was found only in leaf samples from Purus and *Candidatus* Pelagibacter in sapwood samples from Tapajós river. The non-cultivated Bacteria candidate division SR1 (Sulfur-River 1) was also found in the samples. A great number of unclassified members of Acidobacteria was found in *H. brasiliensis* and clustered into 14 Acidobacteria subgroups: Acidobacteria GP 1, 2, 3, 4, 5, 6, 7, 11, 13, 16, 17, 20, 22, and 25. Most of the Acidobacteria subgroups are characterized by not being easily cultivated *in vitro*. Among the fungi, two distinct clades of the Rozellomycota phylum were detected in the basins of Purus and Juruá, GS5 and GS12.

## Core microbiome

The core endophytic microbiome was estimated for each plant organ and for each basin by considering the differential abundance of OTUs and their prevalence in individual samples. The core microbiome estimated for fungal (Table 3) and bacterial (Table 4) communities considered OTUs detected in at least 90% of the samples of each organ/basin and with a relative abundance of at least 0.1%. The leaf core microbiome was composed by 12 species of endophytic fungi that belongs to *Meyerozyma* sp., *Lasiodiplodia* sp., *Phyllosticta* sp., *Diaporthe* sp., *Debaryomyces* sp., *Candida* sp., *Pseudofusicoccum* sp., *Aureobasidium* sp., and *Neostrelitziana* sp. The core microbiome of sapwood and root was composed by 7 and 10 species, respectively, belonging to *Cyberlindnera* sp., *Wickerhamomyces* sp., *Trichoderma* sp., *Nectria* sp., and *Pestalotiopsis* sp. The core microbiome in the basins had a great number of species in Juruá and Tapajós, while Amazonas, Madeira and Purus had a low number of species.

Across the plant organs, *Pantoea*, *Enterobacter*, *Weissella*, *Pediococcus*, *Lactobacillus*, *Leuconostoc*, and *Staphylococcus* were found in leaf samples. In sapwood the only genus occupying the core was *Lactococcus* and in roots the genera were *Lysinibacillus*, *Staphylococcus*, and *Streptomyces* (Table 4). When comparing the microbiome across the basins, the core of the basins of Purus and Juruá shared great similarity, with high number of species. Among these, the most frequent members were *Bacillus* sp., *Pantoea* sp., *Paenibacillus* sp., *Streptomyces* sp., *Pseudomonas* sp., and *Burkholderia* sp., which are genera known to contain both plant-pathogenic and plant beneficial species.

## Functional prediction

Functional prediction using FUNGuild showed 11 possible guilds assigned to the fungal communities found in *H. brasiliensis* (Figure S2). These were Animal Endosymbiont-Undefined Saprotroph (7), Animal pathogen (28), Endophyte-Plant Pathogen (33), Epiphyte (3), Fungal Parasite (10), Lichen Parasite (5), Plant Pathogen (64), Plant Pathogen-Soil Saprotroph-Wood Saprotroph (17), Plant Pathogen-Wood Saprotroph (5), Undefined Saprotroph (193), and Wood Saprotroph (31). The list of species and the corresponding guilds occupied by them is shown in Table S1. Fungal species useful for biocontrol of plant diseases were found in high relative abundance, such as *Clonostachys rosea*, *Trichoderma*, *Acremonium breve*, *Aureobasidium pullulans*, and *Leptobacillium leptobactrum*. Fungal species that form endo and ectomycorrhizal associations with plants found in the microbiome of *H. brasiliensis* include *Erythromyces crocicreas*, *Coprinellus disseminatus*, *Myriotrema urceolare*, *Rhizoscyphus*, and *Entrophospora*.

Approximately 32 fungal diseases have been reported in *H. brasiliensis* (Table S2). We found plant pathogenic species associated with 15 diseases of the rubber tree although only asymptomatic plants were sampled. Thirty-four sequences were classified in one OTU identified as *P. ulei*, the major pathogen of the rubber tree, and these were found in samples from all organs and states. The functional predictions of endophytic fungal communities using FUNguild also showed that many fungal plant pathogens known from other hosts are present in *H. brasiliensis* but have not yet been reported as pathogens of the rubber tree (Table S3). Most of the OTUs assigned to the guild of plant pathogens belong to the Dothideomycetes, Sordariomycetes, Agaricomycetes, Eurotiomycetes, and Leotiomyces classes of Ascomycota. The dominant Dothideomycetes were

represented by plant pathogens belonging to the *Pleosporaceae*, *Botryosphaeriaceae* and *Mycosphaerellaceae*.

Analysis of functional prediction using the functional annotation of prokaryotic taxa (FAPROTAX) found 43 functions linked with bacterial communities in *H. brasiliensis*, accepting only functions with > 1% of representativeness. The 10 more abundant functions found were Chemoheterotrophy (611), Aerobic chemoheterotrophy (356), Fermentation (231), Animal parasites or symbionts (52), Nitrate reduction (47), Aromatic compound degradation (45), Ureolysis (44), Human pathogens (43), Methylophony (33), and Intracellular parasites (32). The functional annotation of microbial communities did not show significant differences among the organs (Figure S3).

## DISCUSSION

The endophytic fungi of rubber tree have been studied, whereas the endophytic bacteria remain poorly explored (Abraham et al. 2013; Glushakova et al. 2016; Rocha et al. 2011; Martin et al. 2015; Gazis and Chaverri 2010; Gazis et al. 2012). Classical methods such as culture-dependent used in these works focus on individuals rather than communities, and generally underestimate the real composition of microorganisms (Glushakova et al. 2016). Due to the great role of microbiome in plant health, deep analysis is necessary to assess the diversity and to understand the complex interactions among the associated microbial species. Thus, we used high-throughput sequencing to investigate the microbiome of rubber tree in its center of origin and explored diversity and abundance of these microorganisms across the plant organs and basins.

Factors such as plant genotype, plant compartment, edaphic factors and biogeography can drive the microbial community assembly and structure (Müller et al. 2016). In our survey, there were differences between fungal and bacterial communities according to the plant organ. High fungal diversity was found in leaves from the basins of Madeira and Purus, while bacteria diversity was higher in sapwood from the basins of Juruá and Purus.

Leaves have a large surface area constantly influenced by the deposition of fungal spores spread by winds and rain. According to Arnold et al. (2003), 10,000 spores of endophytic fungi of tropical trees are estimated to be carried by air and deposited on the leaf surface each day, contributing to the high diversity in the leaves (Arnold et al. 2003). Additionally, the chemical and physical characteristics of the thin leaf blades favor the establishment of fungi (Agler et al. 2016; Andrews and Hirano 1991; Arnold and Herre 2003). When the endophytic

fungi isolated from leaves and sapwood of *H. brasiliensis* were compared, it was found that frequency of isolation was much higher in leaves. However, different estimators always pointed to a greater diversity in the sapwood (Gazis and Chaverri 2010).

Bacterial community for instance, reach the sapwood from the lenticels or by colonization of the lumen of xylem vessels, and are then dispersed vertically in the plant (Compant, Clément, and Sessitsch 2010). The preferential colonization of the sapwood tissues may offer advantages for bacteria, because these are regions rich in carbohydrates and amino acids. Sapwood tissues are considered homogeneous environments that confer protection against antagonists and drastic environmental changes (Abraham et al. 2013; Hardoim et al. 2015; Kandel, Joubert, and Doty 2017).

The bacterial and fungal endophytic communities of *H. brasiliensis* exhibited similar patterns of distribution and composition, with samples from the basins of Juruá and Purus being distinct from those of Amazonas, Madeira and Tapajós rivers. This suggests a potential role of biogeography in community differentiation. The pattern of differentiation between microbiomes from plants collected in different basins coincides with the reports of distinct populations of *H. brasiliensis*, which are known to contain genotypes with high levels of resistance to SALB in Acre (Schultes 1956). This dichotomy between western (Juruá and Purus) and central/eastern portions of the Amazon (Amazonas, Madeira and Tapajós) may be related to the geographic distances, and consequent isolation, between the sampled habitats (Finkel et al. 2011; Lindström and Langenheder 2012).

Additional clues about the origin of this biological compartmentalization are given by the biogeography of this region. Most part of the central-eastern Amazon is located on top of soils derived from the ancient Amazon Craton of Proterozoic and Paleozoic origin (ter Steege 2011). The western Amazon, however, sits on top of much younger Cenozoic sediments originated from erosion after the uplift of the Andean Mountains (Hoorn et al. 2010). This scenario created a gradient of fertility from west to east and is considered a major factor in shaping the diversity patterns currently observed in the Amazon, where the highest values of mammal species richness and plant alpha-diversity are concentrated in the western Amazon, including the state of Acre (Hoorn et al. 2010).

Higher levels of nutrient availability in the Cenozoic sediments led to a higher rate of forest turnover with consequent shorter generation times, faster evolution and faster speciation rates in the western Amazon (ter Steege 2011). It is not clear if these biogeographic patterns also shape the microbial communities directly, although soil properties such as pH can influence the diversity patterns of bacteria in a continental scale (Fierer and Jackson 2006). Nevertheless, the more diverse flora surrounding rubber trees located in west Amazon certainly affects the composition of inoculum available and may contribute to the uniqueness of the microbiome of the rubber trees collected in Acre.

The high number of yeasts detected in our analysis indicate an important role of this group of fungi in the rubber tree microbiome. Yeasts were commonly reported to colonize fresh latex from rubber trees (Glushakova et al. 2016), and in our survey yeasts were abundant in sapwood and root. The more abundant strains such as *Cyberlindnera fabianii* and *Candida* spp. occur in diverse kinds of



alcoholic fermentations and are commonly associated with the phyllosphere of plants (Limtong and Kaewwichian 2015; Doty 2013), while *Hanseniaspora*, *Meyerozyma* and *Wickerhamomyces* are considered as potential biocontrol agents against plant diseases (Oro et al. 2014; Cai et al. 2015; Bautista-Rosales et al. 2013).

The species that are part of the core microbiome have a biological significance for the plant, acting in the growth and health, so they are present in high levels of abundance in the host (Huttenhower et al. 2012). The highest number of species of the core were found in the basins of Juruá and Tapajós. When analyzed by plant organ, the leaf housed the highest number of species. Analysis revealed the consistent presence of *Trichoderma* species and *Clonostachys rosea*, that are mycoparasites and plant symbionts extensively used for the biocontrol of plant diseases (Jensen et al. 2007; Harman 2006; Chatterton, Jayaraman, and Punja 2008), and may be associated with protection of rubber tree. Members of *Diaporthe*, *Phyllosticta* and *Lasiodiplodia* dominated the endophytic fungal assemblages. *Lasiodiplodia* were described in association with diebacks, wood cankers and sap-stains of trees, but they also form persistent endophytic relationships with many woody species (Slippers and Wingfield 2007; Slippers et al. 2013; Coutinho et al. 2017). The pathogenic behavior and onset of disease is almost invariably associated with stressful conditions experimented by the host plant (Slippers and Wingfield 2007). Another point was the absence in our survey of *Colletotrichum* sp., a common genus found in healthy plant tissue of rubber tree (Chaverri and Gazis 2011; Gazis and Chaverri 2015). The absence of *Colletotrichum* species in our study may be related to the fact that we sampled wild trees of *H. brasiliensis*. *Colletotrichum* species were previously found

associated with tree sampled from plantations, *Colletotrichum* species occur in high abundance (Gazis and Chaverri 2015, 2010).

Analysis of the bacterial core microbiome revealed a more diversified picture of the prevalent taxa in different groupings of samples from the basins of Juruá and Purus, and by plant organ in leaf. *Pantoea* is commonly found in the microbiomes of soils and plants, especially in the phyllosphere of crop species, being linked with low overall bacterial diversity and diseased tissues (Bouffaud et al. 2014; Berg et al. 2014). Phylogenetics lineages of *Pantoea* can contain plant and human pathogens, as well as non pathogenic strains (Walterson and Stavrínides 2015), involved with disease control and some strains are employed commercially (Walterson and Stavrínides 2015). Members of *Enterobacter* are commonly found in the indigenous microbiota of plants, but their possible roles in these habitats remain unclear (Berg et al. 2014; Erlacher et al. 2014). Species of *Bacillus* are used for plant growth promotion and biocontrol of diseases (Pérez-García, Romero, and de Vicente 2011). These bacteria produce lipopeptides that act as antimicrobial agents and inducers of plant defense (Ongena and Jacques 2008). High abundances of *Bacillus* in metagenomic surveys of plant microbiomes are generally equated with beneficial effects to the host plant (Müller et al. 2015; Carrell and Frank 2015).

Functional prediction detected plant-beneficial bacteria in the microbiome of the rubber tree associated with plant growth promotion, biological control of diseases and tolerance to the abiotic stress. Some genera of bacteria found here are involved with nitrogen fixation, such as *Rhizobium*, *Azoarcus*, *Azospirillum*, *Burkholderia*, *Enterobacter*, *Gluconacetobacter*, and tolerance of plants to the abiotic stress such as *Achromobacter* (salinity) and *Paenibacillus* (drought

stress). Other functions useful for biotechnological purposes were found, such as chitinolysis (*Lysobacter*, *Clostridium* and *Bacillus*), cellulolysis (*Dyadobacter* and *Cellulomonas*) and degradation of aromatic compound (*Acinetobacter*, *Rhodococcus* and *Nocardioides*). Some endophytic microorganisms of *H. brasiliensis* are associated with human diseases such as bacteria from genera *Salmonella*, *Escherichia*, *Shigella* (Dekker and Frank 2015), and the fungi such as *Mucor circinelloides*, *Candida* spp. *Lodderomyces elongisporus*, *Aspergillus sydowii*, and *Phialemoniopsis oculares* (Fisher et al. 2012; Köhler, Casadevall, and Perfect 2014). Rubber tree as well several plants, harbor a large number of opportunistic species of bacteria and fungi that are pathogenic to humans, however, the impact is low when compared to vegetables such as lettuce and tomato for example (Ottesen et al. 2013; Berg et al. 2014).

The uncultured fungi of the phylum Rozellomycota was recently described and is considered a hyper diverse group of epibiotic and endoparasitic organisms, with members being found in aquatic and terrestrial habitats through metagenomics surveys (Corsaro et al. 2014). Clades of the Rozzelomycota are commonly recovered from soil samples, especially in tundra soils (Tedersoo et al. 2017). Our finding of these taxa in the microbiome of a neotropical tree located in the Equator shows how broad are the geographic and metabolic span of these poorly known early diverging phylogenetic lineages (Tedersoo et al. 2017). Five phyla of uncultured bacteria were found in rubber tree samples. Candidatus division SR1 (Sulphur River 1) is possibly involved in sulfur transformation, because it was found in sulfur-rich marine and river environments (Harris, Kelley, and Pace 2004). The candidate divisions WPS-1 and WPS-2 (Writtenberg Polluted Soil) were named after a study of polychlorinated biphenyl-polluted soil

in Germany. These are present in various environments, but their function is unclear (Nogales et al. 2001). Candidatus *Saccharibacteria* are reported from diverse environments and are generally associated with degradation of organic compounds (Kindaichi et al. 2016). Candidatus *Solibacter* was also found in soils, plants and sediments and plays roles in nitrate and nitrite reduction, and plant cell wall degradation (Ward et al. 2009).

The study of the microbiome of *H. brasiliensis* in its center of origin revealed that the populations are structured according to the type of organ and the basin sampled. Fungal and bacterial communities have shown to be more diverse and richer in the basins located in Acre state (Juruá and Purus). Coincidentally, populations of rubber trees present in this state have higher resistance to SALB. The observed patterns suggest that, in addition to the genotypic composition of plants, the balance of interactions among the components of the microbiome are co-responsible for the higher levels of resistance to SALB in Acre populations of rubber trees. This hypothesis deserves to be tested within the context of the global microbiome of the plants, using strategies of microbiome transfer between native plants and commercial clones, with concomitant evaluation of the disease-resistance patterns and microbial dynamics accessed by metagenomics, aiming to increase the sustainability rubber tree production in areas of occurrence of *P. ulei*, the causal agent of SALB.

## ACKNOWLEDGEMENT

We thank Renato Villaschi for helping us with the sampling of *H. brasiliensis* in Amazonas and Pará states, and for the aid in the processing of the samples. Braz T. Hora-Junior for sampling in Acre state and other contributions with the project. Pablo Alvarez for help with the analyses of microbial diversity. Professor Hilário Mantovani for the help with the analyses. This study was financed in part by the Coordenação de Aperfeiçoamento de Pessoal de Nível Superior - Brasil (CAPES) - Finance Code 001 by the Pró-Amazônia call for proposals.

## REFERENCES

- Abraham, A., Philip, S., Kuruvilla Jacob, C., and Jayachandran, K. 2013. Novel bacterial endophytes from *Hevea brasiliensis* as biocontrol agent against Phytophthora leaf fall disease. **BioControl**. 58:675–684.
- Agler, M. T., Ruhe, J., Kroll, S., Morhenn, C., Kim, S.-T., Weigel, D., et al. 2016. Microbial hub taxa link host and abiotic factors to plant microbiome variation. **Plos Biology**. 14:e1002352.
- Anders, S., and Huber, W. 2010. Differential expression analysis for sequence count data. **Genome Biology**. 11:R106.
- Andreote, F. D., Rocha, U. N. da, Araújo, W. L., Azevedo, J. L., and van Overbeek, L. S. 2010. Effect of bacterial inoculation, plant genotype and developmental stage on root-associated and endophytic bacterial communities in potato (*Solanum tuberosum*). **Antonie van Leeuwenhoek**. 97:389–399.
- Andrews, J. H., and Hirano, S. S., eds. 1991. Microbial ecology of leaves. New York, NY: Springer New York.
- Aprill, A., McNally, S., Parsons, R., and Weber, L. 2015. Minor revision to V4 region SSU rRNA 806R gene primer greatly increases detection of SAR11 bacterioplankton. **Aquatic Microbial Ecology**. 75, 129-137.
- Arnold, A. E., and Herre, E. A. 2003. Canopy cover and leaf age affect colonization by tropical fungal endophytes: Ecological pattern and process in *Theobroma cacao* (Malvaceae). **Mycologia**. 95:388–398.
- Arnold, A. E., Mejía, L. C., Kyllö, D., Rojas, E. I., Maynard, Z., Robbins, N., et al. 2003. Fungal endophytes limit pathogen damage in a tropical tree. **Proceedings of the National Academy of Sciences of the United States of America**. 100:15649–54.
- Bálint, M., Tiffin, P., Hallström, B., O'Hara, R. B., Olson, M. S., Fankhauser, J. D., et al. 2013. Host genotype shapes the foliar fungal microbiome of balsam poplar (*Populus balsamifera*). **PLoS One**. 8:e53987.
- Bardou, P., Mariette, J., Escudié, F., Djemiel, C., and Klopp, C. 2014. jvenn: an interactive Venn diagram viewer. **BMC Bioinformatics**. 15:293.
- Bautista-Rosales, P. U., Calderon-Santoyo, M., Servín-Villegas, R., Ochoa-Álvarez, N. A., and Ragazzo-Sánchez, J. A. 2013. Action mechanisms of the yeast *Meyerozyma caribbica* for the control of the phytopathogen *Colletotrichum gloeosporioides* in mangoes. **Biological Control**. 65:293–301.

- Berendsen, R. L., Pieterse, C. M. J., and Bakker, P. A. H. M. 2012. The rhizosphere microbiome and plant health. **Trends in Plant Science**. 17:478–486.
- Berg, G., Erlacher, A., Smalla, K., and Krause, R. 2014. Vegetable microbiomes: is there a connection among opportunistic infections, human health and our ‘gut feeling’? **Microbial Biotechnology**. 7:487–495.
- Bouffaud, M.-L., Poirier, M.-A., Muller, D., and Moënne-Loccoz, Y. 2014. Root microbiome relates to plant host evolution in maize and other poaceae. **Environmental Microbiology**. 16:2804–2814.
- Cai, Z., Yang, R., Xiao, H., Qin, X., and Si, L. 2015. Effect of preharvest application of *Hanseniaspora uvarum* on postharvest diseases in strawberries. **Postharvest Biology and Technology**. 100:52–58.
- Caporaso, J. G., Lauber, C. L., Walters, W. A., Berg-Lyons, D., Huntley, J., Fierer, N., et al. 2012. Ultra-high-throughput microbial community analysis on the Illumina HiSeq and MiSeq platforms. **The ISME Journal**. 6:1621–1624.
- Caporaso, J. G., Lauber, C. L., Walters, W. A., Berg-Lyons, D., Lozupone, C. A., Turnbaugh, P. J., et al. 2011. Global patterns of 16S rRNA diversity at a depth of millions of sequences per sample. **Proceedings of the National Academy of Sciences of the United States of America**. 108 Suppl 1:4516–22.
- Carrell, A. A., and Frank, A. C. 2015. Bacterial endophyte communities in the foliage of coast redwood and giant sequoia. **Frontiers in Microbiology**. 6:1008.
- Chao, A., Gotelli, N. J., Hsieh, T. C., Sander, E. L., Ma, K. H., Colwell, R. K., et al. 2014. Rarefaction and extrapolation with Hill numbers: a framework for sampling and estimation in species diversity studies. **Ecological Monographs**. 84:45–67.
- Chatterton, S., Jayaraman, J., and Punja, Z. K. 2008. Colonization of cucumber plants by the biocontrol fungus *Clonostachys rosea* f. *catenulata*. **Biological Control**. 46:267–278.
- Chaverri, P., and Gazis, R. O. 2011. Linking ex planta fungi with their endophytic stages: *Perisporiopsis*, a common leaf litter and soil fungus, is a frequent endophyte of *Hevea* spp. and other plants. **Fungal Ecology**. 4:94–102
- Chee, K. H., and Holliday, P. 1986. South American leaf blight of *Hevea* rubber. **South American leaf blight of Hevea rubber**. 13.
- Compant, S., Clément, C., and Sessitsch, A. 2010. Plant growth-promoting bacteria in the rhizo- and endosphere of plants: their role, colonization,

mechanisms involved and prospects for utilization. **Soil Biology and Biochemistry**. 42:669–678.

Corsaro, D., Walochnik, J., Venditti, D., Müller, K.-D., Hauröder, B., and Michel, R. 2014. Rediscovery of *Nucleophaga amoebae*, a novel member of the Rozellomycota. **Parasitology Research**. 113:4491–4498.

Coutinho, I. B. L., Freire, F. C. O., Lima, C. S., Lima, J. S., Gonçalves, F. J. T., Machado, A. R., et al. 2017. Diversity of genus *Lasiodiplodia* associated with perennial tropical fruit plants in northeastern Brazil. **Plant Pathology**. 66:90–104.

Deiner, K., Bik, H. M., Mächler, E., Seymour, M., Lacoursière-Roussel, A., Altermatt, F., et al. 2017. Environmental DNA metabarcoding: transforming how we survey animal and plant communities. **Molecular Ecology**. 26:5872–5895.

Dekker, J. P., and Frank, K. M. 2015. *Salmonella*, *Shigella*, and *Yersinia*. **Clinics in laboratory medicine**. 35:225–46.

Doty, S. L. 2013. Endophytic yeasts: biology and applications. In **Symbiotic Endophytes**, Springer, Berlin, Heidelberg, p. 335–343.

Eren, A. M., Vineis, J. H., Morrison, H. G., and Sogin, M. L. 2013. A Filtering method to generate high quality short reads using Illumina paired-end technology. **PLoS One**. 8:e66643.

Erlacher, A., Cardinale, M., Grosch, R., Grube, M., and Berg, G. 2014. The impact of the pathogen *Rhizoctonia solani* and its beneficial counterpart *Bacillus amyloliquefaciens* on the indigenous lettuce microbiome. **Frontiers in Microbiology**. 5:175.

Fierer, N., and Jackson, R. B. 2006. The diversity and biogeography of soil bacterial communities. **Proceedings of the National Academy of Sciences**. 103:626–631.

Finkel, O. M., Burch, A. Y., Lindow, S. E., Post, A. F., and Belkin, S. 2011. Geographical location determines the population structure in phyllosphere microbial communities of a salt-excreting desert tree. **Applied and Environmental Microbiology**. 77:7647–55.

Fisher, M. C., Henk, D. A., Briggs, C. J., Brownstein, J. S., Madoff, L. C., McCraw, S. L., et al. 2012. Emerging fungal threats to animal, plant and ecosystem health. **Nature**. 484:186–194.

Garcia, D., Carels, N., Koop, D. M., de Sousa, L. A., Andrade Junior, S. J. de, Pujade-Renaud, V., et al. 2011. EST profiling of resistant and susceptible *Hevea*



infected by *Microcyclus ulei*. **Physiological and Molecular Plant Pathology**. 76:126–136.

Garcia, D., Mattos, C. R. R., Goncalves, P. D. S., and Guen, V. Le. 2004. Selection of rubber clones for resistance to South American leaf blight and latex yield in the germplasm of the Michelin plantation of Bahia (Brazil). **Journal of Rubber Research**. 7(3), 188-198.

Gazis, R., and Chaverri, P. 2010. Diversity of fungal endophytes in leaves and stems of wild rubber trees (*Hevea brasiliensis*) in Peru. **Fungal Ecology**. 3:240–254.

Gazis, R., and Chaverri, P. 2015. Wild trees in the Amazon basin harbor a great diversity of beneficial endosymbiotic fungi: is this evidence of protective mutualism? **Fungal Ecology**. 17:18–29.

Gazis, R., Miadlikowska, J., Lutzoni, F., Arnold, A. E., and Chaverri, P. 2012. Culture-based study of endophytes associated with rubber trees in Peru reveals a new class of Pezizomycotina: Xylonomycetes. **Molecular Phylogenetics and Evolution**. 65:294–304.

Glushakova, A. M., Kachalkin, A. V, Maksimova, I. A., and Chernov, I. Y. 2016. Yeasts in *Hevea brasiliensis* latex. **Mikrobiologiya**. 85:466–471.

Guyot, J., and Le Guen, V. 2018. A review of a century of studies on South American Leaf Blight of the rubber tree. **Plant Disease**. 102:1052–1065.

Le Guen, V., Doaré, F., Weber, C., and Seguin, M. 2009. Genetic structure of Amazonian populations of *Hevea brasiliensis* is shaped by hydrographical network and isolation by distance. **Tree Genetics & Genomes**. 5:673–683.

Le Guen, V., Garcia, D., Doaré, F., Mattos, C. R. R., Condina, V., Couturier, C., et al. 2011. A rubber tree's durable resistance to *Microcyclus ulei* is conferred by a qualitative gene and a major quantitative resistance factor. **Tree Genetics & Genomes**. 7:877–889.

Le Guen, V., Garcia, D., Mattos, C. R. R., Doaré, F., Lespinasse, D., and Seguin, M. 2007. Bypassing of a polygenic *Microcyclus ulei* resistance in rubber tree, analyzed by QTL detection. **New Phytologist**. 173:335–345.

Hardoim, P. R., van Overbeek, L. S., Berg, G., Pirttilä, A. M., Compant, S., Campisano, A., et al. 2015. The hidden world within plants: ecological and evolutionary considerations for defining functioning of microbial endophytes. **Microbiology and Molecular Biology Reviews**. 79:293–320.

Harman, G. E. 2006. Overview of mechanisms and uses of *Trichoderma* spp. **Phytopathology**. 96:190–194.

Harris, J. K., Kelley, S. T., and Pace, N. R. 2004. New perspective on uncultured bacterial phylogenetic division OP11. **Applied and Environmental Microbiology**. 70:845–9.

Hennings, P. 1904. Über die auf *Hevea*-Arten bisher beobachteten parasitischen Pilze. **Notizblatt des Königl. Botanischen Gartens und Museums zu Berlin**. 4:133.

Horn, C., Wesselingh, F. P., ter Steege, H., Bermudez, M. A., Mora, A., Sevink, J., et al. 2010. Amazonia through time: andean uplift, climate change, landscape evolution, and biodiversity. **Science**. 330:927–931.

Hora Júnior, B. T. da, de Macedo, D. M., Barreto, R. W., Evans, H. C., Mattos, C. R. R., Maffia, L. A., et al. 2014. Erasing the past: a new identity for the damoclean pathogen causing south american leaf blight of rubber. **PLoS One**. 9:e104750.

Hsieh, T. C., Ma, K. H., and Chao, A. 2016. iNEXT: an R package for rarefaction and extrapolation of species diversity (Hill numbers). **Methods in Ecology and Evolution**. 7:1451–1456.

Huttenhower, C., Gevers, D., Knight, R., Abubucker, S., Badger, J. H., Chinwalla, A. T., et al. 2012. Human Microbiome Project Consortium. Structure, function and diversity of the healthy human microbiome. **Nature**. 486:207–214.

Jensen, D. F., Knudsen, I. M. B., Lübeck, M., Mamarabadi, M., Hockenhull, J., and Jensen, B. 2007. Development of a biocontrol agent for plant disease control with special emphasis on the near commercial fungal antagonist *Clonostachys rosea* strain “IK726.” **Australasian Plant Pathology**. 36:95.

Kandel, S., Joubert, P., and Doty, S. 2017. Bacterial endophyte colonization and distribution within plants. **Microorganisms**. 5:77.

Kindaichi, T., Yamaoka, S., Uehara, R., Ozaki, N., Ohashi, A., Albertsen, M., et al. 2016. Phylogenetic diversity and ecophysiology of Candidate phylum *Saccharibacteria* in activated sludge. **FEMS Microbiology Ecology**. 92:fiw078.

Köhler, J. R., Casadevall, A., and Perfect, J. 2014. The spectrum of fungi that infects humans. **Cold Spring Harbor perspectives in medicine**. 5:a019273.

Köljalg, U., Nilsson, R. H., Abarenkov, K., Tedersoo, L., Taylor, A. F. S., Bahram, M., et al. 2013. Towards a unified paradigm for sequence-based identification of fungi. **Molecular Ecology**. 22:5271–5277.

Lieberei, R. 2007. South American leaf blight of the rubber tree (*Hevea* spp.): new steps in plant domestication using physiological features and molecular markers. **Annals of Botany**. 100:1125–42.

Limtong, S., and Kaewwichian, R. 2015. The diversity of culturable yeasts in the phylloplane of rice in Thailand. **Annals of Microbiology**. 65:667–675.

Lindström, E. S., and Langenheder, S. 2012. Local and regional factors influencing bacterial community assembly. **Environmental Microbiology Reports**. 4:1–9.

Louca, S., Parfrey, L. W., and Doebeli, M. 2016. Decoupling function and taxonomy in the global ocean microbiome. **Science** (New York, N.Y.). 353:1272–7.

Lundberg, D. S., Yourstone, S., Mieczkowski, P., Jones, C. D., and Dangl, J. L. 2013. Practical innovations for high-throughput amplicon sequencing. **Nature Methods**. 10:999–1002.

Martin, R., Gazis, R., Skaltsas, D., Chaverri, P., and Hibbett, D. 2015. Unexpected diversity of basidiomycetous endophytes in sapwood and leaves of *Hevea*. **Mycologia**. 107:284–97.

McMurdie, P. J., and Holmes, S. 2013. phyloseq: An R package for reproducible interactive analysis and graphics of microbiome census data. **PLoS One**. 8:e61217.

Mendes, R., Kruijt, M., de Bruijn, I., Dekkers, E., van der Voort, M., Schneider, J. H. M., et al. 2011. Deciphering the rhizosphere microbiome for disease-suppressive bacteria. **Science** (New York, N.Y.). 332:1097–100.

Moissl-Eichinger, C., Grasis, J. A., Hardoim, P. R., Gopal, M., and Gupta, A. 2016. Microbiome selection could spur next-generation plant breeding strategies. **Frontiers in Microbiology**, 7, 1971.

Müller, D. B., Vogel, C., Bai, Y., and Vorholt, J. A. 2016. The plant microbiota: systems-level insights and perspectives. **Annual Review of Genetics**. 50:211–234.

Müller, H., Berg, C., Landa, B. B., Auerbach, A., Moissl-Eichinger, C., and Berg, G. 2015a. Plant genotype-specific archaeal and bacterial endophytes but similar *Bacillus* antagonists colonize Mediterranean olive trees. **Frontiers in Microbiology**. 6:138.

Nguyen, N. H., Song, Z., Bates, S. T., Branco, S., Tedersoo, L., Menke, J., et al.

2016. FUNGuild: An open annotation tool for parsing fungal community datasets by ecological guild. **Fungal Ecology**. 20:241–248.

Nogales, B., Moore, E. R., Llobet-Brossa, E., Rossello-Mora, R., Amann, R., and Timmis, K. N. 2001. Combined use of 16S ribosomal DNA and 16S rRNA to study the bacterial community of polychlorinated biphenyl-polluted soil. **Applied and Environmental Microbiology**. 67:1874–84.

Ongena, M., and Jacques, P. 2008. *Bacillus* lipopeptides: versatile weapons for plant disease biocontrol. **Trends in Microbiology**. 16:115–125.

Oro, L., Feliziani, E., Ciani, M., Romanazzi, G., and Comitini, F. 2014. Biocontrol of postharvest brown rot of sweet cherries by *Saccharomyces cerevisiae* Disva 599, *Metschnikowia pulcherrima* Disva 267 and *Wickerhamomyces anomalus* Disva 2 strains. **Postharvest Biology and Technology**. 96:64–68.

Ottesen, A. R., Peña, A. G., White, J. R., Pettengill, J. B., Li, C., Allard, S., Rideout, S., Allard, M., Hill, T., Evans, P., Strain, E., Musser, S., Knight, R., and Brown, E. 2013. Baseline survey of the anatomical microbial ecology of an important food plant: *Solanum lycopersicum* (tomato). **BMC Microbiology**. 13:114.

Oyserman, B. O., Medema, M. H., and Raaijmakers, J. M. 2018. Road MAPs to engineer host microbiomes. **Current Opinion in Microbiology**. 43:46–54.

Parada, A. E., Needham, D. M., and Fuhrman, J. A. 2016. Every base matters: assessing small subunit rRNA primers for marine microbiomes with mock communities, time series and global field samples. **Environmental Microbiology**. 18:1403–1414.

Pérez-García, A., Romero, D., and de Vicente, A. 2011. Plant protection and growth stimulation by microorganisms: biotechnological applications of *Bacilli* in agriculture. **Current Opinion in Biotechnology**. 22:187–193.

Priyadarshan, P. M., and Goncalves, P. de S. 2003. *Hevea* gene pool for breeding. **Genetic Resources and Crop Evolution**. 50:101–114.

Quast, C., Pruesse, E., Yilmaz, P., Gerken, J., Schweer, T., Yarza, P., et al. 2013. The SILVA ribosomal RNA gene database project: improved data processing and web-based tools. **Nucleic Acids Research**. 41:D590-6.

Rocha, A. C. S., Garcia, D., Uetanabaro, A. P. T., Carneiro, R. T. O., Araújo, I. S., Mattos, C. R. R., et al. 2011. Foliar endophytic fungi from *Hevea brasiliensis* and their antagonism on *Microcyclus ulei*. **Fungal Diversity**. 47:75–84.

Rognes, T., Flouri, T., Nichols, B., Quince, C., and Mahé, F. 2016. VSEARCH: a versatile open source tool for metagenomics. **PeerJ**. 4:e2584.

Schloss, P. D., Westcott, S. L., Ryabin, T., Hall, J. R., Hartmann, M., Hollister, E. B., et al. 2009. Introducing mothur: open-source, platform-independent, community-supported software for describing and comparing microbial communities. **Applied and Environmental Microbiology**. 75:7537–41.

Schultes, R. E. (1956). The Amazon Indian and evolution in *Hevea* and related genera. **Journal of the Arnold Arboretum**, 37(2), 123-152.

Serier, J.-B. 1993. *Histoire du caoutchouc*. **Desjonquères**.

Sethuraj, M. R., & Mathew, N. M. 1992. Natural rubber: biology, cultivation and technology. Amsterdam, **NL: Elsevier Science Publisher**. 633.895.

Slippers, B., Boissin, E., Phillips, A. J. L., Groenewald, J. Z., Lombard, L., Wingfield, M. J., et al. 2013. Phylogenetic lineages in the Botryosphaerales: a systematic and evolutionary framework. **Studies in Mycology**. 76:31–49.

Slippers, B., and Wingfield, M. J. 2007. Botryosphaeriaceae as endophytes and latent pathogens of woody plants: diversity, ecology and impact. **Fungal Biology Reviews**. 21:90–106.

Smith, D. P., and Peay, K. G. 2014. Sequence depth, not pcr replication, improves ecological inference from next generation DNA sequencing. **PLoS One**. 9:e90234.

ter Steege, H. 2011. Contribution of current and historical processes to patterns of tree diversity and composition of the amazon. In **Amazonia: landscape and species evolution: A look into the past**. Oxford, UK: Wiley-Blackwell Publishing 347–359.

Tedersoo, L., Bahram, M., Polme, S., Koljalg, U., Yorou, N. S., Wijesundera, R., et al. 2014. Global diversity and geography of soil fungi. **Science**. 346:1256688–1256688.

Tedersoo, L., Bahram, M., Puusepp, R., Nilsson, R. H., and James, T. Y. 2017. Novel soil-inhabiting clades fill gaps in the fungal tree of life. **Microbiome**. 5:42.

Walterson, A. M., and Stavrinides, J. 2015. *Pantoea*: insights into a highly versatile and diverse genus within the Enterobacteriaceae. **FEMS Microbiology Reviews**. 39:968–984.

Ward, N. L., Challacombe, J. F., Janssen, P. H., Henrissat, B., Coutinho, P. M.,

Wu, M., et al. 2009. Three genomes from the phylum *Acidobacteria* provide insight into the lifestyles of these microorganisms in soils. **Applied and Environmental Microbiology**. 75:2046–2056.

White, T. J., T. D. Bruns, S. B. Lee, and J. W. T. 1990. Amplification and direct sequencing of fungal ribosomal RNA genes for phylogenetics. In **PCR Protocols: A Guide to Methods and Applications**. Academic Press. 482.

Yilmaz, P., Parfrey, L. W., Yarza, P., Gerken, J., Pruesse, E., Quast, C., et al. 2014. The SILVA and “All-species living tree project (LTP)” taxonomic frameworks. **Nucleic Acids Research**. 42:D643–D648.

## FIGURE LEGENDS

**Figure 1.** Map of Brazil showing the sampling points (red dots) of *Hevea brasiliensis*. The dashed area corresponds to the center of origin of *H. brasiliensis* (Wicherley 1992).

**Figure 2.** Alpha diversity metrics (Species richness, Shannon, and Simpson indices) of fungal communities of *Hevea brasiliensis* by plant organs and basin. Center line in rectangles represents the median value. The upper end lower lines of the boxes represent the third and first quartiles, respectively. Whiskers represent  $\pm 1.5$  times the interquartile range. The black dots represent outliers.

**Figure 3.** Alpha diversity metrics (Species richness, Shannon, and Simpson indices) of bacteria communities of *Hevea brasiliensis* by plant organs and basin. Center line in rectangles represents the median value. The upper end lower lines of the boxes represent the third and first quartiles, respectively. Whiskers represent  $\pm 1.5$  times the interquartile range. The black dots represent outliers.

**Figure 4.** Beta diversity estimates using Principal Coordinates Analysis (PCoA) weighted Uni-Frac distances calculated from relative OTU abundances for (A) fungi and (B) bacteria communities in the basins of Amazonas, Juruá, Madeira, Purus and Tapajós river.

**Figure 5.** Beta diversity estimates using Principal Coordinates Analysis (PCoA) weighted Uni-Frac distances calculated from relative OTU abundances for fungi and bacteria into communities in the basins of Amazonas, Juruá, Madeira, Purus and Tapajós river.

**Figure 6.** Relative abundance of fungal endophytic community of *Hevea brasiliensis* across the plant organs and basins. (A) order and (B) family.

**Figure 7.** Relative abundance with the 35 most abundant fungal endophytic community of *Hevea brasiliensis* across the plant organs and basins.

**Figure 8.** Relative abundance of bacterial endophytic community of *Hevea brasiliensis* across the plant organs and basins. (A) class and (B) family.

**Figure 9.** Relative abundance with the 35 most abundant bacterial endophytic community of *Hevea brasiliensis* across the plant organs and basins.

**Figure S1.** Venn diagrams for **(A)** fungal and **(B)** bacterial endophytic communities of *Hevea brasiliensis* showing the unique and shared OTUs among plant organs and basins.

**Figure S2.** Prediction ecological guild of endophytic fungi present in *Hevea brasiliensis*. The y axis represents the guild and x axis represent the relative abundance of OTUs assigned.

**Figure S3.** Functional prediction annotation of bacterial community in *Hevea brasiliensis* across the organs. The x axis represents the functional groups and y axis represents the relative abundance of OTUs assigned.



## FIGURES AND TABLES

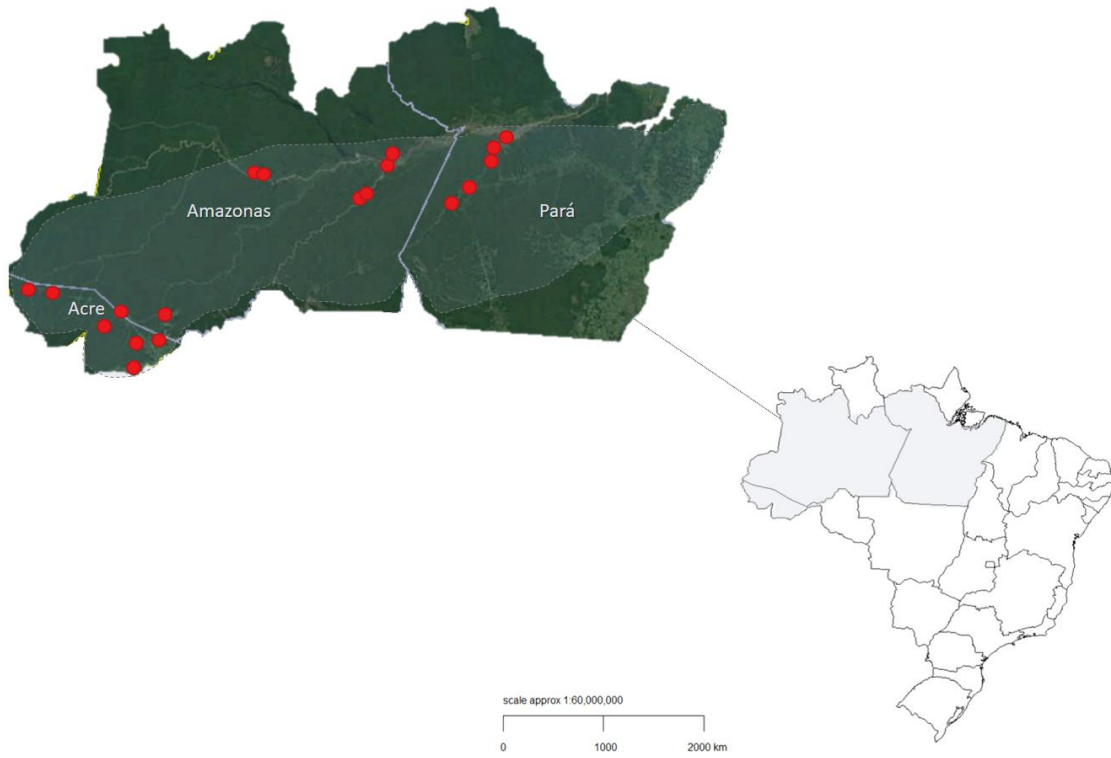


**Figure 1. Ferreira et al. 2018.**

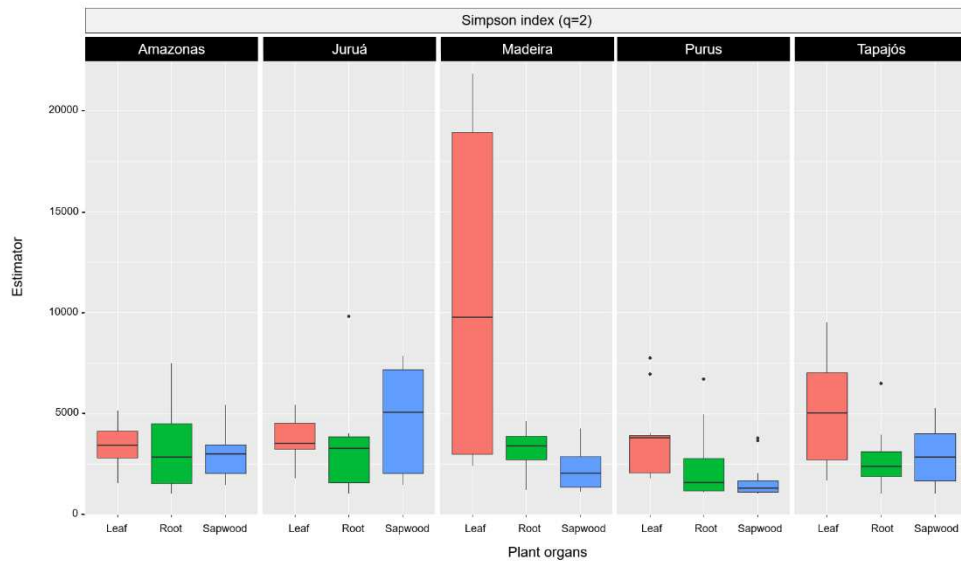
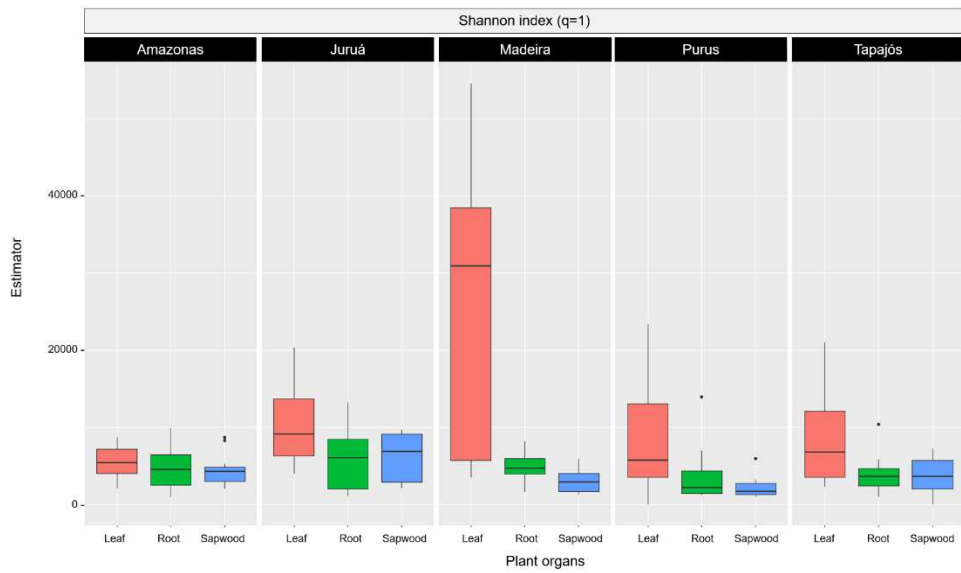
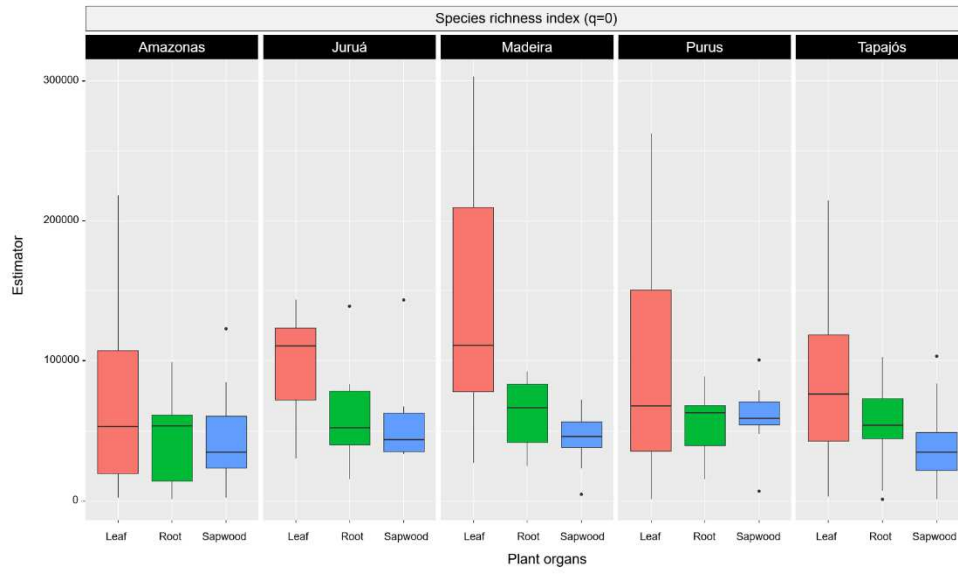
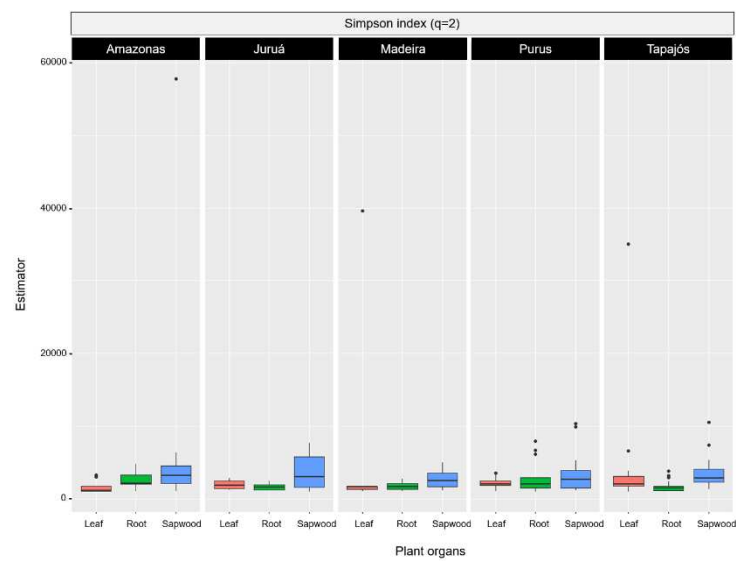
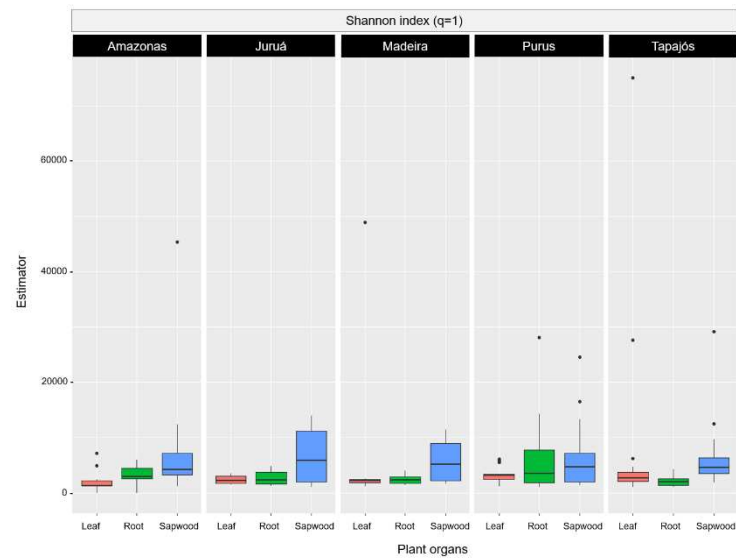
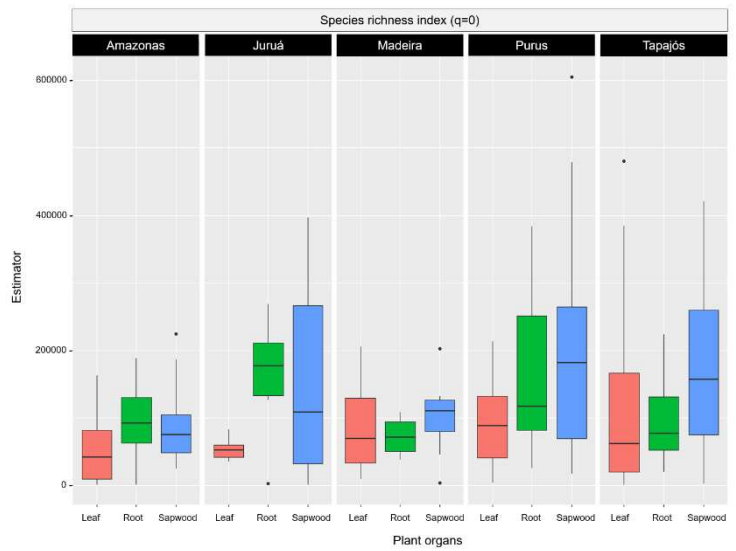


Figure 2. Ferreira et al. 2018.



**Figure 3. Ferreira et al. 2018.**

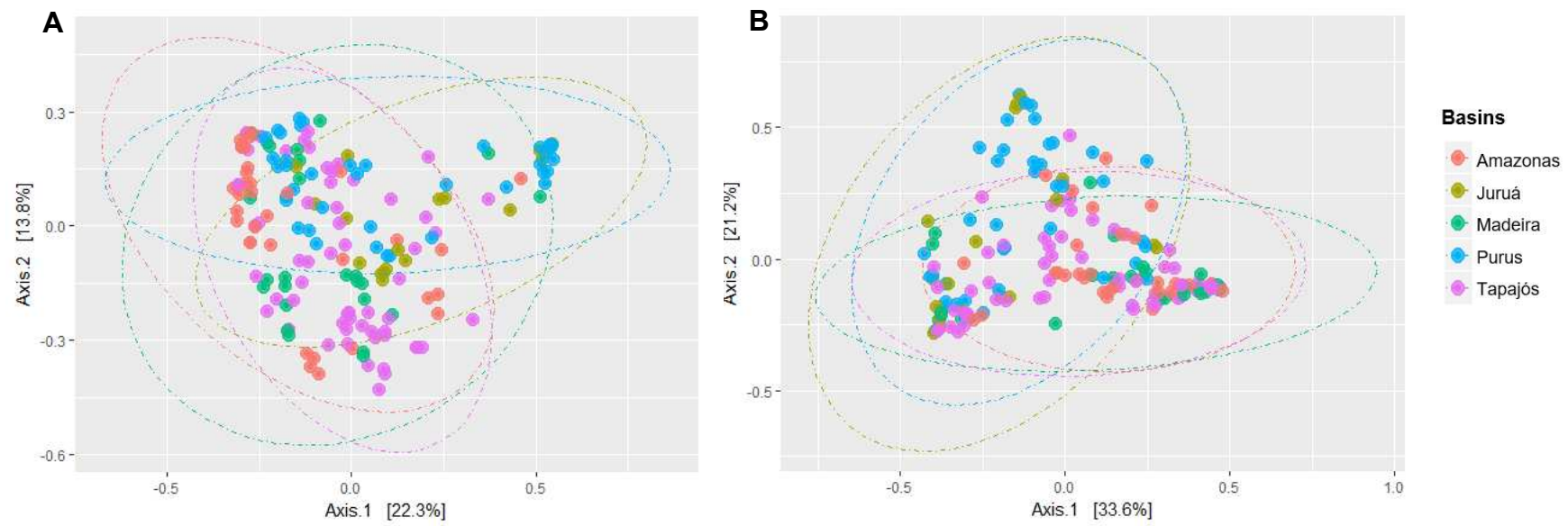


Figure 4. Ferreira et al. 2018.

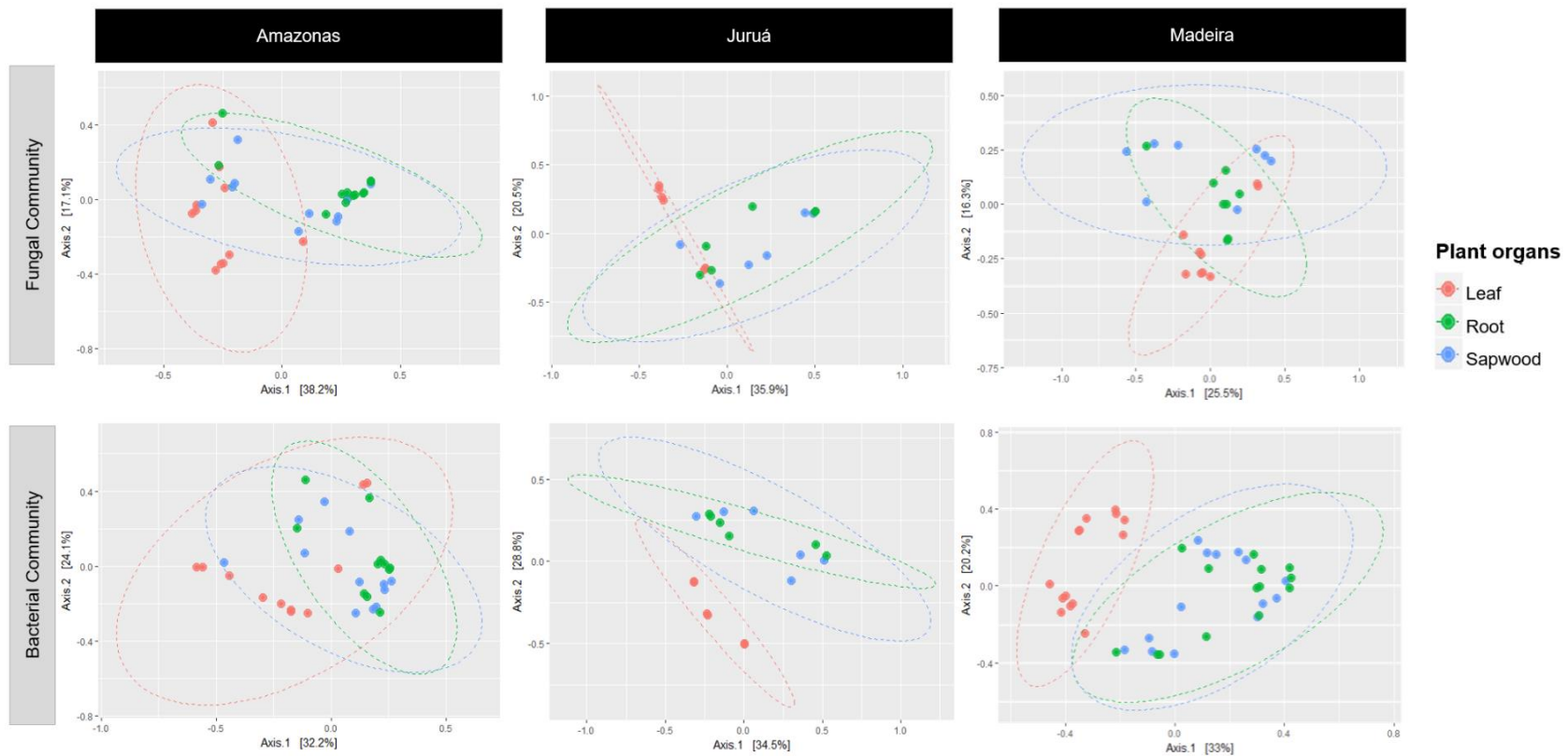


Figure 5. Ferreira et al. 2018.

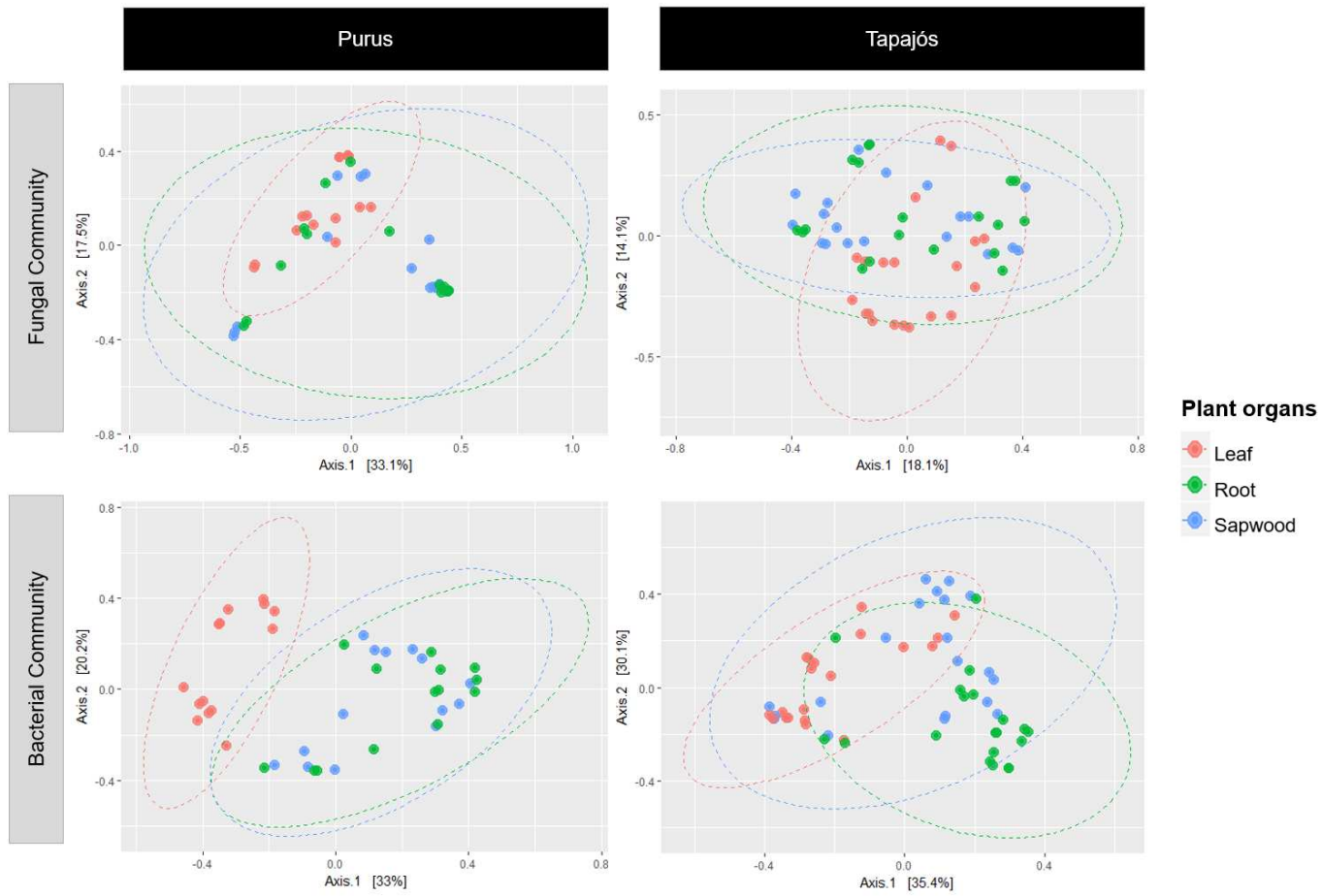
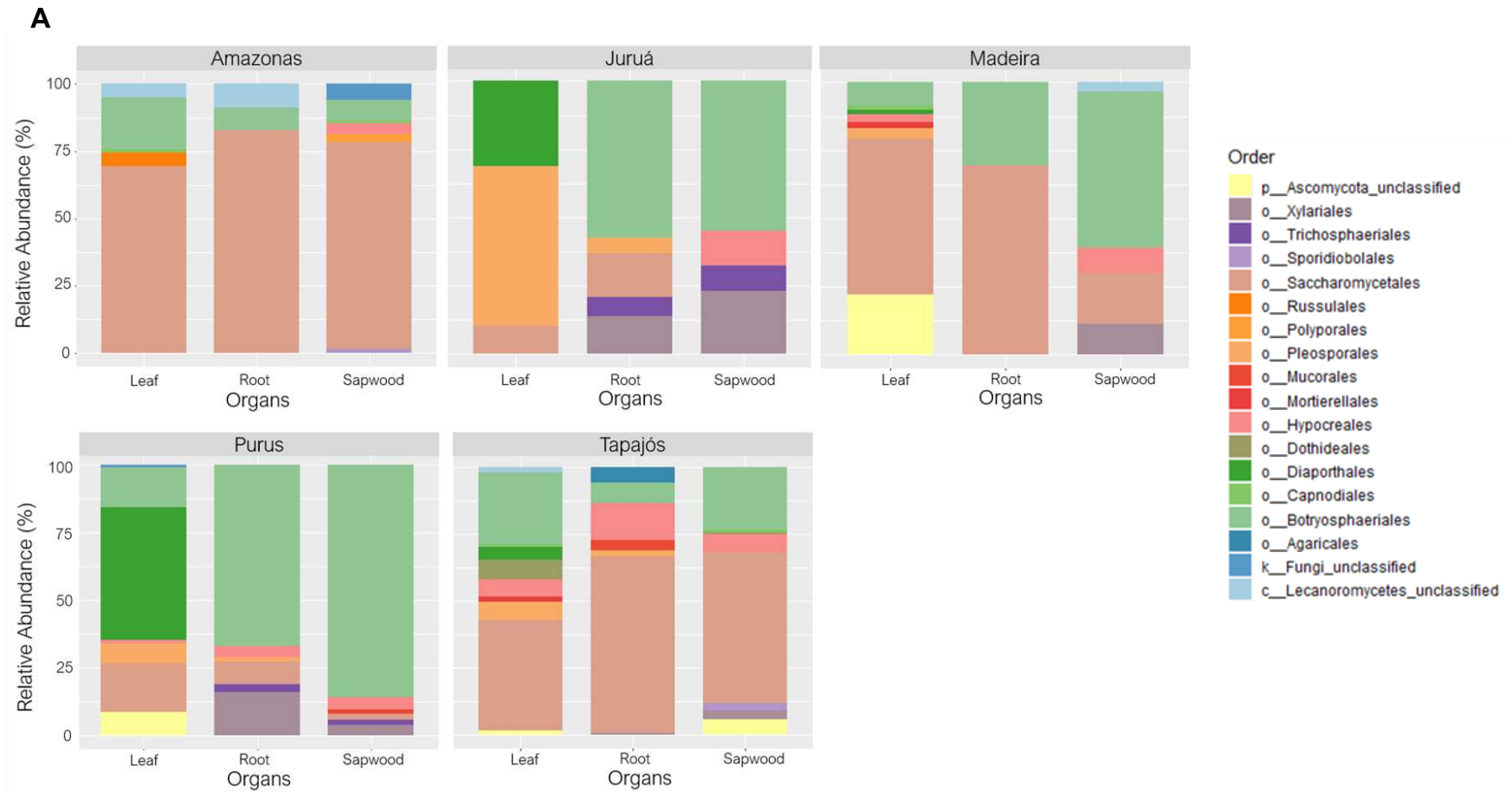


Figure 5. Ferreira et al. 2018.



**Figure 6. Ferreira et al. 2018.**

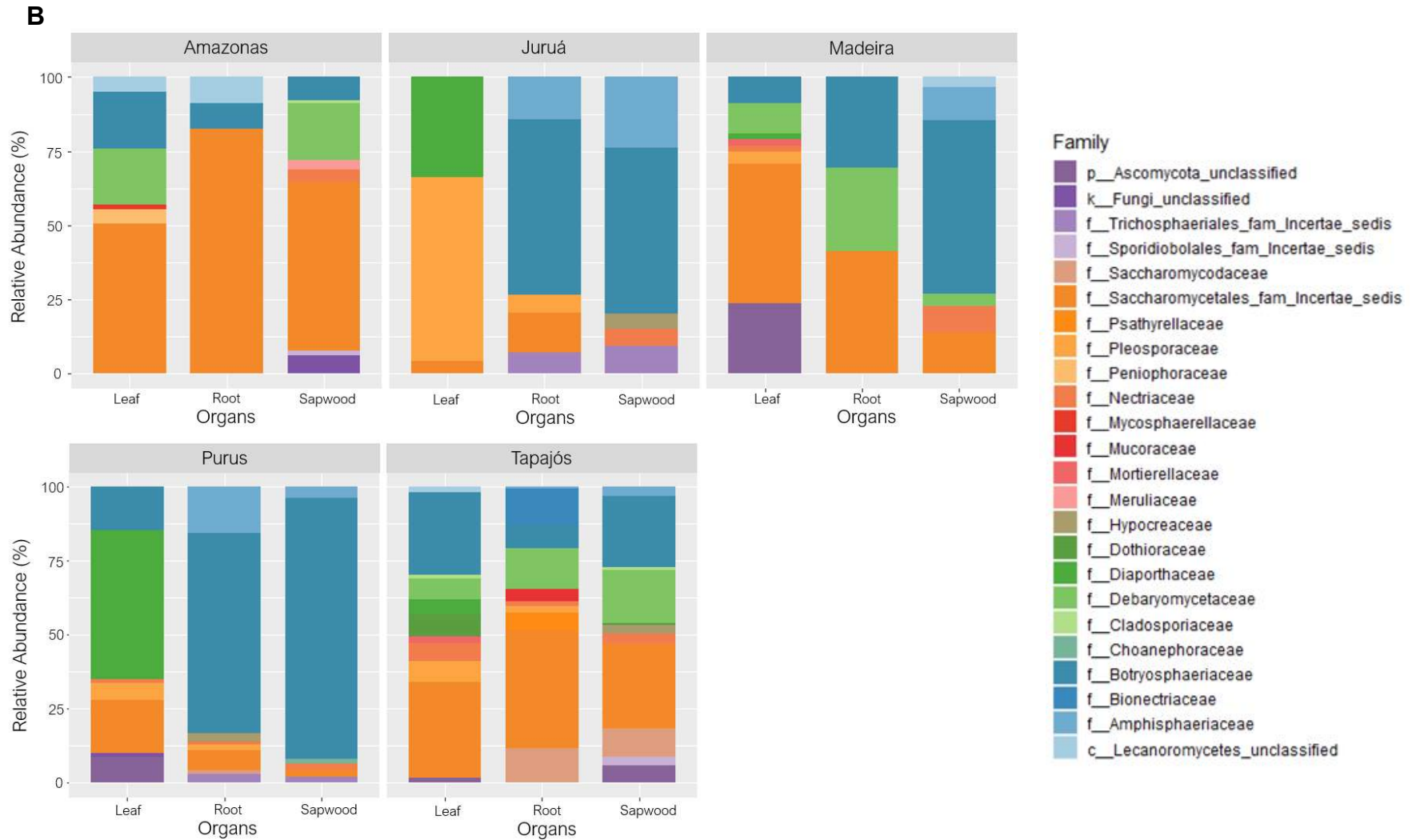
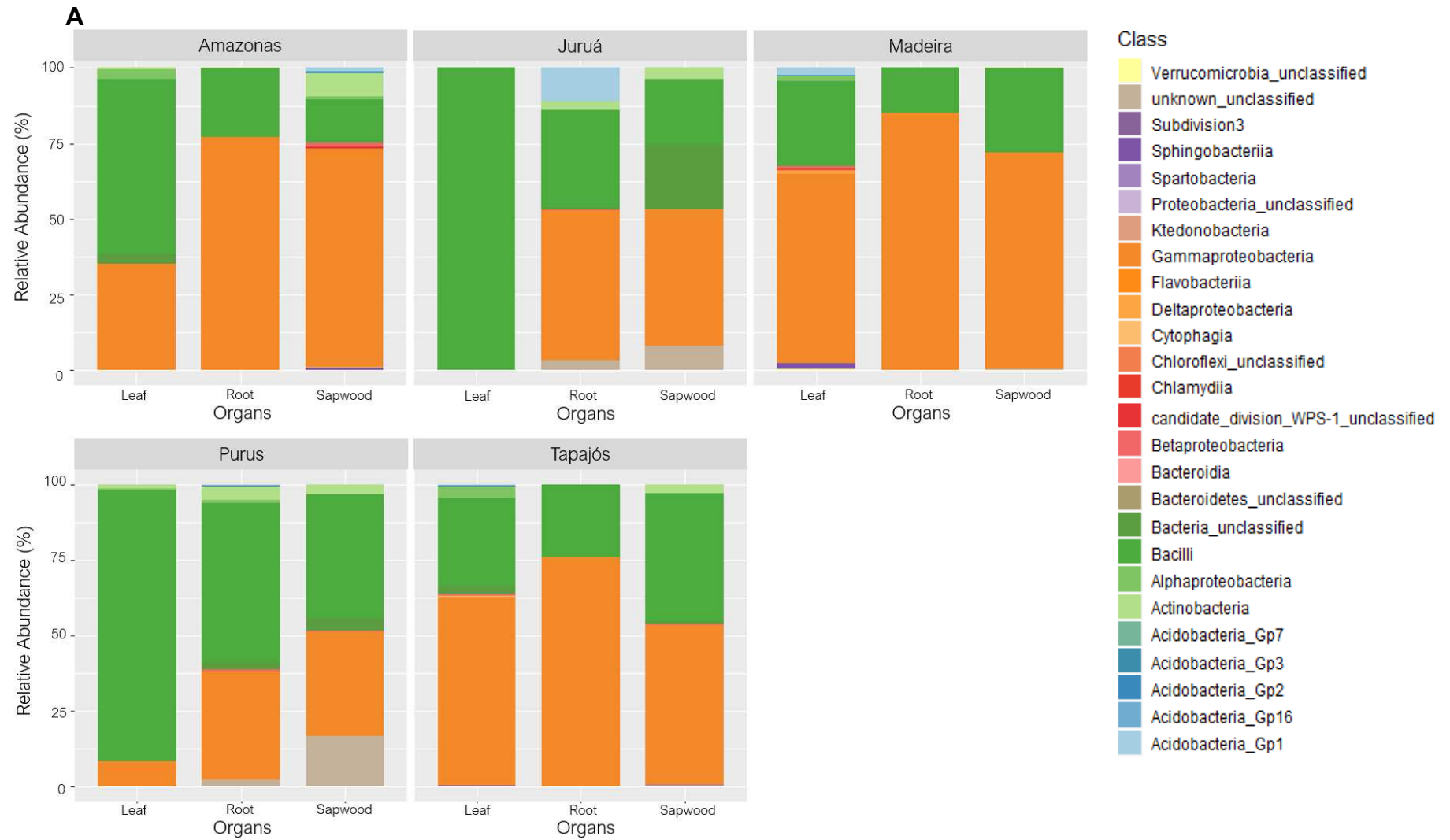


Figure 6. Ferreira et al. 2018.



	Amazonas			Juruá			Madeira			Purus			Tapajós		
Ascomycota; Lasiodiplodia-	4.7	9	7.7	1	49	44.2	0.2	27.8	54	13	59.7	79.8	0.5	8.8	22.6
Ascomycota; f__Saccharomycetales_fam_Incertae_sedis_unclassified-	9.5	68.1	42.2	2.1	10.6	0.5	1	7.6	9.4	3.2	6.3	2.3	6	18.4	11.8
Ascomycota; Meyerozyma-	17.8	2.7	19.4	1.1	0.2	0.1	7.1	23.6	4.4	0.4	0.2	0	7.2	13	16.9
Ascomycota; Wickerhamomyces-	29.7	3.7	5.4	4.1	0.1	0.1	18.6	12	2.4	0.8	0.4	0	15	3.2	0.5
Ascomycota; Candida-	4.2	1.1	3.1	0.4	1.6	0.3	1.7	12.7	0.9	10.9	0.5	0.1	2.1	12.3	12.3
Ascomycota; Diaporthe-	1	0	0.1	20.5	0.7	0.1	3.7	0	0	40.6	0.4	0.1	5.5	0.2	0
Ascomycota; Phyllosticta-	13.9	0	0	1.3	0	0	6.5	0	0	0.3	0	0	19.8	0	0
Ascomycota; Alternaria-	0.8	0.6	0.8	36.1	5.3	1.8	2.8	1.4	0.6	4.3	2.4	0.3	6.7	2.3	0.3
Ascomycota; f__Amphisphaeriaceae_unclassified-	0.2	0.3	1.5	0.3	10.7	12.2	0.1	0.3	8.6	1.9	10.1	3.9	0.1	0.6	2
Ascomycota; p__Ascomycota_unclassified-	0.2	0.1	0.1	4.5	0.3	0.1	16.3	0.1	0.1	8.2	0.2	0.1	3.1	0	5.4
Ascomycota; Hanseniaspora-	0	0.3	0.1	0.2	0.8	0.2	0	0	0	0.1	1.1	0	0	10.5	9
Ascomycota; Debaryomyces-	3.3	3.7	1.2	0	0	0	12.1	0.3	1	0.1	0.1	0	4.7	2.8	1.7
Ascomycota; f__Nectriaceae_unclassified-	0.1	0.2	2.8	0.7	1	4.1	0.6	2	0.9	0.1	1.4	0.3	5.3	1.4	2.5
k__Fungi_unclassified; k__Fungi_unclassified-	0.3	0.2	5.6	5.9	1.1	0.2	4.1	0.1	0.1	3.5	0.5	0.2	1.8	0.2	0.2
Ascomycota; Aureobasidium-	0.1	0.1	1	0.1	0.4	0.2	0.1	2	1.1	0	0.3	0	7.1	1.4	1.4
Ascomycota; c__Lecanoromycetes_unclassified-	4.6	8.3	0	0.1	0	0	0.5	0	3.1	0.3	0	0	1.7	0	0
Ascomycota; Clonostachys-	0	0.2	0	0	0	0	0	0.2	0	0	0	0	0.1	10.8	0
Ascomycota; Nigrospora-	0	0	0	0.1	7	9.5	0	0.1	0.6	0.2	3.8	2.2	0.2	0.4	0.2
Ascomycota; Trichoderma-	0	0.1	0	0.1	1.3	6.7	0.2	0.3	0	0.2	3.8	1.7	0	0.6	2.5
Ascomycota; Gibberella-	0.2	0	0.1	0.1	0.6	0	0.2	0.4	6.4	0.2	0.3	1.7	0.2	0.6	2.1
Ascomycota; Cladosporium-	0.2	0	1	1.3	1	1.8	0.1	1.7	0.5	0.3	0.2	0	1.2	1.1	1.7
Ascomycota; Pestalotiopsis-	0	0	0.1	0	1.5	4.3	0.2	0.9	0.1	0.2	1.9	0.2	0.2	0.7	1.5
Basidiomycota; Rhodotorula-	0.1	0.2	1.7	0.2	0.3	0	0.6	2.3	0	0.2	0	0	0.2	0	2.7
Ascomycota; Pseudoestalotiopsis-	0	0	0.3	0	0.6	4.4	0	0	2.2	0.1	2.8	0.8	0	0.1	0
Basidiomycota; Coprinopsis-	0	0	0	0.1	0	0	0	0	0	0	0	0	0	5.3	0
Ascomycota; Fusarium-	0	0	0.9	0.3	0.5	2.1	1.3	0.5	1.1	1.6	0.1	1.1	0.1	0	0
Ascomycota; Pseudofusicoccum-	0	0	0	0	0	0	0.1	0	0	0	0	0	3.8	0	0
Mucoromycota; Mucor-	0	0	0	0.2	0	0	0.1	0	0	0	0	0.1	0	3.5	0
Ascomycota; Endomelanconiopsis-	0	0	0	0	0.7	4.6	0	0	1	0.1	0.4	1.1	0	0	0.4
Ascomycota; Neostrelitziana-	0.4	0	0	4.1	0.4	0	1.1	0	0	0.8	0.1	0	0.1	0	0.2
Mortierellomycota; Mortierella-	0	0	0	0.2	0	0	1.9	0	0	0	0	0	1.8	0	0
Basidiomycota; Peniophora-	4.6	0	0	0	0	0	0	0	0	0	0	0	0	0	0
Basidiomycota; Phlebia-	0	0	2.8	0.3	0.2	0	0.1	0	0	0.2	0.1	0	0.1	0.1	0
Ascomycota; Curvularia-	0	0	0	0.1	0.1	0.7	0.3	0	0.1	1.6	0.3	0.1	0.1	0.1	0.2
Ascomycota; Colletotrichum-	0.2	0	0	0.7	0	0	1.3	0	0	0.8	0	0	0.2	0.4	0
	leaf-	root-	sapwood-	leaf-	root-	sapwood-	leaf-	root-	sapwood-	leaf-	root-	sapwood-	leaf-	root-	sapwood-

Figure 7. Ferreira et al. 2018



**Figure 8. Ferreira et al. 2018.**

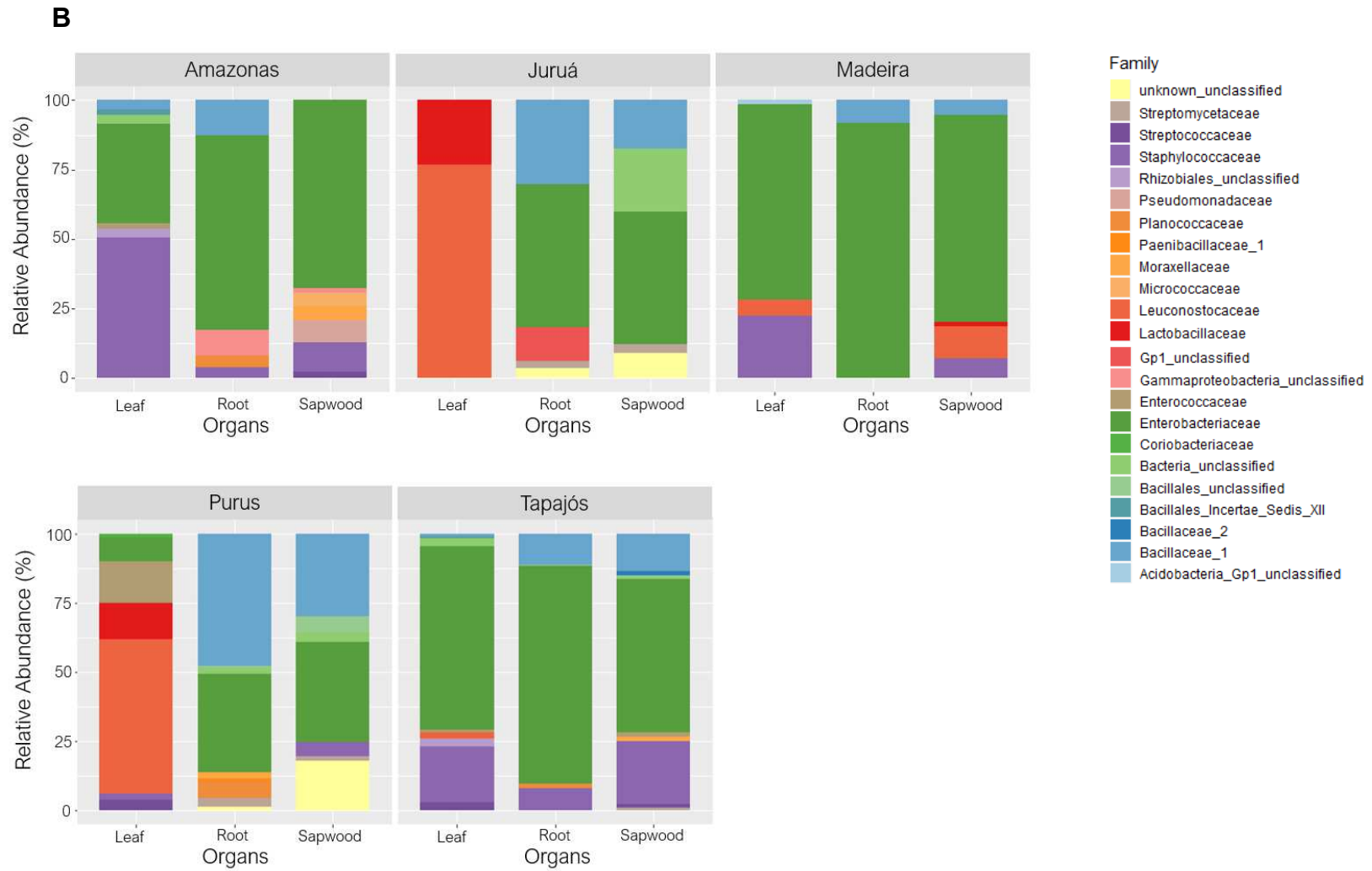


**Figure 8. Ferreira et al. 2018.**

	Amazonas			Juruá			Madeira			Purus			Tapajós		
Proteobacteria; Pantoea-	24.3	39	47.5	0	2.4	1.4	34.7	39.5	65.1	3.3	7.7	5.9	54.1	16.3	30.1
Proteobacteria; Enterobacter-	10.8	28.2	9.7	0.1	45.8	41.6	28.9	45.4	5.3	4.9	24.5	27.8	7.3	58.8	17.9
Firmicutes; Bacillus-	3.3	12.4	1.1	0	29.2	16.9	0.1	11.8	7.2	0	41.9	28.2	1.3	12.6	14.1
Firmicutes; Staphylococcus-	49.7	5.7	9.3	0.2	0.3	2.2	20.1	1	7.6	2.5	1	4.9	20.1	8.3	21.1
Firmicutes; Weissella-	0.3	0	0.1	75.4	1.4	0	5	0.1	11	47.8	0	0	2.2	0	0.1
unknown_unclassified; unknown_unclassified-	0	0	0	0	3.3	8	0	0	0.5	0.2	2.3	16.6	0.1	0	0.6
Bacteria_unclassified; Bacteria_unclassified-	3	0	0.8	0	0.5	21.2	0.6	0	0.2	0.2	2.5	4.2	2.5	0	1
Firmicutes; Enterococcus-	1.9	0.2	0.1	0.7	0.3	0	0.8	0.1	0	15.3	0	0.1	1.1	0	1.6
Firmicutes; Lactococcus-	0.1	0.1	2.1	0.7	0	0	1.5	0.1	0	6.2	0	0	3.2	0	1.7
Firmicutes; Pediococcus-	0	0	0	8.5	0	0	0	0	1.5	10.2	0	0	0	0	0
Firmicutes; Bacillales_unclassified-	0.1	0.1	0.4	0	0.4	2.1	0	1.2	0.1	0	2	5.5	0	0.6	1.2
Firmicutes; Lysinibacillus-	0	4	0.1	0	0	0	0	0.5	0	0	5.1	0.1	0	2.4	0
Proteobacteria; Acinetobacter-	0	0.2	4.6	0	0.2	1.6	0.2	0.1	0.2	0	2.4	0.2	0.1	0.2	2.2
Actinobacteria; Streptomyces-	0	0	0	0	2.7	3.2	0	0	0	0	3.8	2.8	0	0	0.9
Firmicutes; Lactobacillus-	0.2	0	0	14.3	0.2	0	0	0	0	2.9	0	0	0	0	0
Proteobacteria; Pseudomonas-	0	0.1	8.1	0	0.4	0.1	0.2	0	0.4	0	0.2	0.5	0.3	0	0.1
Proteobacteria; Gammaproteobacteria_unclassified-	0	9.1	1.1	0	0	0	0.1	0	0	0	0	0	0.1	0	0
Proteobacteria; Rhizobiales_unclassified-	3	0	0	0	0	0	0.6	0	0	0.2	0.1	0	3	0	0
Actinobacteria; Arthrobacter-	0.1	0	4.8	0	0	0.1	0	0	0	0	0.1	0.1	0	0	0.6
Acidobacteria; Gp1_unclassified-	0	0	0	0	11.1	0	0.4	0	0	0	0.1	0	0	0	0
Firmicutes; Leuconostoc-	0	0	0	0.1	0	0	0.1	0	0	3.7	0	0	0.4	0	0.1
Actinobacteria; Curtobacterium-	0.4	0.1	1.9	0	0	0.3	0	0	0.1	0.1	0.1	0	0.1	0	0.9
Firmicutes; Exiguobacterium-	2	0.3	0	0	0	0	0	0	0	0	0	0	0.6	0	0
Firmicutes; Terribacillus-	0	0	0	0	0	0	0	0	0	0	0	0.4	0	0	1.4
Firmicutes; Paenibacillus-	0	0	0	0	0.1	0.2	0	0	0.1	0	1.2	0.8	0	0.1	0.1
Proteobacteria; Burkholderia-	0	0	0.4	0	0.1	0.2	0.3	0	0.1	0	0.3	0.3	0.1	0	0.3
Acidobacteria; Acidobacteria_Gp1_unclassified-	0	0	0.4	0	0	0	1.3	0	0	0	0.3	0	0.1	0	0.1
Proteobacteria; Serratia-	0	0	0	0	0	0	0	0	0	0	0	0	0	0.2	0.8
Proteobacteria; Escherichia/Shigella-	0	0	0	0	0	0	0	0	0	0	0	0	0	0	0.9
Firmicutes; Kurthia-	0.6	0	0.4	0	0	0	0	0	0	0	0.4	0	0	0	0
Proteobacteria; Enterobacteriaceae_unclassified-	0.2	0.1	0.1	0	0	0	0.2	0.1	0.1	0	0	0.1	0.1	0.1	0.2
Actinobacteria; Coriobacteriaceae_unclassified-	0	0	0	0	0	0	0	0	0	1.2	0	0	0	0	0
Bacteroidetes; Chitinophagaceae_unclassified-	0	0	0.8	0	0	0	0.4	0	0	0	0	0	0	0	0
Acidobacteria; Granulicella_unclassified-	0	0	0.8	0	0	0	0.2	0	0	0	0.1	0	0.1	0	0
Proteobacteria; Stenotrophomonas-	0	0.2	0.4	0	0.1	0	0	0	0	0	0	0	0	0	0.2
	leaf-	root-	sapwood-	leaf-	root-	sapwood-	leaf-	root-	sapwood-	leaf-	root-	sapwood-	leaf-	root-	sapwood-

Figure 9. Ferreira et al. 2018.

**Table 1.** Origin of *Hevea brasiliensis* samples.

Plant	State	Local	Latitude	Longitude	Collector	Year
1	Amazon	Itacoatiara	-3,04378	-58,5033	Ferreira e Villaschi	2014
6	Amazon	Arari	-3,40706	-58,4941	Ferreira e Villaschi	2014
8	Amazon	Itacoatiara	-3,14969	-58,438	Ferreira e Villaschi	2014
14	Amazon	Nova Olinda do Norte	-3,72553	-59,0709	Ferreira e Villaschi	2014
19	Amazon	Coari	-3,84558	-63,3415	Ferreira e Villaschi	2014
22	Amazon	Coari	-3,76464	-63,3978	Ferreira e Villaschi	2014
23	Amazon	Coari	-3,76464	-63,3978	Ferreira e Villaschi	2014
24	Amazon	Coari	-3,75775	-63,4096	Ferreira e Villaschi	2014
25	Amazon	Coari	-3,75761	-63,4096	Ferreira e Villaschi	2014
29	Amazon	Coari	-3,71944	-63,4656	Ferreira e Villaschi	2014
1	Acre	Xapuri	-9,95097	-67,2226	Hora Junior	2014
5	Acre	Xapuri	-10,8344	-68,3869	Hora Junior	2014
6	Acre	Boca do Acre*	-10,038	-67,6793	Hora Junior	2014
10	Acre	Boca do Acre*	-9,12672	-67,2494	Hora Junior	2014
11	Acre	Cruzeiro do Sul	-7,76414	-72,2521	Hora Junior	2014
13	Acre	Cruzeiro do Sul	-7,76414	-72,2509	Hora Junior	2014
15	Acre	Cruzeiro do Sul	-7,73481	-72,2509	Hora Junior	2014
18	Acre	Sena Madureira	-9,13381	-68,9513	Hora Junior	2014
20	Acre	Sena Madureira	-9,13525	-68,952	Hora Junior	2014
22	Acre	Sena Madureira	-9,13694	-68,9516	Hora Junior	2014
6	Pará	Itaituba	-4,3175	-56,0087	Ferreira e Villaschi	2015
7	Pará	Itaituba	-4,31778	-56,0086	Ferreira e Villaschi	2015
9	Pará	Fordlândia	-3,82942	-55,4989	Ferreira e Villaschi	2015
18	Pará	Belterra	-2,59869	-54,9741	Ferreira e Villaschi	2015
19	Pará	Belterra	-2,60681	-54,9773	Ferreira e Villaschi	2015
22	Pará	Santarém	-2,50478	-54,943	Ferreira e Villaschi	2015
24	Pará	Santarém	-2,41925	-54,7386	Ferreira e Villaschi	2015
32	Pará	Belterra	-2,80619	-55,0359	Ferreira e Villaschi	2015
33	Pará	Belterra	-2,79717	-55,0306	Ferreira e Villaschi	2015
38	Pará	Santarém	-2,49983	-54,7347	Ferreira e Villaschi	2015

\* The samples belong to Amazonas state but were included in the Acre dataset due to proximity to this state.

**Table 2.** Primer sequence used in the gene amplification for accessing bacteria, archaea and fungi community of *Hevea brasiliensis*.

Primer	Orientation	Sequence (5' – 3')	Gene Target	Longitude	Reference
515	Forward	GTGCCAGCMGCCGCGGTAA	V4 region of 16S SSU rRNA	Bacteria and Archaea	(Caporaso et al. 2011, 2012; Parada, Needham, and Fuhrman 2016)
806	Reverse	GGACTACHVGGGTWTCTAAT	V4 region of 16S SSU rRNA	Bacteria and Archaea	(Caporaso et al. 2011, 2012; Apprill et al. 2015)
ITS1f	Forward	CTTGGTCATTTAGAGGAAGTAA	ITS region of the rRNA	Fungi	(Smith and Peay 2014; Caporaso et al. 2012)
ITS2	Reverse	GCTGCGTTCTTCATCGATGC	ITS region of the rRNA	Fungi	(Smith and Peay 2014; Caporaso et al. 2012; White, T. J., T. D. Bruns, S. B. Lee 1990)

**Table 3.** Core microbiome of fungal endophyte in *Hevea brasiliensis*.

Taxonomy	Basins					Organs		
	AM	JU	MA	PU	TA	L	S	R
<i>Cyberlindnera fabianii</i>							x	x
<i>Lasiodiplodia theobromae</i>		x	x	x				
<i>Meyerozyma athensensis</i>						X	x	x
<i>Lasiodiplodia iranensis</i>			x		x	X		
<i>Lasiodiplodia parva</i>		x			x			
<i>Wickerhamomyces anomalus</i>					x	X		x
<i>Pestalotiopsis sp.</i>		x				X		x
<i>Phyllosticta capitalensis</i>	x		x		x	X		
<i>Candida naeodendra</i>					x		x	x
<i>Diaporthe miriciae</i>	x	x		x		X		
<i>Debaryomyces hansenii</i>						X		
<i>Hanseniaspora opuntiae</i>					x		x	
<i>Clonostachys rosea</i>					x			
<i>Aureobasidium pullulans</i>						X		x
<i>Wickerhamomyces anomalus</i>					x	X		x
<i>Pestalotiopsis disseminata</i>		x			x			
<i>Pseudopestalotiopsis cocos</i>		x		x				x
<i>Trichoderma spirale</i>		x		x			x	x
<i>Fusarium sp.</i>							x	
<i>Trichoderma koningiopsis</i>		x						
<i>Candida metapsilosis</i>						X		
<i>Nigrospora oryzae</i>		x						
<i>Pseudofusicoccum stromaticum</i>					x	X		
<i>Nectria pseudotrichia</i>		x					x	
<i>Gibberella intricans</i>					x			
<i>Diaporthe eucalyptorum</i>					x	X		
<i>Endomelanconiopsis endophytica</i>		x						
<i>Phyllosticta sp.</i>	x				x			
<i>Candida unclassified</i>				x				
<i>Diaporthe unclassified</i>		x						
<i>Ascomycota unclassified</i>			x					
<i>Diaporthe cf. heveae</i>					x			
<i>Ascomycota unclassified</i>			x					
<i>Pestalotiopsis unclassified</i>								x
<i>Neostrelitziana acaciigena</i>		x						
<i>Curvularia unclassified</i>		x						
<i>Ascomycota unclassified</i>					x			
<i>Cladosporium unclassified</i>		x						
<i>Mycosphaerellaceae unclassified</i>			x					
<i>Fusarium nelsonii</i>		x						
<i>Candida boidinii</i>		x						
<i>Ochroconis cordanae</i>		x						
<i>Ascomycota unclassified</i>			x					
<i>Fusarium unclassified</i>		x						
<i>Penicillium sclerotiorum</i>		x						
<i>Fusarium pseudensiforme</i>		x						

Basins: **AM:** Amazonas; **JU:** Juruá; **MA:** Madeira; **PU:** Purus; **TA:** TapajósOrgans: **L:** leaf; **S:** sapwood; **R:** root.**X** represent the occurrence of taxa in the samples.

**Table 4.** Core microbiome of bacteria endophyte in *Hevea brasiliensis*.

Taxonomy	Basins					Organs		
	AM	JU	MA	PU	TA	L	S	R
<i>Pantoea</i>				X		X		
<i>Enterobacter</i>		X		X		X		
<i>Staphylococcus</i>								X
<i>Bacillus</i>		X		X	X			
<i>Weissella</i>		X		X		X		
<i>Bacillus</i>	X		X	X	X			
<i>Weissella</i>		X		X		X		
<i>Enterococcus</i>				X				
<i>Pediococcus</i>	X	X		X		X		
<i>Lysinibacillus</i>			X					X
<i>Bacillales unclassified</i>		X		X	X			
<i>Lactococcus</i>			X	X			X	
<i>Acinetobacter</i>	X				X			
<i>Pseudomonas</i>		X		X				
<i>Lactococcus</i>				X				
<i>Lactobacillus</i>		X		X		X		
<i>Leuconostoc</i>				X		X		
<i>Arthrobacter</i>		X						
<i>Curtobacterium</i>	X				X			
<i>Streptomyces</i>		X		X				X
<i>Streptomyces</i>				X				
<i>Streptomyces</i>		X		X				
<i>unknown unclassified</i>				X				
<i>Streptomyces</i>		X		X				
<i>Staphylococcus</i>						X		
<i>Paenibacillus</i>				X				
<i>Burkholderia</i>		X		X				
<i>Pediococcus</i>		X		X				
<i>Bacteria unclassified</i>				X				
<i>Acinetobacter</i>		X		X				

Basins: **AM**: Amazonas; **JU**: Juruá; **MA**: Madeira; **PU**: Purus; **TA**: Tapajós

Organs: **L**: leaf; **S**: sapwood; **R**: root.

**X** represent the occurrence of taxa in the samples.



## SUPPORTING INFORMATION

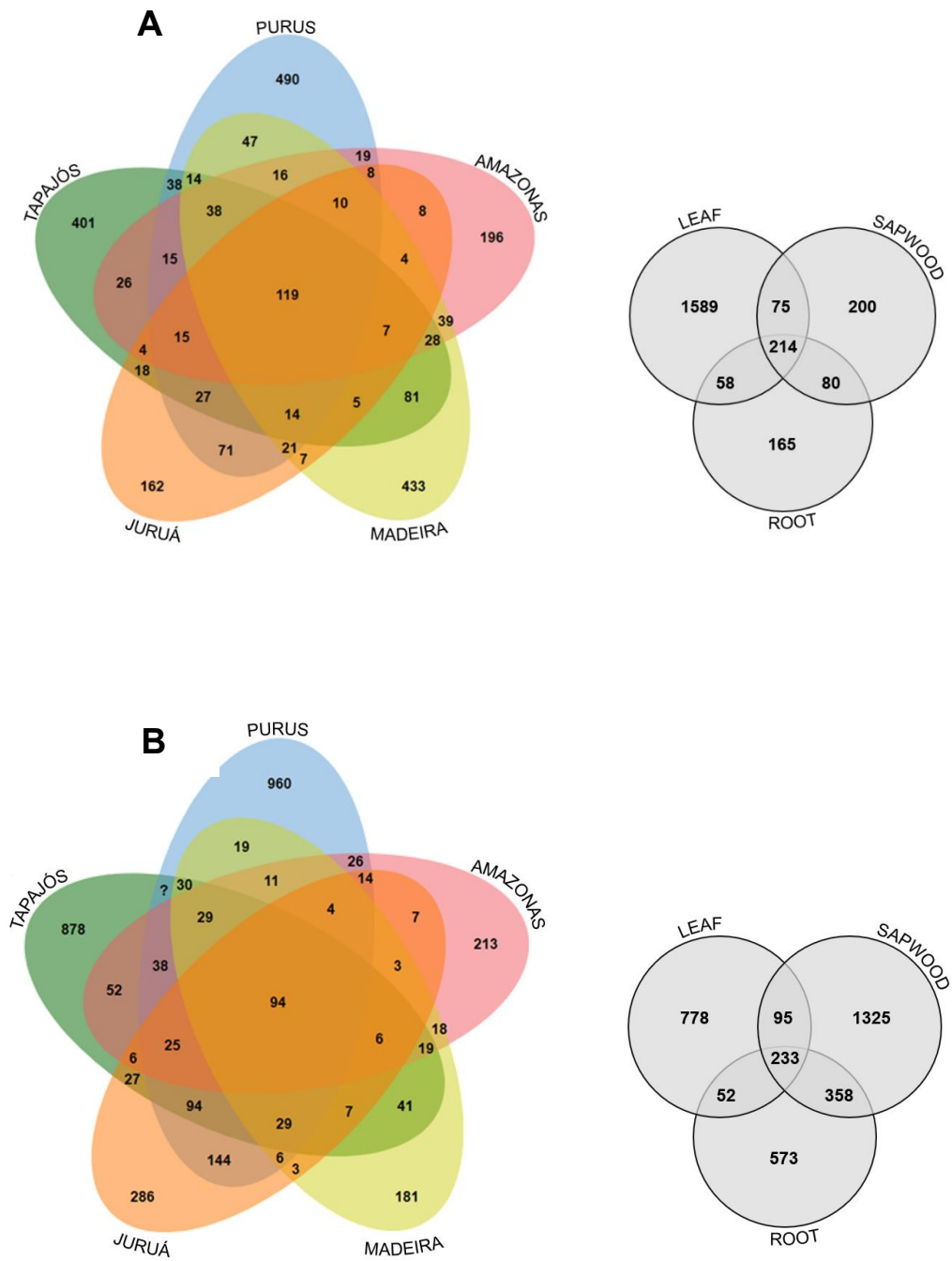


**Figure S1. Ferreira et al. 2018.**

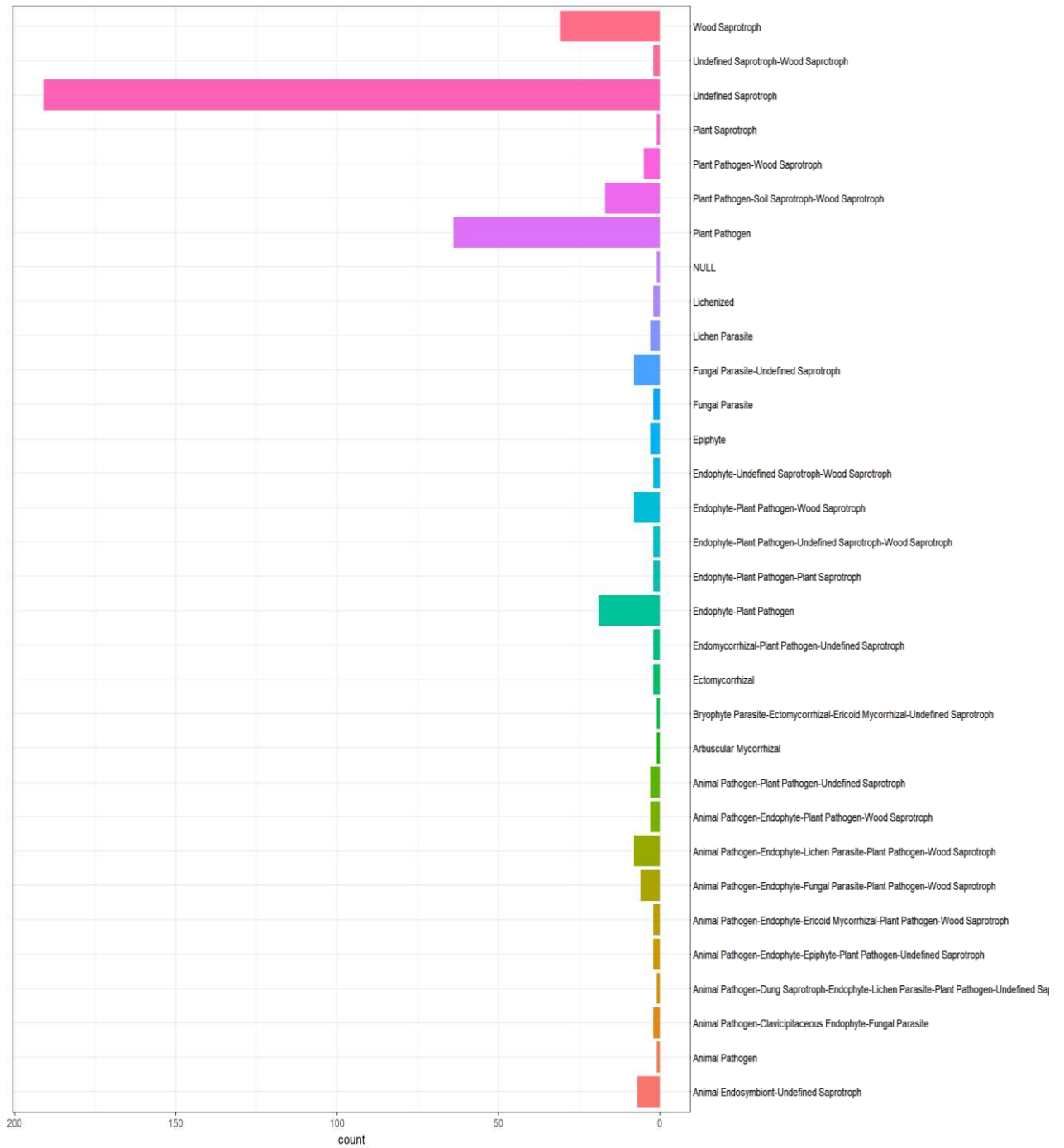


Figure S2. Ferreira et al. 2018.

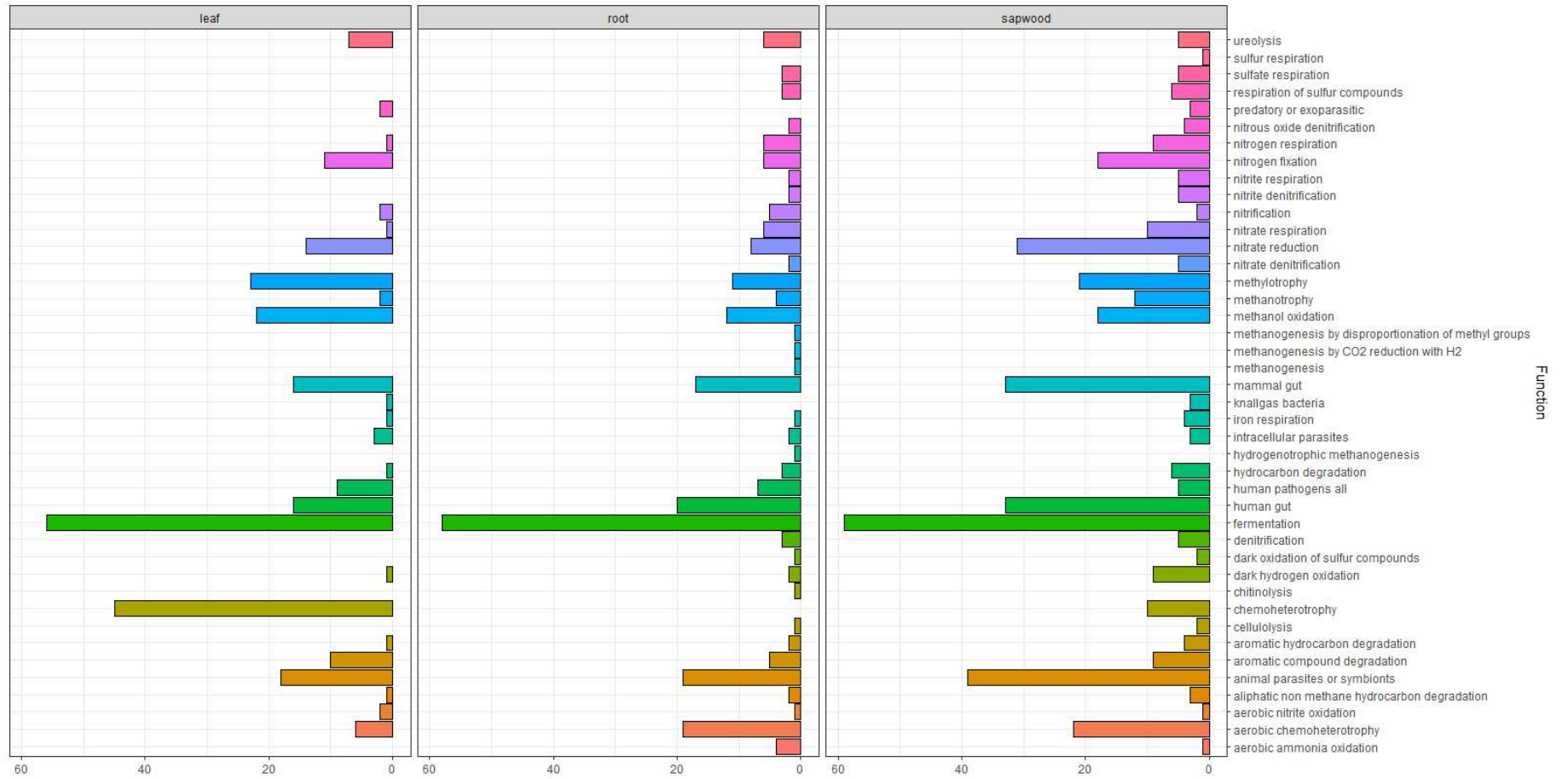


Figure S3. Ferreira et al. 2018.

**Table S1.** Ecological guild of fungal endophyte in *Hevea brasiliensis*.

<b>Taxonomy</b>	<b>Guild</b>	<b>Mode</b>
<b>Saprotroph</b>	Wood Saprotroph	<i>Corioloopsis</i> sp., <i>Phlebia subochracea</i> , <i>Rigidoporus</i> sp., <i>Schizophyllum unclassified</i> , <i>Phlebia acanthocystis</i> , <i>Favolus grammacephalus</i> , <i>Phlebia unclassified</i> , <i>Bjerkandera atroalba</i> , <i>Phlebia floridensis</i> , <i>Trametes elegans</i> , <i>Phlebia brevispora</i> , <i>Phlebia</i> sp., <i>Nigroporus vinosus</i> , <i>Fomes fasciatus</i> , <i>Gloeoporus</i> sp., <i>Ceriporia camaresiana</i> , <i>Psathyrella candolleana</i> , <i>Junghuhnia</i> sp, <i>Trametes cubensis</i> , <i>Polyporus tricholoma</i> , <i>Irpex lacteus</i> , <i>Trichaptum</i> sp., <i>Ceriporia alachuana</i> , <i>Phanerochaete unclassified</i> , <i>Pycnoporus cinnabarinus</i> , <i>Phlebia chrysocreas</i> , <i>Phylloporia ribis</i> , <i>Pyrenochaeta</i> sp., <i>Humicola unclassified</i>
<b>Pathotroph-Saprotroph</b>	Plant Pathogen-Soil Saprotroph-Wood Saprotroph	<i>Fusarium unclassified</i> , <i>Fusarium domesticum</i> , <i>Fusarium nelsonii</i> , <i>Fusarium pseudensiforme</i> , <i>Fusarium keratoplasticum</i> , <i>Fusarium albosuccineum</i> ,
<b>Symbiotroph</b>	Lichenized	<i>Bacidia unclassified</i> , <i>Myriotrema urceolare</i> , <i>Trimmatostroma cordae</i> ,
<b>Pathotroph</b>	Fungal Parasite	<i>Cosmospora unclassified</i> , <i>Kwoniella unclassified</i> , <i>Naganishia diffluens</i> , <i>Bionectria wenpingii</i> , <i>Naganishia adeliensis</i> , <i>Kwoniella heveanensis</i>
<b>Pathotroph-Symbiotroph</b>	Epiphyte	<i>Cyphellophora eucalypti</i> , <i>Chaetothyriaceae unclassified</i>
<b>Pathotroph-Symbiotroph</b>	Endophyte-Plant Pathogen	<i>Diaporthe</i> sp, <i>Diaporthe unclassified</i> , <i>Diaporthe foeniculina</i> , <i>Microdochium unclassified</i> , <i>Diaporthaceae unclassified</i> , <i>Xylariaceae unclassified</i> , <i>Phyllosticta capitalensis</i> , <i>Microdochium</i> sp., <i>Phyllosticta</i> sp., <i>Botryosphaeriaceae unclassified</i> , <i>Phomopsis unclassified</i> , <i>Cytospora eucalyptina</i> , <i>Xylaria hypoxylon</i> , <i>Xylaria grammica</i> , <i>Colletotrichum unclassified</i> , <i>Colletotrichum annellatum</i> , <i>Diaporthe pseudomangiferae</i> , <i>Colletotrichum gigasporum</i> , <i>Periconia</i> sp.,
<b>Symbiotroph</b>	Endomycorrhizal- Plant Pathogen- Undefined Saprotroph	<i>Ceratobasidiaceae unclassified</i> , <i>Russulaceae unclassified</i> , <i>Ceratobasidium unclassified</i>
<b>Symbiotroph</b>	Arbuscular Mycorrhizal	<i>Entrophospora</i> sp.

Table S1. Continued

<b>Taxonomy</b>	<b>Guild</b>	<b>Mode</b>
<b>Pathotroph-Saprotroph-Symbiotroph</b>	Animal Pathogen- Endophyte-Plant Pathogen-Wood Saprotroph	<i>Coniosporium sp.</i> , <i>Coniosporium apollinis</i> , <i>Alternaria unclassified</i> , <i>Alternaria longissimi</i> , <i>Cladosporium delicatulum</i> , <i>Cladosporium unclassified</i> , <i>Cladosporium dominicanum</i> , <i>Cladosporium flabelliforme</i> , <i>Cladosporium sphaerospermum</i>
<b>Pathogen-Saprotroph-Symbiotroph</b>	Animal Pathogen- Endophyte-Fungal Parasite-Plant Pathogen-Wood Saprotroph	<i>Acremonium hennebertii</i> , <i>Acremonium persicinum</i> , <i>Acremonium unclassified</i> , <i>Acremonium breve</i> ,
<b>Pathotroph-Saprotroph-Symbiotroph</b>	Animal Pathogen- Endophyte-Ericoid Mycorrhizal-Plant Pathogen-Wood Saprotroph	<i>Phialophora livistonae</i> , <i>Phialophora sp.</i> ,
<b>Pathotroph-Saprotroph-Symbiotroph</b>	Animal Pathogen- Endophyte-Epiphyte- Plant Pathogen- Undefined Saprotroph	<i>Aureobasidium pullulans</i> , <i>Aureobasidium thailandense</i>
<b>Pathotroph-Saprotroph-Symbiotroph</b>	Animal Pathogen- Dung Saprotroph- Endophyte-Lichen Parasite-Plant Pathogen-Undefined Saprotroph	<i>Coniochaetaceae sp.</i>
<b>Pathotroph-Symbiotroph</b>	Animal Pathogen- Clavicipitaceous Endophyte-Fungal Parasite	<i>Tolypocladium album</i>

Table S1. Continued

Taxonomy	Guild	Mode
Pathotroph	Animal Pathogen	<i>Medicopsis romeroi</i>
Pathotroph-Saprotroph	Animal Endosymbiont- Undefined Saprotroph	<i>Rhodotorula unclassified</i> , <i>Pichia myanmarensis</i> , <i>Rhodotorula paludigena</i> , <i>Rhodotorula taiwanensis</i> , <i>Rhodotorula toruloides</i> , <i>Rhodotorula</i> sp.,
Saprotroph	Undefined Saprotroph	<p><i>Saccharomycetales</i> fam <i>Incertae sedis</i> unclassified, <i>Meyerozyma unclassified</i>, <i>Wickerhamomyces anomalus</i>, <i>Amphisphaeriaceae unclassified</i>, <i>Candida unclassified</i>, <i>Debaryomyces unclassified</i>, <i>Hanseniaspora unclassified</i>, <i>Pseudopestalotiopsis cocos</i>, <i>Trichoderma unclassified</i>, <i>Nectriaceae unclassified</i>, <i>Candida metapsilosis</i>, <i>Nigrospora oryzae</i>, <i>Lodderomyces elongisporus</i>, <i>Mucor circinelloides</i>, <i>Nakazawaea ernobii</i>, <i>Phylacia</i> sp., <i>Aspergillus unclassified</i>, <i>Candida palmioleophila</i>, <i>Aspergillus sydowii</i>, <i>Candida boidinii</i>, <i>Umbelopsis isabellina</i>, <i>Pyrenochaetopsis leptospora</i>, <i>Ochroconis cordanae</i>, <i>Biscogniauxia capnodes</i>, <i>Penicillium unclassified</i>, <i>Blakeslea trispora</i>, <i>Mortierella macrocystopsis</i>, <i>Candida michaelii</i>, <i>Candida orthopsilosis</i>, <i>Mucor nederlandicus</i>, <i>Sarocladium bactrocephalum</i>, <i>Albonectria rigidiuscula</i>, <i>Candida insectorum</i>, <i>Clitopilus</i> sp., <i>Ascocoryne</i> sp., <i>Erythromyces crocicreas</i>, <i>Hypochnicium punctulatum</i>, <i>Chaetothyrium agathis</i>, <i>Gilbertella persicaria</i>, <i>Preussia persica</i>, <i>Resinicium saccharicola</i>, <i>Coprinellus disseminates</i>, <i>Penicillium hetheringtonii</i>, <i>Yamadazyma Mexicana</i>, <i>Hypocreales unclassified</i>, <i>Mortierella unclassified</i>, <i>Pleurostoma ootheca</i>, <i>Corticium</i> sp., <i>Eichleriella alliciens</i>, <i>Peniophorella odontiformis</i>, <i>Scopuloides hydnoides</i>, <i>Sugiyamaella paludigena</i>, <i>Fuscoporia senex</i>, <i>Paraphaeosphaeria areacearum</i>, <i>Lipomyces</i> sp., <i>Uwebraunia unclassified</i>, <i>Mortierella clonocystis</i>, <i>Coprinellus brevisetulosus</i>, <i>Capnodium coffeae</i>, <i>Meyerozyma caribbica</i>, <i>Peniophora laxitexta</i>, <i>Campylocarpon</i> sp., <i>Resinicium confertum</i>, <i>Hymenochaete luteobadia</i>, <i>Ogataea unclassified</i>, <i>Wickerhamomyces unclassified</i>, <i>Exidia unclassified</i>, <i>Schwanniomyces yamadae</i>, <i>Penicillium adametzii</i>, <i>Coprinopsis candidolanata</i>, <i>Zasmidium dalbergiae</i>, <i>Wickerhamomyces sydowiorum</i>, <i>Candida theae</i>, <i>Cyberlindnera subsufficiens</i>, <i>Beltraniella unclassified</i>, <i>Peniophora</i> sp., <i>Choanephora cucurbitarum</i>, <i>Stachybotrys parvispora</i>, <i>Pseudeurotium hygrophilum</i>, <i>Myxospora crassiseta</i>, <i>Bionectriaceae unclassified</i>, <i>Saccharomycopsis fibuligera</i>, <i>Hypoxylon</i> sp., <i>Umbelopsis unclassified</i>, <i>Preussia pilosella</i>, <i>Mortierella exigua</i>, <i>Candida glabrosa</i>, <i>Peniophora albobadia</i>, <i>Marasmius unclassified</i>, <i>Tetracladium</i> sp., <i>Articulospora proliferata</i>, <i>Phaeosphaeria podocarpis</i>, <i>Coprinellus radians</i>, <i>Fibrodontia alba</i>, <i>Ceramothyrium unclassified</i>, <i>Sistotremastrum guttuliferum</i>, <i>Penicillium paxillin</i>, <i>Scolecobasidium</i> sp., <i>Sidera lowei</i>, <i>Psilocybe</i> sp., <i>Brycekendrickomyces acaciae</i>, <i>Resinicium mutabile</i>, <i>Mucor ardhlaengiktus</i>, <i>Mortierella ambigua</i>, <i>Yamadazyma</i> sp., <i>Fusicolla violacea</i>, <i>Meruliopsis</i> sp., <i>Penicillium rolfsii</i>, <i>Deconica phyllogena</i>, <i>Pterula</i></p>

		<p><i>echo</i>, <i>Phaeococcomyces rothmanniae</i>, <i>Biscogniauxia</i> sp., <i>Paraconiothyrium unclassified</i>, <i>Hyphodontia</i> sp., <i>Agaricus unclassified</i>, <i>Aspergillus caesiellus</i>, <i>Marasmius</i> sp., <i>Scopuloides</i> sp., <i>Candelabrochaete</i> sp., <i>Wickerhamomyces ciferrii</i>, <i>Fusicolla aquaeductuum</i>, <i>Henningsomyces puber</i>, <i>Candida sanyaensis</i>, <i>Cystiodontia laminifera</i>, <i>Saccharomycetaceae unclassified</i>, <i>Myxocephala albida</i>, <i>Clitopilus unclassified</i>, <i>Geosmithia unclassified</i>, <i>Mucor irregularis</i>, <i>Exophiala xenobiotica</i>, <i>Blastobotrys malaysiensis</i>, <i>Ceramothyrium thailandicum</i>, <i>Gymnopus unclassified</i>, <i>Peniophora pithya</i>, <i>Arthrimum marii</i></p>
--	--	--

**Table S2.** Fungal disease of *Hevea brasiliensis*.

Plant pathogen	Disease	N° of OTUs
<b>Leaf</b>		
<i>Bipolaris heveae</i>	Bird's Eye Spot	6
<i>Alternaria</i>	Alternaria leaf blight	97
<i>Cephaleuros</i>	Algal leaf spot disease	-
<i>Colletotrichum acutatum</i>	Colletotrichum leaf disease	3
<i>Colletotrichum gloeosporioides</i>	Colletotrichum secondary leaf fall	54
<i>Corticium salmonicolor</i>	Pink disease	20
<i>Corynespora cassiicola</i>	Corynespora leaf fall	13
<i>Oidium heveae</i>	Oidium secondary leaf fall	-
<i>Periconia manihoticola</i>	Periconia blight	21
<i>Phyllachora huberi</i>	Black scab	-
<i>Phytophthora botryose</i>	Abnormal leaf fall	-
<i>Phytophthora cactorum</i>	Abnormal leaf fall	-
<i>Phytophthora capsici</i>	Abnormal leaf fall	-
<i>Phytophthora citricola</i>	Abnormal leaf fall	-
<i>Phytophthora citrophthora</i>	Leaf fall disease	-
<i>Phytophthora meadii</i>	Abnormal leaf fall	-
<i>Phytophthora nicotianae</i>	Abnormal leaf fall	-
<i>Phytophthora palmivora</i>	Leaf fall and black stripe diseases	-
<i>Phytophthora parasitica</i>	Abnormal leaf fall	-
<i>Pseudocercospora ulei</i>	South American Leaf Blight	31
<i>Pseudoidium</i>	Powdery mildew of rubber tree	321
<i>Rosenscheldiella</i>	False black scab	-
<i>Thanatephorus cucumeris</i>	Target leaf spot	10
<b>Stem</b>		
<i>Ceratocystis fimbriata</i>	Mouldy rot of rubber	-
<i>Corticium salmonicolor</i>	Pink disease	20
<i>Lasiodiplodia theobromae</i>	Stem cankers	12
<i>Phytophthora</i>	Black stripe disease	-
<i>Ustilina deusta</i>	Dry rot	-
<b>Root</b>		
<i>Ganoderma philippii</i>	Red root disease	6
<i>Helicobasidium compactum</i>	Purple root disease	-
<i>Phellinus noxius</i>	Brown root disease	49
<i>Rigidoporus lignosus</i>	White Root Rot Disease	224



**Table S3.** List of possible plant pathogens found in *Hevea brasiliensis*.

Class	Order	Family	Species	N° of OTUs	
<b>Agaricomycetes</b>	Polyporales	Ganodermataceae	<i>Ganoderma australe</i>	121	
		Meripilaceae	<i>Meripilus giganteus</i>	87	
	Hymenochaetales	Hymenochaetaceae	<i>Phellinus gilvus</i>	49	
			<i>Phellinus noxius</i>	22	
			<i>Fomitiporia unclassified</i>	23	
<b>Dothideomycetes</b>	Botryosphaeriales	Aplosporellaceae	<i>Aplosporella javeedii</i>	95	
		Botryosphaeriaceae	<i>Endomelanconiopsis endophytica</i>	6180	
			<i>Endomelanconiopsis microspora</i>	93	
			<i>Endomelanconiopsis unclassified</i>	748	
			<i>Lasiodiplodia unclassified</i>	103368	
			<i>Lasiodiplodia venezuelensis</i>	364	
			<i>Macrophomina phaseolina</i>	29	
			<i>Neofusicoccum unclassified</i>	30	
			<i>Pseudofusicoccum stromaticum</i>	8721	
	Capnodiales	Mycosphaerellaceae	<i>Mycosphaerella pseudomarksii</i>	19	
			<i>Mycosphaerella tassiana</i>	24	
			<i>Mycosphaerella unclassified</i>	972	
			<i>Phaeophleospora hymenocallidicola</i>	1266	
			<i>Phaeophleospora parsoniae</i>	100	
			<i>Pseudocercospora lonicericola</i>	65	
			<i>Pseudocercospora luzardii</i>	389	
			<i>Pseudocercospora norchiensis</i>	98	
			<i>Pseudocercospora unclassified</i>	882	
			<i>Passalora haldinae</i>	115	
Pleosporales	Pleosporaceae	<i>Curvularia lunata</i>	33		
		<i>Curvularia oryzae</i>	47		
		<i>Curvularia pseudorobusta</i>	128		
		<i>Curvularia sorghina</i>	433		
		<i>Curvularia unclassified</i>	329		
		<i>Curvularia verruculosa</i>	1294		
			Teratosphaeriaceae	<i>Devriesia strelitziicola</i>	40
				<i>Penidiella aggregata</i>	21
				<i>Penidiella sp</i>	20
		<b>Eurotiomycetes</b>	Chaetothyriales	Chaetothyriales	<i>Strelitziana syzygii</i>
	<i>Strelitziana unclassified</i>			2	
<b>Leotiomycetes</b>	Erysiphales	Erysiphaceae	<i>Pseudoidium neolycopersici</i>	321	
<b>Sordariomycetes</b>	Diaporthales	Togniniaceae	<i>Phaeoacremonium hungaricum</i>	22	
		Schizoparmaceae	<i>Coniella eucalyptigena</i>	41	
			<i>Coniella wangiensis</i>	21	
	Hypocreales	Nectriaceae	<i>Fusarium albosuccineum</i>	65	
			<i>Calonectria unclassified</i>	29	
			<i>Fusarium domesticum</i>	1217	
			<i>Fusarium keratoplasticum</i>	585	
			<i>Fusarium nelsonii</i>	944	
			<i>Fusarium pseudensiforme</i>	590	
		<i>Fusarium unclassified</i>	707		

		<i>Gibberella intricans</i>	2557
		<i>Volutella consors</i>	32
	Plectosphaerellaceae	<i>Verticillium leptobactrum</i>	53
Meliolales	Meliolaceae	<i>Irenopsis vincensii</i>	40
Xylariales	Amphisphaeriaceae	<i>Pestalotiopsis anacardiacearum</i>	459
		<i>Pestalotiopsis unclassified</i>	1650

## CHAPTER 2

**Genetic variability and evolution of putative effector genes of  
*Pseudocercospora ulei* in Amazonian and Non-Amazonian  
populations of the pathogen**

## ABSTRACT

Allelic variation in five effector proteins (PuAve1, PuAvr4, PuEcp2, PuEcp5, and PuECP6), known as core effector genes in Dothideomycetes, was investigated in two populations of the causal agent of South American Leaf Blight of rubber tree, *Pseudocercospora ulei*, one derived from native plants in the Amazon region (AM population) and the other from commercial plantations in the Northeast and Southeast regions in Brazil (N-AM). The highest levels of polymorphisms for three effector genes (PuAve1, PuEcp2 and PuEcp6) were recorded for AM populations. There was genetic division between groups of haplotypes of the AM and N-AM populations when PEcp6 and PuAve1 genes were assessed. Two evolutionary forces influencing the diversification of the five *P. ulei* effector genes were recombination and selection. Evidences of deviations from the neutrality model suggest the existence of selective pressures acting on these genes in the N-AM population, probably in response to the deployment of resistant clones in some commercial rubber tree plantations. Isolates of the oriental Amazon (Manaus region) showed low levels of genetic diversity in all genes and formed distinct clusters in the haplotype networks, pointing to a natural subdivision of the AM population between oriental and occidental regions. Two mechanisms could be associated with recognition avoidance by rubber tree: an indel in PuAve1 gene (pseudogenization event), and a complete deletion of the effector protein in PuEcp5. The pseudogenization event in PuAve1 clearly separates the AM of the N-AM populations of *P. ulei*. Thus, distinct evolutionary processes seems to be acting on these populations. These findings highlight the importance of the ongoing efforts towards the selection of new plant genotypes with resistance to SALB and point to strategies that involve the combination of

qualitative and quantitative resistance in the development of rubber tree clones for durable resistance.

**Key words:** SALB, effector genes, intragenic recombination, positive selection and indel

## INTRODUCTION

*Hevea brasiliensis* (Willd. Ex A. Juss.) Müll. Arg., the rubber tree, is an endemic species of the Amazon region and the only one among 200 other species within the genus *Hevea* that is commercially exploited for the production of latex (van Beilen and Poirier 2007). Other plants can provide latex, such as guayule (*Parthenium argentatum*) and the Russian dandelion (*Taraxacum koksaghyz*), but they are not able to supply the market demands. In addition, the physicochemical characteristics of these alternatives sources of latex are inferior to those found in the latex of *H. brasiliensis* (Lieberei 2007).

The market appreciation for the natural rubber eventually led to the exploitation of rubber trees in Pará state, in the Amazon region, pioneered in the 1930s by Henry Ford, with large-scale rubber plantations in monoculture. However, the outbreaks of South American Leaf Blight (SALB), caused by the fungus *Pseudocercospora ulei*, led to the complete failure of the plantations (Guyot and Le Guen 2018; Grandin 2009). The lack of knowledge on the epidemiological aspects of the disease and the genetic resistance of the host were the main factors responsible for the discontinuity of the rubber tree exploitation in wetlands in the Amazon (Le Guen et al. 2011).

The endemic occurrence of SALB in the Northern region redirected the rubber tree plantations to other regions in Brazil: Central (Mato Grosso state), Southeast (Espírito Santo, São Paulo and Minas Gerais states) and Northeast (Bahia state). In these areas, clones with partial resistance to SALB, are planted and epidemics are of lower intensity (Lespinasse et al. 2000; Garcia et al. 2004; Le Guen et al. 2007). SALB resistance is associated with quantitative trait loci (QTL) and general resistance phenotypes are commonly observed. There are

few commercial clones available that combine high levels of stable resistance and good latex yields (Garcia et al. 2002, 2011; Lieberei 2007).

The knowledge about the evolutionary and ecological processes that shape the populations of plant pathogens is essential to understand their life history and the potential to overcome the disease-resistant phenotypes deployed in agro-ecosystems (Stukenbrock and McDonald 2008; McDonald and Linde 2002). The variability of *P. ulei* populations in commercial plantation areas in Brazil, assessed by single sequence repeats (SSR), revealed a high level of genetic variability between spatially structured populations and accelerated rates of genetic differentiation in the populations of the pathogen, mainly due to selection (host-resistance effect) (Hora Júnior 2012). In this context, it is of great importance to elucidate the genes encoding proteins putatively involved in the biochemical interactions between *P. ulei* and the rubber tree, and that can lead to selection events.

Effector proteins are molecules secreted by pathogens that modify the structure and functions of the affected host cells, suppressing the signaling of defense responses and promoting parasitism by the pathogen (Hogenhout et al. 2009). To recognize these genes and avoid infection, plants use immune receptors called NB-LRR domains (*Nucleotide binding- Leucin rich repeat*), that encoded dominant resistance (R) genes, which recognize effector proteins (Avr) and activate defense (Dangl and Jones 2001). On the other hand, plant pathogens evade recognition imposed by R genes with evolutionary adaptations, like deletions and insertions (Stukenbrock and McDonald 2009).

Genomic studies revealed that some genes encoding effector proteins are homologous in species of the Dothideomycetes class, including *P. ulei*

(Stergiopoulos et al. 2009, 2010; Ohm et al. 2012). These include homologs for the avirulence protein 4 (Avr4) and the extracellular proteins Ecp2, Ecp5 and Ecp6 firstly described in *Cladosporium fulvum* (de Wit 2016).

Previous screenings in a draft genome of *P. ulei* conducted in our laboratory revealed the existence of putative homologs of the genes encoding for the effector proteins Avr4, Ecp2, Ecp5 and Ecp6. Additionally, a homolog of the avirulence Ve1 protein (Ave1) gene, from *Verticillium dahliae* (Castroverde, Nazar, and Robb 2016), was also found in the genome of *P. ulei* (Hora-Júnior, 2012, unpublished). A comparative analysis between the populations in the center of origin of the pathogen (Amazon region) and those found in commercial plantations of rubber trees in southern states of Brazil can provide a more complete landscape of pathogen dispersal and short-term evolution. These comparisons also allow for inferences on the potential risks of a major overcome of disease resistance in the field (McDonald and Linde 2002). Thus, we investigated allelic polymorphism in the five putative effector genes of *P. ulei* isolates collected in different locations in Brazil and in native populations of *P. ulei* from the Amazon. The nucleotide and haplotype diversities were compared between the populations of *P. ulei* found in the Amazon region, and those found in association with rubber tree plantations in other Brazilian states. Evidences of gene recombination, selection and mutation within and between populations were also investigated.



## MATERIAL AND METHODS

### Sampling and isolation of *P. ulei*

In the Amazon, sampling was carried out in endemic areas of South American Leaf Blight located in the states of Acre and Amazonas. Infected plants were also collected in plantation areas located in the Brazilian states of Bahia, Mato Grosso, Minas Gerais, Rio de Janeiro, Rondônia, and São Paulo (Figure 1). Young leaves in the B1/B2 and C stages showing asexual and sexual reproduction structures of *P. ulei* were collected and stored in dry paper bags. The material was washed with sterilized water and dried in a laminar flow hood to reduce the number of contaminants. Under a stereoscopic microscope, conidia were individually picked and transferred to plates containing a modified version of the M3 medium (sucrose - 10 g, neopeptone - 6 g, smashed potatoes - 250 g,  $\text{KH}_2\text{PO}_4$  - 2 g,  $\text{MgSO}_4 \cdot 7\text{H}_2\text{O}$  - 1 g, lysine hydrochloride - 10 mg, threonine - 0.25 mg, tryptophan - 0.25 mg, bacteriological agar - 20 g, chloramphenicol - 50 mg, distilled water - 1 L, final pH - 5.0) (Junqueira et al. 1984). Plates containing single conidia were placed in an incubator at  $25 \pm 1$  °C under a specific 24-h light regime for 1 h of light and 3 h of dark, repeated 3 times followed by a period of 12 h of dark for approximately 15 days. The fungal colonies that grew from germinated single conidia were preserved in test tubes containing 5 mL of M3 medium for further experiments. A total of 64 isolates of *P. ulei* were obtained for this study (Table S1).

### DNA extraction and sequencing

Strains of *P. ulei* were cultivated in 125 mL Erlenmeyer flasks containing 30 mL of liquid M3 medium (Junqueira et al. 1984) kept under agitation in an orbital shaker (125 rpm) at 25 °C in the dark for 30 days. The fungal biomass was collected on a filter paper, dried at room temperature and ground with liquid

nitrogen in a mortar. Twenty-five mg of fungal tissue were subjected to genomic DNA extraction using the protocol of extraction of high quality DNA for genome sequencing available at: <http://1000.fungalgenomes.org/home/protocols/high-quality-genomic-dna-extraction/>. Upon the addition 1,183  $\mu$ L of lysis buffer (2.5 volume of buffer A: 0.35 M sorbitol, 0.1 M Tris-HCl (pH 9), 5 mM EDTA (pH 8); 2.5 volume of buffer B: 0.2 M Tris-HCl (pH 9) 50 mM EDTA (pH 8) 2 M NaCl, 2% CTAB; 1.0 volume of buffer C: 5% Sarkosyl; 0.1% PVP and 20 mg/ml Proteinase K) to the tubes and complete homogenization by vortex agitation, the microtubes were kept in a dry bath at 65 °C for 30 min and mixed frequently by gentle tube inversion. This was followed by the addition of 0.33 volumes of potassium acetate 5M (pH 7.5) to the tubes and storage on ice for 30 min. The tubes were centrifuged for 20 min at 5,000 g at 4 °C and the supernatant was transferred to new microtubes with 1 volume of Chloroform: Isoamylalcohol (24:1), followed by another centrifugation for 10 min at 4,000g at 4°C. The aqueous phases were transferred to new tubes and 100  $\mu$ l of RNase A (10mg/ml) was added. Tubes were incubated for 2 h at 37 °C. After the addition of 1/10 volume of sodium acetate and 1 volume of isopropanol (100%), the tubes were kept for 5 min at room temperature and centrifuged for 30 min at 10,000 g at 4°C. The supernatants were discarded, the residual pellets formed were washed twice with 2 mL of ethanol (70%) and the tubes were centrifuged for 10 min at 10,000 g at 4°C. Dried pellets were resuspended in 50  $\mu$ L of TE at 65°C and stored at -80 °C until further use. The DNA quality and concentration were checked using NanoDrop® 2000 spectrophotometer (Thermo Fisher Scientific) (260/280 nm ratio), and agarose gel electrophoresis (0.8%) using Lambda DNA (PROMEGA). The final concentration of DNA was adjusted to 50 ng/ $\mu$ L. The primers used for

the amplification of putative effector genes were designed based on homologous sequences detected after querying the draft genome of *P. ulmi*, obtained with 454 sequencing, with sequences of the genes coding for the effectors Avr4, Ecp2, Ecp5 and Ecp6 from *Cladosporium fulvum* and Ave1 from *Verticillium dahliae* (Hora-Júnior 2014, unpublished). The polymerase chain reactions were done in final volumes of 12  $\mu$ L, including 1  $\mu$ L DNA template, 0.5  $\mu$ L of each primer (10  $\mu$ M), 1  $\mu$ L of dimethyl-sulfoxide (Sigma), 2.4  $\mu$ L of Colorless GoTaq® Flexi Buffer (5X), 0.75  $\mu$ L of MgCl<sub>2</sub> Solution (25mM), 0.5  $\mu$ L of PCR Nucleotide Mix (10mM), 0,05  $\mu$ L of GoTaq® G2 Flexi DNA Polymerase and 5.30  $\mu$ L of Nuclease-Free Water. The amplification reactions were run on a T100™ thermal cycler (Bio-Rad, USA) and the PCR conditions were: initial denaturing step at 95 °C for 3 min, followed by 35 cycles of 95 °C for 45 s, annealing for 60 s, 72 °C for 90 s and final extension of 10 min at 72 °C. Primer descriptions including primer sequence, annealing temperature and expected fragment size are described in Table 1. The quality of amplicons was assessed in agarose gel electrophoresis (1%) and fragment sizes were checked using a 100 bp DNA ladder (Thermo Fisher Scientific, Massachusetts, USA). PCR amplicons were purified by ExoSAP treatment (Amersham Biosciences, Buckinghamshire, UK). The purified amplicons were sequenced using Sanger sequencing by Macrogen (Geumcheon-gu, Seoul, South Korea). Generated sequences were edited and assembled using Gap4 in Staden software package (Staden, Beal, and Bonfield 2000), and the sequences alignment were made in MEGA 7 (Kumar, Stecher, and Tamura 2016).

## **DNA polymorphism**

For the analyses the populations were separated in Amazonian, comprised of isolates sampled in Amazonas, Acre and Rondônia state; and Non-Amazonian, comprised of isolates sampled in São Paulo, Rio de Janeiro, Minas Gerais, Espírito Santo, Mato Grosso, and Bahia states. The standard diversity indices based on nucleotide sequence alignments (exon and intron region) were calculated with DnaSP version 6.11.01 (Rozas et al. 2017). These included the number of polymorphic (segregating) sites (S), number of haplotypes (h), Nei's haplotype (Hd) and nucleotide diversity ( $\pi$ ), total number of mutations (Eta) and G+C content. Haplotypes were inferred based on the allelic variation in each individual effector gene and a parsimony haplotype network was made for each coding region using TCS method implemented in the PopART package v. 1.7 (Leigh and Bryant 2015).

## **Recombination and mutation analysis**

Recombination in putative effectors genes were detected first by the SplitNetwork using NeighborNet methods with uncorrected *p-distances* implemented in SplitsTree4 software (Huson and Bryant 2006). The Pairwise Homoplasy Index (PHI test) was used to distinguish recurrent mutation from recombination (Bruen, Philippe, and Bryant 2005). The following methods were used to detect recombination breakpoints: Bootscan (B) and RDP (R), which are based on phylogeny (Martin et al. 2005; Martin and Rybicki 2000); Chimaera (C), GENECONV (G), MaxChi (M), SiScan (S) and 3SEQ (3S), which are based on nucleotide substitutions (Posada and Crandall 2001; Padidam, Sawyer, and Fauquet 1999; Smith 1992; Gibbs, Armstrong, and Gibbs 2000; Boni, Posada, and Feldman 2007). These tests were implemented in RDP (Recombination

Detection Program) version 4.95 (Martin et al. 2015), using default settings for all methods and a Bonferroni corrected  $p$ -value of 0.05. Recombination events detected in at least four methods by RDP were considered consistent. Breakpoints in the nucleotide sequences were detected using GARD (Genetic Algorithm for Recombination Detection) (Kosakovsky Pond et al. 2006) implemented in DataMonkey server (Delpont et al. 2010). The LDHat software version 2.2 (Auton and McVean 2007) was used to estimate the recombination rates ( $\rho$ ), recombination rates by site ( $\rho_{\text{site}}$ ), mutation rates ( $\Theta$ ), mutation rates by site ( $\Theta_{\text{site}}$ ) and the occurrence of recombination over mutation for each gene.

### **Selection analysis**

Adaptive selection was detected by the neutrality tests Tajima's D, Fu and Li's D\* and F\* calculated in DnaSP v6.11 (Rozas et al. 2017). Selection in each gene was detected by SLAC (Single Likelihood Ancestor Counting), FEL (Fixed Effects Likelihood) and REL (Random Effects Likelihood) methods implemented in DataMonkey server (Delpont et al. 2010).

## RESULTS

### Description of putative effector genes

A total of 5 putative effector genes were explored *in silico* and their genic organization is described in Figure 2. The PuAve1 is a homolog of the avirulence on Ve1 protein (Ave1) from *Verticillium dahliae* in tomato. In *P. ulei*, the effector gene coding a protein of 135 amino acids, with DPBB (double-psi beta-barrel) domains, a typical domain found in Ve1, being an outer membrane protein that is a lytic transglycosylase with specificity for peptidoglycan lacking stem peptides. PuAve1 have 6 cysteine residues and into the exon's region a sequence of 848 bp which corresponds to a pseudogenization event. The evidences for this event are: 1) presence of premature stop codon in exon region (Figure S1), 2) indels in exons regions, 3) high mutation rates (Table 3) and 4) synonymous and non-synonymous mutations in the same proportion. In the AM population, only 18 of 39 isolates had the pseudogene (isolates sampled in Acre and Rondônia states), while in N-AM population only 1 (RJ12) had the pseudogene.

The effector genes PuAvr4, PuEcp2, PuEcp5, and PuEcp6 were identified based on the effector genes of *Cladosporium fulvum* (de Wit 2016). PuAvr4 codes for a protein of 117 amino acids with 9 cysteines residues. In plant pathogenic fungi, the Avr4 binds to the CBM 14 domain of the chitin gene and protects the chitin from host-derived chitinases during infection (Kohler et al. 2016). PuEcp2 codes a 159 amino acid-protein with 4 cysteines residues, and a Hce2 domain (homologs of *C. fulvum* Ecp2 effector). The most accepted function of ECP2 during parasitism is a factor that induces plant necrosis (Stergiopoulos et al. 2010). PuEcp5 codes a small protein of 96 amino acids and 5 cysteines residues. In both the AM and N-AM populations of *P. ulei* this protein was completely deleted, in 11 isolates from AM population and in 7 isolates from N-AM

population. The PuEcp6 codes a protein with 283 amino acids and 8 cysteines residues. PuEcp6 has a LysM domain, which is found in bacteria, plants and fungi, and it is involved in peptidoglycan binding. We also found a repetition of serine and glycine amino acids (SG repetition), probably associated with transposable elements, and when compared to ECP6 sequences from other fungi, this pattern was only found in *Mycosphaerella fijiensis*.

### **DNA polymorphisms**

DNA polymorphisms were evaluated for each of the five genes separately (Table 2), and differences in the types and number of polymorphisms were observed. The number of isolates included in the analyses varied from 55 to 63 and the alignments ranged from 641 to 1448 bp. The highest numbers of segregating sites were found in PuEcp2 (48), PuEcp6 (41), and PuAve1 (27), while the least polymorphic loci were PuEcp5 (23) and PuAvr4 (10). Nucleotide diversity was higher in PuAve1 and PuECP6, and haplotype diversity was higher in PuECP6, followed by PuAve1 and PuEcp5. The highest number of haplotypes was found in PuEcp6 (24), followed by PuEcp2 (13), PuAve1 (11), PuAvr4 and PuECP5 (8). Comparisons between AM and N-AM populations revealed that the number of segregating sites, the nucleotide and haplotype diversity indices were always higher in AM population, except in PuAver4 gene. The total number of mutations (Eta) was higher in PuEcp2 (48) and in PuEcp6 (43).

The haplotype networks constructed for each gene (Figure 3) showed distinct patterns of distribution of the haplogroups in AM and N-AM populations. The isolates corresponding to each haplogroup are described in Table S1. In the networks of PuAve1, PuAvr4 and PuEcp2 the dominant haplogroups were composed by roughly 2/3 to 1/2 of isolates from AM population. On the other hand,

the networks of PuEcp5 and PuEcp6 tended to split the haplogroups between AM and N-AM. Most isolates of N-AM population shared a single haplotype of PuAve1. In the more diverse PuEcp6, most isolates from the N-AM population formed a group of related rare haplotypes, distinct from most of the haplotypes of the AM population. Interestingly, the haplogroups H20 and H21 belongs to AM population in PuEcp6 appear to derive from haplotypes of the N-AM population (Figure 3).

### **Mutation and Recombination**

Networks evidenced reticulated connections between isolates in all genes (Figure 4). There is evidence for the occurrence of recombination events. Some patterns of isolate distribution between subpopulations of the AM and N-AM populations could be assigned to mutation signatures and indel events observed in some genes. In PuAve1, all isolates from the oriental Amazon (Manaus region: Beruri, Manicoré and Manaus) formed a single haplogroup (ellipse 1, Figure 4). In addition to shared synapomorphies, all of those isolates were characterized by a 12 bp insertion between the positions 355 and 367 of the original alignment, and lack of 849 bp insertion of DNA between the positions 518 and 1368, corresponding to the pseudogenization event. The ellipse 2 in the split graph of PuAve1 identifies the haplogroup containing all, but two isolates of the N-AM population (BA27, RJ12). This haplogroup is also characterized by the absence of the 849 bp DNA insertion but does not have the 12 bp insertion characteristic of the isolates from the Manaus region (Figure S1).

Isolates of oriental Amazon (Manaus region) grouped in a single haplogroup or in a cluster of very closely related haplotypes in the split graphs of the other four genes (Figure 4). The haplogroup highlighted in the split graph of



PuEcp5 (Figure 4), formed by isolates of the N-AM population and three isolates of the eastern AM population (Table S1), are characterized by the deletion of 273 bp out of the 288 bp corresponding to the coding region of this gene (Figure S2).

Mutation events were more frequent and important than recombination events in the evolution of the analyzed effector genes of *P. ulmi* (Table 3). The PHI test, which compares the number of observed homoplasies in haplotype trees with the expected number derived from mutation events only, indicated the presence of recombination only in PuEcp6 (Mean  $\phi_w = 0.10$ ; *p-value* = 0.034) (Table 3, Figure 4). The topology of the haplotype networks, however, had reticulations in all genes. Three out of the five methods of recombination detection implemented by the RDP software identified intragenic recombination in the genes PuEcp2 and PuEcp6 (Table 4). Finally, the software GARD identified recombination breakpoints in the genes PuAve1, PuEcp2 and PuEcp5 (Figure 5).

### **Selection analyses**

Significant negative results were obtained for neutrality test statistics of Tajima's D, Fu and Li's D\* and F\* for PuEcp6 in the N-AM population, indicating purifying selection or the result of a recent population expansion after a bottleneck or founder effect (Table 5). The number of sites under negative selection in PuEcp6 estimated by FEL and REL methods were 15 and 21, respectively. A similar, although not statistically supported, pattern of negative selection was found for PuAve1 in the N-AM population. On the other hand, significant positive values for PuAve1 (Fu and Li's D\* and F\*) and PuEcp2 (Fu and Li's D\*) in the AM population indicate the existence of balanced selection acting on those genes.

## DISCUSSION

The rubber tree breeding programs for SALB resistance were initiated more than 90 years ago and resulted in the selection of several clones with partial (quantitative) resistance or complete immune reactions (qualitative resistance) to *P. ulei* (Zhang et al. 2016). The qualitative resistance of many clones was quickly overcome by new variants of the pathogen. Apparently, the selection pressure imposed by the resistant host population affects the genetic variability in local populations of *P. ulei*. The partial resistance traits of clones currently found in rubber tree plantations mostly located in the Atlantic Coast of Brazil are controlled by a combination of quantitative loci (Le Guen et al. 2007, 2011, 2013). However, the history of severe outbreaks of SALB in rubber tree plantations in Brazil, especially in the northern regions, should raise awareness to the risks of resistance overcome by selected *P. ulei* individuals carrying new versions and combinations of pathogenic traits. This risk should be quantified including resistance breakdown in “escape” areas, i.e. regions where environmental conditions are not conducive to severe epidemics of SALB (Furtado et al. 2015). Good comprehension of the evolutionary mechanisms affecting the populations of *P. ulei* is required to properly assess the risks of resistance overcome. We used the patterns of allelic variability found in the sequences of five putative effector genes of *P. ulei* to compare the pathogen populations from the Amazon region with those from commercial rubber tree plantations located outside the center of origin of this pathogen.

DNA polymorphism analyses revealed different patterns of evolution among the five putative effector genes under investigation. The PuEcp6 gene showed the highest level of polymorphisms, with 24 allelic versions found in a collection of 63 isolates of *P. ulei*, almost twice the number of haplogroups found

in PuEcp2 and PuAvr4 (13). The remaining genes were less diverse and represented by 11 (PuAve1) and seven (PuAvr4) haplogroups, although the number of segregating sites found in PuAve1 was four to five times higher than those found in PuEcp5 and PuAvr4, indicating concerted mutations in PuAve1. In a related study on the allelic diversity of effector genes present in a global collection of isolates of the banana black leaf strike pathogen *Pseudocercospora fijiensis*, similar values of nucleotide and haplotype diversity were found in the MfAvr4 and MfEcp2-3, which are homologs of PuAvr4 and PuEcp2 (Stergiopoulos et al. 2014).

A similar pattern of splitting between the haplotypes of AM and N-AM populations was found in the networks of PuAve1 and PuEcp6; however, the distribution of isolates among haplogroups in the AM population varied according to the genomic region analyzed. In the case of PuAve1, 19 of 21 isolates belonging to the N-AM population shared the same haplogroup. On the other hand, most isolates were dispersed along a cluster of eight closely related haplogroups in PuEcp6, distinguished by one or two mutations between them. Significant negative values obtained in the neutrality tests conducted with PuEcp6 are indicative of a recent expansion of the allelic diversity within the N-AM population, or the result of admixtures with alleles derived from the occidental AM population, as implied in the haplotype network analyses. In this scenario and considering the putative active role of the PuEcp6 protein in the interactions between *P. ulei* and the rubber tree (de Jonge et al. 2010), the allelic expansion associated with this gene in the N-AM population may be part of a response to the selective pressures imposed by the clones expressing high levels of partial resistance to SALB. On the other hand, selection analyses of PuEcp6 revealed

the predominance of synonymous over non-synonymous mutations in N-AM population, suggesting the existence of barriers to allelic diversification imposed by structural and functional constraints in the amino acid sequence of the active protein (Stavriniades, McCann, and Guttman 2007). This result reinforces that PuEcp6 is an active effector gene in *P. ulei*.

The fact that most isolates of the N-AM population share the same haplotype of PuAve1 can be the result of a possible directional selection towards a specific allele conferring adaptive advantages to the pathogen population (Stergiopoulos et al. 2014), a trend supported by unitary negative values obtained for the N-AM population in the neutrality tests conducted with this gene. However, the low PuAve1 haplotype diversity in the BR population may also be the result of genetic drift (Barrett et al. 2009). Significant positive values obtained in the neutrality tests conducted with PuAve1 in the AM population suggest an opposite trend of conservation of the allelic diversity within this population (balanced selection), which is also corroborated by the haplotype networks.

In this study the Brazilian isolates of *P. ulei* were divided between AM and N-AM populations, but apparently there is a more complex genetic structure of these populations. Based on the haplotype diversity analyses of all investigated genes there is a subdivision in the AM population with isolates from oriental Amazon (Manaus region) exhibiting lower levels of allelic diversity and grouping in one or few related clusters. Conversely, the isolates from the occidental Amazon (AC, ERN and AM isolates) were distributed along several distinct haplotypes, including those composed by isolates of the N-AM population. The low allelic and haplotype diversity among the isolates of oriental Amazon region may reflect a geographic isolation of this subpopulation. Additionally, selection

and genetic drift may have contributed to reduce the genetic diversity. On the other hand, the sharing of alleles between isolates of the occidental Amazon and those of the AM population suggest the existence of gene flow between these populations (Zhan, Pettway, and McDonald 2003).

The diversification of the effectors of *P. ulei* is also influenced by intragenic recombination events. Evidences of recombination were observed in the reticulated haplotype networks and additional recombination tests showed that all genes, except PuAvr4, had signals of recombination events, although in some genes this evidence is weak. Intragenic recombination was strongly detected in PuEcp6 and PuEcp2 genes, while in PuAve1 and PuEcp5 evidence was weak. Recombination has a strong impact on the diversification of *P. ulei* effector genes. In the context of the arms race, the presence of recombination in the effector genes leads to a rapid genomic rearrangement where new alleles can emerge in the populations and overcome the recognition of R genes of the host (Croll et al. 2015; McDonald and Linde 2002), which was observed in *P. ulei* genes.

New functional isomorphs of effector proteins that retain their function may be generated and can bypass the host protein receptors or result in nonfunctional or truncate versions of the effectors. Two mechanisms were identified in *P. ulei*, a complete protein deletion in PuEcp5 and an insertion of 849 bp in PuAve1. The long insertion in PuAve1 has typical characteristics of a pseudogene, such as the presence of premature stop codon in exon region and higher mutation rates (Yang et al. 2011). In *P. ulei*, this pseudogene can separate the populations in non-arbitrary way. The population from the Amazon (18 isolates) has an indel while only one isolate from the N-AM population (RJ12) had the indel, which may reflect some evolutionary event in these populations (van der Burgt et al. 2014).

The loss of effector protein will only be fixed in the pathogen population if there is no fitness cost (de Jonge et al. 2012). In the case of PuAve1 and Ecp5, it is not possible at this point to predict the consequences of the insertion and deletion, respectively, observed in some haplotypes. Additional studies with a larger number of isolates will help elucidate the fate of such mutations in the pathogen population.

Our investigation revealed high levels of polymorphisms in sequences of five putative effector genes from Amazonian and Non-Amazonian populations of *P. ulei*. Based on evidence from at least two genes (PuEcp6, PuAve1) distinct evolutionary processes are acting on the AM and N-AM populations. The loss of allelic diversity in PuAve1 and expansion of rare allelic variants in PuEcp6 points to selective pressures acting in the N-AM population, in response to the widespread deployment of resistant clones in commercial plantations. In addition, the evidence of gene flow between the N-AM and occidental Amazon populations also implies that new sources of genetic variation derived from the Amazonian region may be regularly being introduced to rubber tree plantations in the Atlantic Coast of Brazil. This scenario suggests that *P. ulei* has high potential to overcome rubber tree resistance, even outside the Amazon region. Thus, we must reinforce the importance of continuous efforts for breeding programs for SALB resistance, with deployment of clones with new allelic combinations and the mixed of qualitative and quantitative resistance to be effective against the SALB pathogen.

## **ACKNOWLEDGMENTS**

We thank Braz T. Hora-Junior for help with this research. We thank Taciana Santos for help with DNA extractions. This study was financed in part by the Coordenação de Aperfeiçoamento de Pessoal de Nível Superior - Brasil (CAPES) - Finance Code 001.

## REFERENCES

- Auton, A., and McVean, G. 2007. Recombination rate estimation in the presence of hotspots. **Genome Research**. 17:1219–1227.
- Barrett, L. G., Thrall, P. H., Dodds, P. N., van der Merwe, M., Linde, C. C., Lawrence, G. J., et al. 2009. Diversity and evolution of effector loci in natural populations of the plant pathogen *Melampsora lini*. **Molecular Biology and Evolution**. 26:2499–2513.
- van Beilen, J. B., and Poirier, Y. 2007. Establishment of new crops for the production of natural rubber. **Trends in Biotechnology**. 25:522–529.
- Boni, M. F., Posada, D., and Feldman, M. W. 2007. An exact nonparametric method for inferring mosaic structure in sequence triplets. **Genetics**. 176:1035–47.
- Bruen, T. C., Philippe, H., and Bryant, D. 2005. A simple and robust statistical test for detecting the presence of recombination. **Genetics**. 172:2665–2681.
- van der Burgt, A., Karimi Jashni, M., Bahkali, A. H., and de Wit, P. J. G. M. 2014. Pseudogenization in pathogenic fungi with different host plants and lifestyles might reflect their evolutionary past. **Molecular Plant Pathology**. 15:133–144.
- Castroverde, C. D. M., Nazar, R. N., and Robb, J. 2016. *Verticillium* Ave1 effector induces tomato defense gene expression independent of Ve1 protein. **Plant Signaling & Behavior**. 11:e1245254.
- Croll, D., Lendenmann, M. H., Stewart, E., and McDonald, B. A. 2015. The impact of recombination hotspots on genome evolution of a fungal plant pathogen. **Genetics**. 201:1213–1228.
- Dangl, J. L., and Jones, J. D. G. 2001. Plant pathogens and integrated defence responses to infection. **Nature**. 411:826–833.
- Delport, W., Poon, A. F. Y., Frost, S. D. W., and Kosakovsky Pond, S. L. 2010. Datamonkey 2010: a suite of phylogenetic analysis tools for evolutionary biology. **Bioinformatics**. 26:2455–2457.
- Furtado, E. L., Cunha, A. R. da, Alvares, C. A., Bevenuto, J. A. Z., and Passos, J. R. 2015. Ocorrência de epidemia do mal das folhas em regiões de escape do Brasil. **Arquivos do Instituto Biológico**. 82:1–6.
- Garcia, D., Carels, N., Koop, D. M., de Sousa, L. A., Andrade Junior, S. J. de, Pujade-Renaud, V., et al. 2011. EST profiling of resistant and susceptible *Hevea* infected by *Microcyclus ulei*. **Physiological and Molecular Plant Pathology**.



76:126–136.

Garcia, D., Guen, V. Le, Mattos, C. R. R., Goncalves, P. D. S., and Clement-Demange, A. 2002. Relationships between yield and some structural traits of the laticiferous system in *Hevea* clones resistant to South American leaf blight. **Crop Breeding and Applied Biotechnology**. 2:307–317.

Garcia, D., Mattos, C. R. R., Goncalves, P. D. S., and Guen, V. Le. 2004. Selection of rubber clones for resistance to South American leaf blight and latex yield in the germplasm of the Michelin plantation of Bahia (Brazil). **Journal of Rubber Research**. 7.

Gibbs, M. J., Armstrong, J. S., and Gibbs, A. J. 2000. Sister-scanning: a Monte Carlo procedure for assessing signals in recombinant sequences. **Bioinformatics** (Oxford, England). 16:573–82.

Grandin, G. 2009. Fordlandia : the rise and fall of Henry Ford's forgotten jungle city. **New York**.

Le Guen, V., Garcia, D., Doaré, F., Mattos, C. R. R., Condina, V., Couturier, C., et al. 2011. A rubber tree's durable resistance to *Microcyclus ulei* is conferred by a qualitative gene and a major quantitative resistance factor. **Tree Genetics & Genomes**. 7:877–889.

Le Guen, V., Garcia, D., Mattos, C., Fouet, O., Doaré, F., Condina, V., et al. 2013. A newly identified locus controls complete resistance to *Microcyclus ulei* in the Fx2784 rubber clone. **Tree Genetics & Genomes**. 9:805–812.

Le Guen, V., Garcia, D., Mattos, C. R. R., Doaré, F., Lespinasse, D., and Seguin, M. 2007. Bypassing of a polygenic *Microcyclus ulei* resistance in rubber tree, analyzed by QTL detection. **New Phytologist**. 173:335–345.

Guyot, J., and Le Guen, V. 2018. A review of a century of studies on South American Leaf Blight of the Rubber Tree. **Plant Disease**. 102:1052–1065.

Hogenhout, S. A., Van der Hoorn, R. A. L., Terauchi, R., and Kamoun, S. 2009. Emerging Concepts in Effector Biology of Plant-Associated organisms. **Molecular Plant-Microbe Interactions**. 22:115–122.

Hora Júnior, B. T. da. 2012. Molecular phylogeny and population genetics of *Microcyclus ulei*, causal agent of the South American leaf blight of *Hevea brasiliensis*. Available at: <http://www.locus.ufv.br/handle/123456789/1046> [Accessed May 6, 2018].

Huson, D. H., and Bryant, D. 2006. Application of phylogenetic networks in

evolutionary studies. **Molecular Biology and Evolution**. 23:254–267.

de Jonge, R., Peter van Esse, H., Kombrink, A., Shinya, T., Desaki, Y., Bours, R., et al. 2010. Conserved fungal LysM effector Ecp6 prevents chitin-triggered immunity in plants. **Science**. 329:953–955.

de Jonge, R., Peter van Esse, H., Maruthachalam, K., Bolton, M. D., Santhanam, P., Saber, M. K., et al. 2012. Tomato immune receptor Ve1 recognizes effector of multiple fungal pathogens uncovered by genome and RNA sequencing. **Proceedings of the National Academy of Sciences**. 109:5110–5115.

Junqueira, N. T. V., Chavees, G. M., Zambolim, L., Romeiro, R. da S., and Gasparotto, L. 1984. Isolamento, cultivo e esporulação de *Microcyclus ulei*, agente etiológico do mal-das-folhas da seringueira. **Revista Ceres**. 31:322–331.

Kohler, A. C., Chen, L.-H., Hurlburt, N., Salvucci, A., Schwessinger, B., Fisher, A. J., et al. 2016. Structural analysis of an Avr4 effector ortholog offers insight into chitin binding and recognition by the cf-4 receptor. **The Plant cell**. 28:1945–65.

Kosakovsky Pond, S. L., Posada, D., Gravenor, M. B., Woelk, C. H., and Frost, S. D. W. 2006. Automated phylogenetic detection of recombination using a genetic algorithm. **Molecular Biology and Evolution**. 23:1891–1901.

Kumar, S., Stecher, G., and Tamura, K. 2016. MEGA7: Molecular Evolutionary Genetics Analysis Version 7.0 for Bigger Datasets. **Molecular Biology and Evolution**. 33:1870–1874.

Leigh, J. W., and Bryant, D. 2015. Popart: full-feature software for haplotype network construction ed. Shinichi Nakagawa. **Methods in Ecology and Evolution**. 6:1110–1116.

Lespinasse, D., Grivet, L., Troispoux, V., Rodier-Goud, M., Pinard, F., and Seguin, M. 2000. Identification of QTLs involved in the resistance to South American leaf blight ( *Microcyclus ulei* ) in the rubber tree. **Theoretical and Applied Genetics**. 100:975–984.

Lieberji, R. 2007. South American leaf blight of the rubber tree (*Hevea* spp.): new steps in plant domestication using physiological features and molecular markers. **Annals of botany**. 100:1125–42.

Martin, D. P., Murrell, B., Golden, M., Khoosal, A., and Muhire, B. 2015. RDP4: Detection and analysis of recombination patterns in virus genomes. **Virus evolution**. 1:vev003

- Martin, D. P., Posada, D., Crandall, K. A., and Williamson, C. 2005. A modified bootscan algorithm for automated identification of recombinant sequences and recombination breakpoints. **AIDS Research and Human Retroviruses**. 21:98–102.
- Martin, D., and Rybicki, E. 2000. RDP: detection of recombination amongst aligned sequences. **Bioinformatics** (Oxford, England). 16:562–3.
- McDonald, B. A., and Linde, C. 2002. Pathogen population genetics, evolutionary potential, and durable resistance. **Annual review of phytopathology**. 40:349–79.
- Ohm, R. A., Feu, N., Henrissat, B., Schoch, C. L., Horwitz, B. A., Barry, K. W., et al. 2012. Diverse lifestyles and strategies of plant pathogenesis encoded in the genomes of eighteen Dothideomycetes fungi. **PLoS Pathogens**. 8:e1003037.
- Padidam, M., Sawyer, S., and Fauquet, C. M. 1999. Possible emergence of new geminiviruses by frequent recombination. **Virology**. 265:218–225.
- Posada, D., and Crandall, K. A. 2001. Evaluation of methods for detecting recombination from DNA sequences: computer simulations. **Proceedings of the National Academy of Sciences of the United States of America**. 98:13757–62.
- Rozas, J., Ferrer-Mata, A., Sánchez-DelBarrio, J. C., Guirao-Rico, S., Librado, P., Ramos-Onsins, S. E., et al. 2017. DnaSP 6: DNA sequence polymorphism analysis of large data sets. **Molecular Biology and Evolution**. 34:3299–3302.
- Smith, J. M. 1992. Analyzing the mosaic structure of genes. **Journal of molecular evolution**. 34:126–9.
- Staden, R., Beal, K. F., and Bonfield, J. K. 2000. The Staden Package, 1998. In **Bioinformatics Methods and Protocols**, New Jersey: Humana Press, p. 115–130.
- Stavrinos, J., McCann, H. C., and Guttman, D. S. 2007. Host–pathogen interplay and the evolution of bacterial effectors. **Cellular Microbiology**. 0:071127144819001.
- Stergiopoulos, I., Beenen, H., Burg, H. van den, Kourmpetis, Y. I. A., Okmen, B., and Wit, P. J. G. M. de. 2010. Functional analysis of homologues of the *Cladosporium fulvum* Avr4 and ECp2 effectors present in other (pathogenic) fungal species. In: **Book of Abstracts 10th European Conference on Fungal Genetics, Noordwijkerhout, the Netherlands**, 29 March–1 April 2010. 149–149.

Stergiopoulos, I., Burg, H. van den, Okmen, B., Beenen, H., Kema, G. H. J., and Wit, P. J. G. M. de. 2009. Homologues of the *Cladosporium fulvum* effector proteins are present in *Mycosphaerella* species. n: **Book of Abstracts 25th Fungal Genetics Conference, Pacific Grove, California, USA, 17-22 March 2009**. 218 (539)-218 (539).

Stergiopoulos, I., Cordovez, V., Ökmen, B., Beenen, H. G., Kema, G. H. J., and de Wit, P. J. G. M. 2014. Positive selection and intragenic recombination contribute to high allelic diversity in effector genes of *Mycosphaerella fijiensis*, causal agent of the black leaf streak disease of banana. **Molecular Plant Pathology**. 15:447–460.

Stukenbrock, E. H., and McDonald, B. A. 2009. Population genetics of fungal and oomycete effectors involved in gene-for-Gene Interactions. **Molecular Plant-Microbe Interactions**. 22:371–380.

Stukenbrock, E. H., and McDonald, B. A. 2008. The origins of plant pathogens in agro-ecosystems. **Annual Review of Phytopathology**. 46:75–100.

de Wit, P. J. G. M. 2016. *Cladosporium fulvum* Effectors: Weapons in the Arms Race with Tomato. *Annual Review of Phytopathology*. 54:1–23 Available at: <http://www.ncbi.nlm.nih.gov/pubmed/27215970> [Accessed May 18, 2018].

Yang, L., Takuno, S., Waters, E. R., and Gaut, B. S. 2011. Lowly expressed genes in *Arabidopsis thaliana* bear the signature of possible pseudogenization by promoter degradation. **Molecular Biology and Evolution**. 28:1193–1203.

Zhan, J., Pettway, R. E., and McDonald, B. A. 2003. The global genetic structure of the wheat pathogen *Mycosphaerella graminicola* is characterized by high nuclear diversity, low mitochondrial diversity, regular recombination, and gene flow. **Fungal genetics and biology**. 38:286–97.

Zhang, X., Wang, L., He, C., and Luo, H. 2016. An efficient transient mesophyll protoplast system for investigation of the innate immunity responses in the rubber tree (*Hevea brasiliensis*). **Plant Cell, Tissue and Organ Culture (PCTOC)**. 126:281–290.

## FIGURE LEGEND

**Figure 1.** Sampling areas of *Pseudocercospora ulei*.

**Figure 2.** Design of amplification region of putative effector genes of *Pseudocercospora ulei*. Black boxes represent the primers used to amplifying each putative effector gene. Dark grey boxes represent the intron region and gold boxes represent the exons. Indel are show in light gray boxes, and conserved domains are show in orange boxes. The mature protein is indicated with N-terminal and C-terminal and the cysteine residues are represented by letter C in red.

**Figure 3.** Parsimony haplotype networks for the loci PuAve1, PuAvr4, PuEcp2, PuEcp5 and PuECP6 of *Pseudocercospora ulei*. The blue color represents the haplogroups from Amazonia population and the green color represent the haplogroups from Non-Amazonian population. The hatch marks represent the synonymous and non-synonymous mutations. The description of each haplogroup is listed in the Table S2.

**Figure 4.** Split tree graphs based on populations of *P. ulei* using 5 putative effectors genes. Graphs were constructed with reticulate phylogenetic relationships among PuAve1, PuAvr4, PuEcp2, PuEcp5 and PuEcp6 using NeighborNet. Least Square (LS) fit and PHI test values are shown. The codes in green represent the isolates from Amazonia population and in blue resent the isolates from Non-Amazonian population.

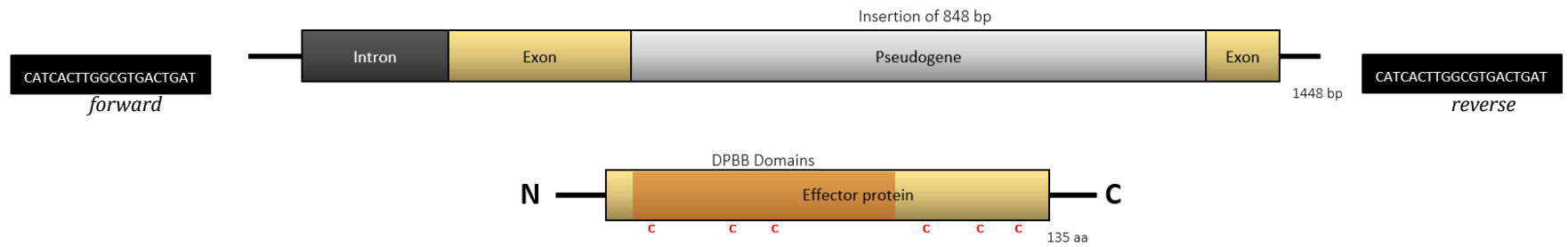
**Figure 5.** Analysis of recombination of PuAve1, PuEcp2 and PuEcp5 genes of *Pseudocercospora ulei* performed in GARD software implemented in DataMonkey server. **BPs:** Numbers of breakpoints detected in the alignment; **AICc:** Small-sample correct Akaike information criterion;  $\square$  **AICc:** Change in AICc of best scoring models with one fewer breakpoint; **LHS and RHS p-value:** P-value for left and right side; **Significance:** Visual indicator of statistical significance.

## FIGURES AND TABLES

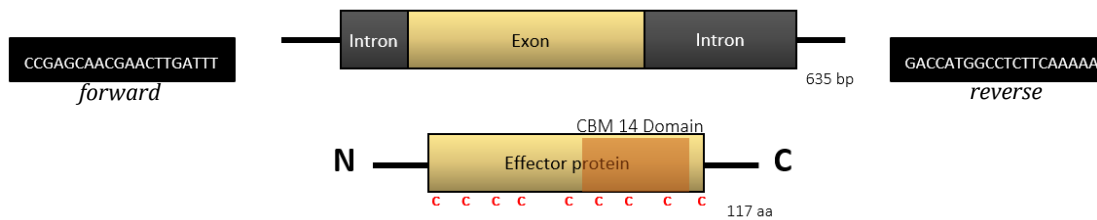


**Figure 1. Ferreira et al. 2018**

**A) PuAve1**



**B) PuAvr4**



**C) PuECP2**

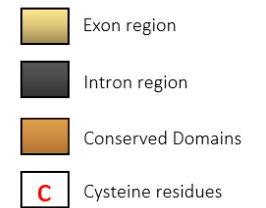
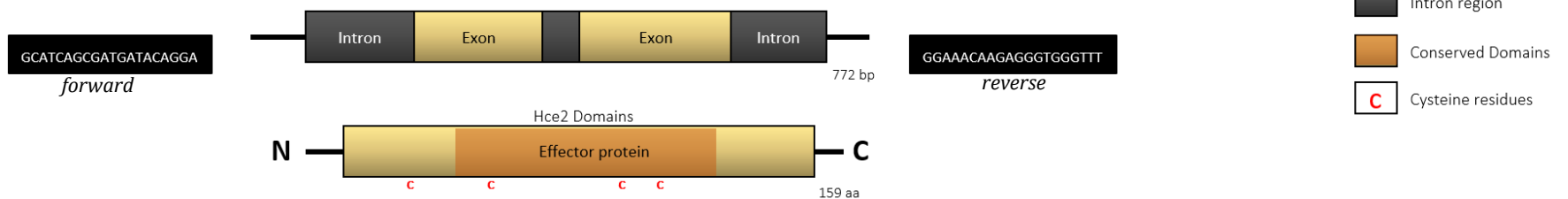
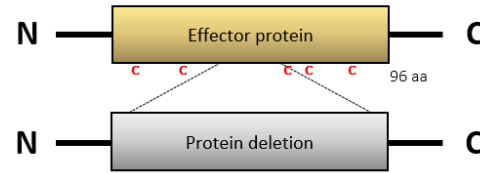
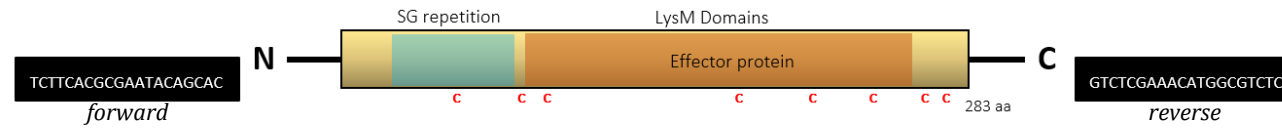


**Figure 02. Ferreira et al. 2018**

**D) PuECP5**



**E) PuECP6**

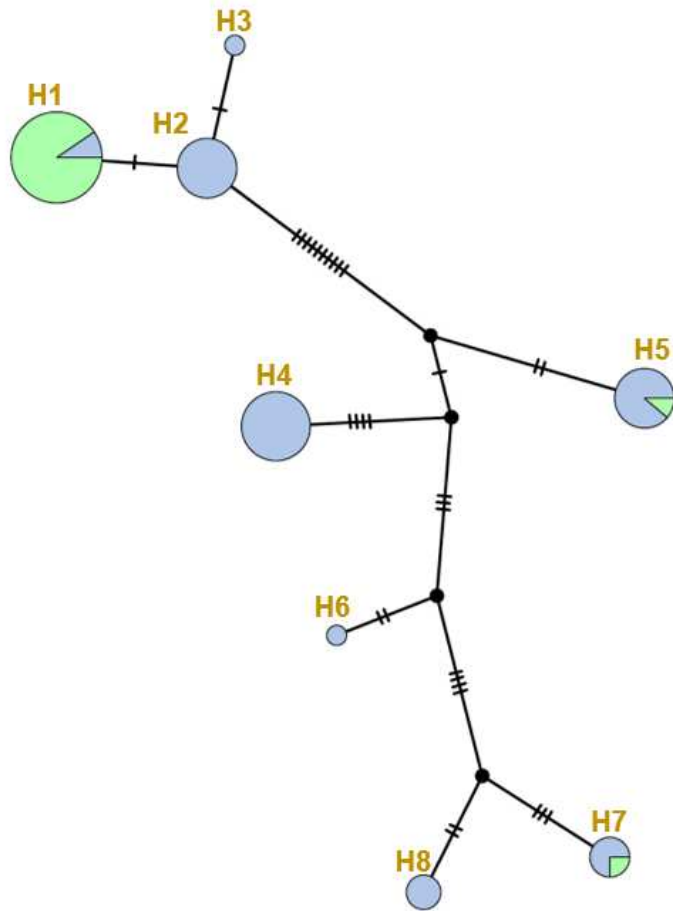


- Exon region
- Intron region
- Conserved Domains
- C Cysteine residues
- SG repetition
- Indels

**Figure 02. Ferreira et al. 2018**



A) PuAve1



B) PuAvr4

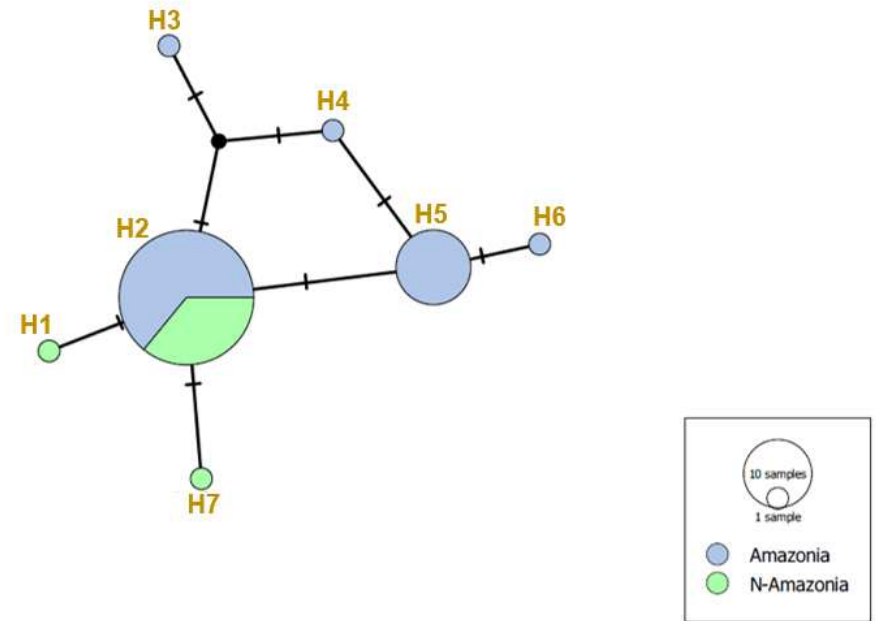
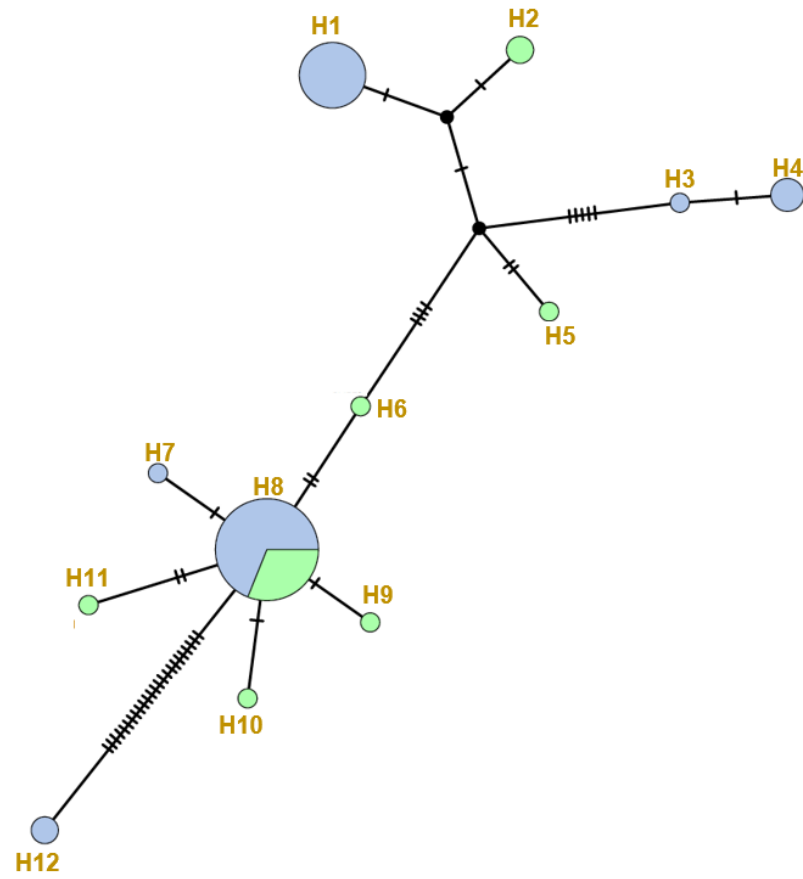


Figure 3. Ferreira et al. 2018

C) PuEcp2



D) PuEcp5

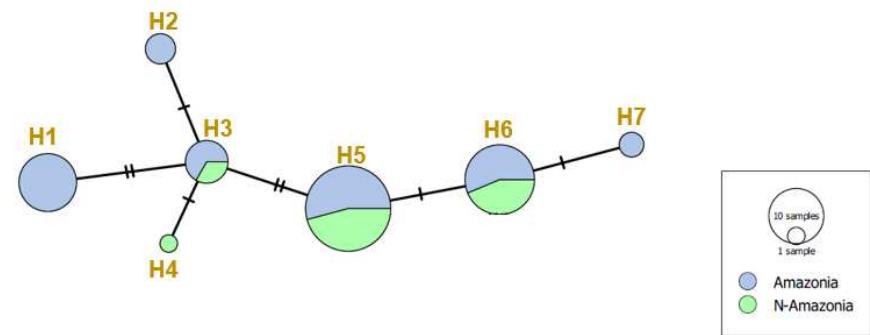


Figure 3. Ferreira et al. 2018

### E) PuEcp6

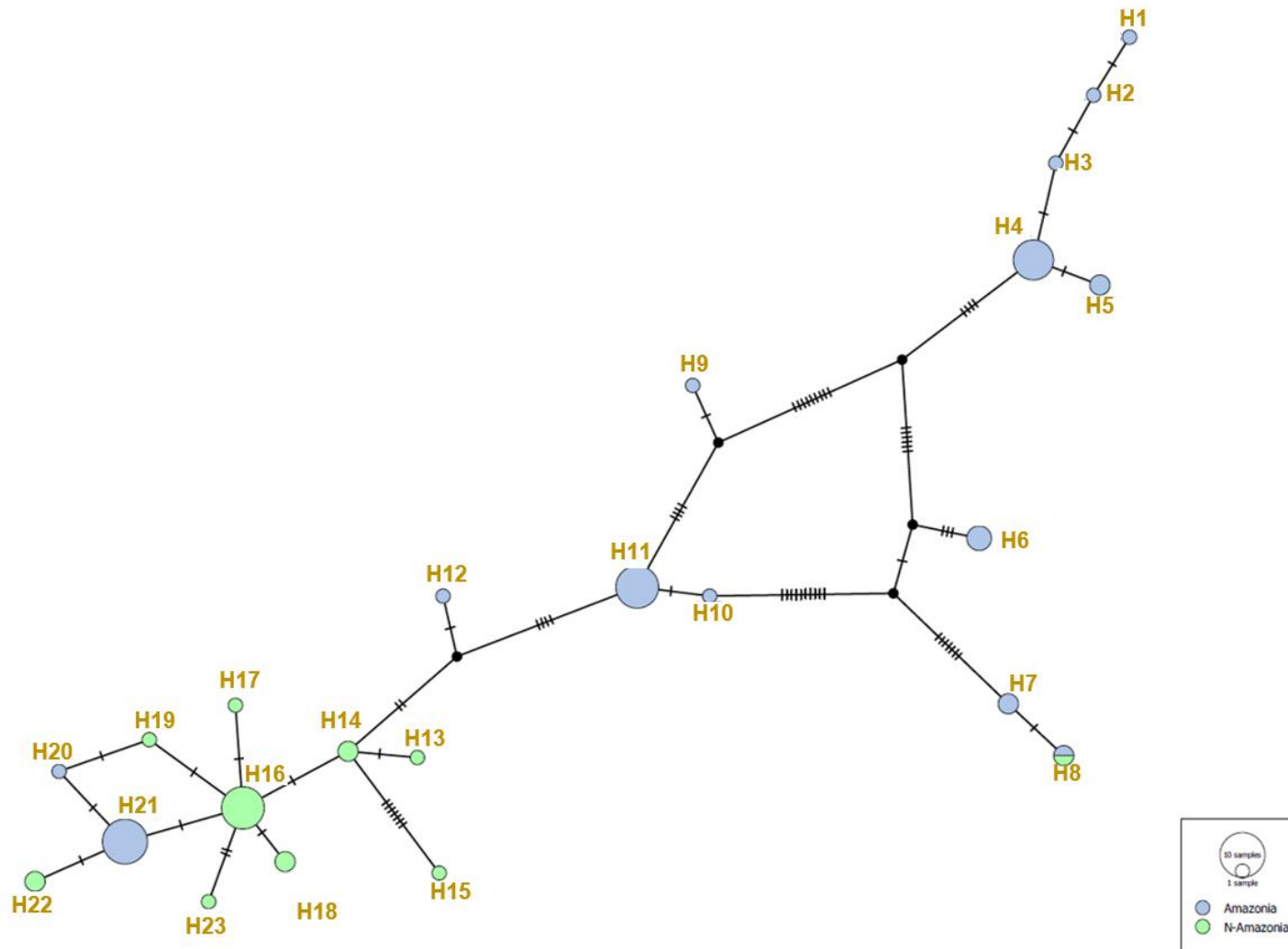


Figure 3. Ferreira et al. 2018

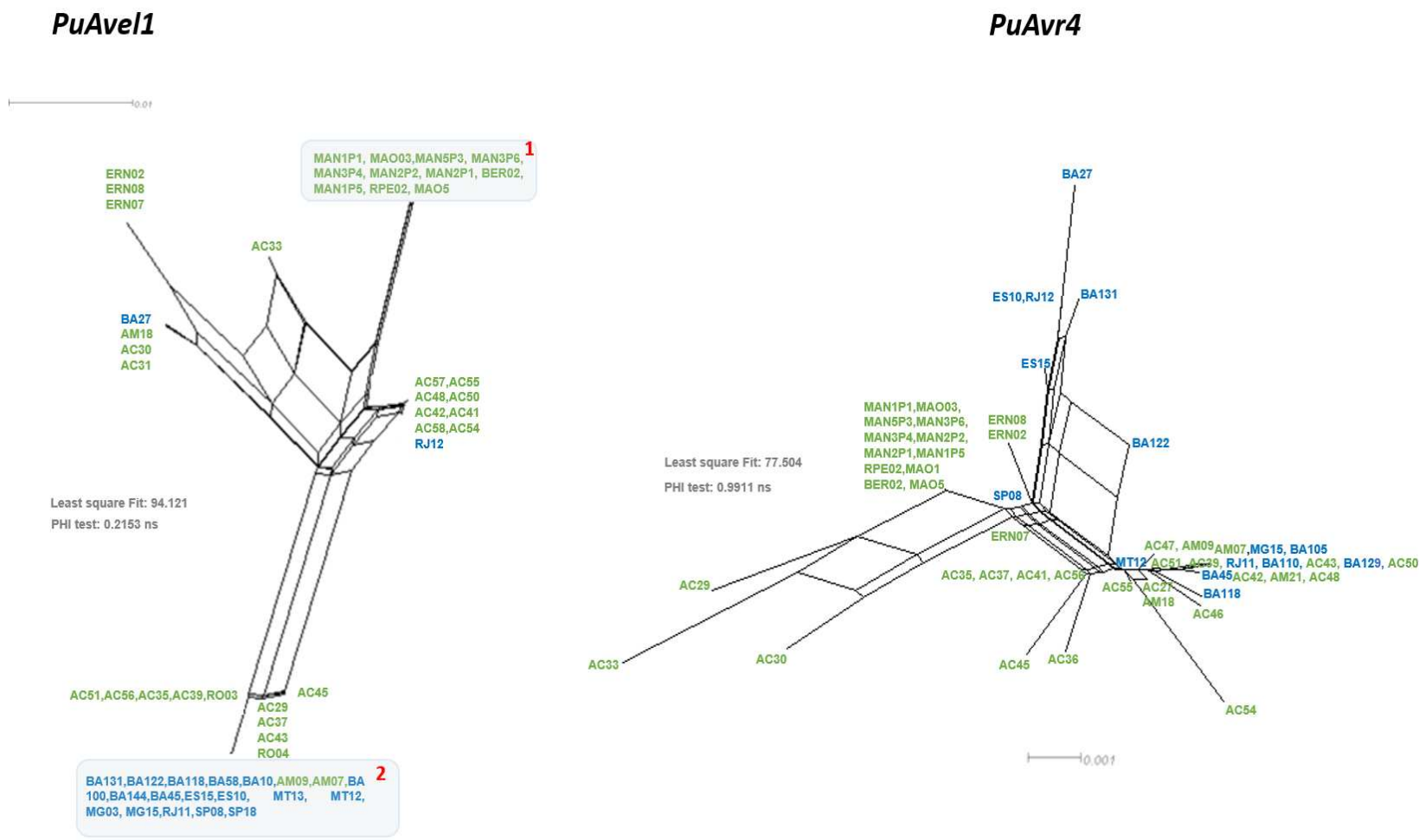
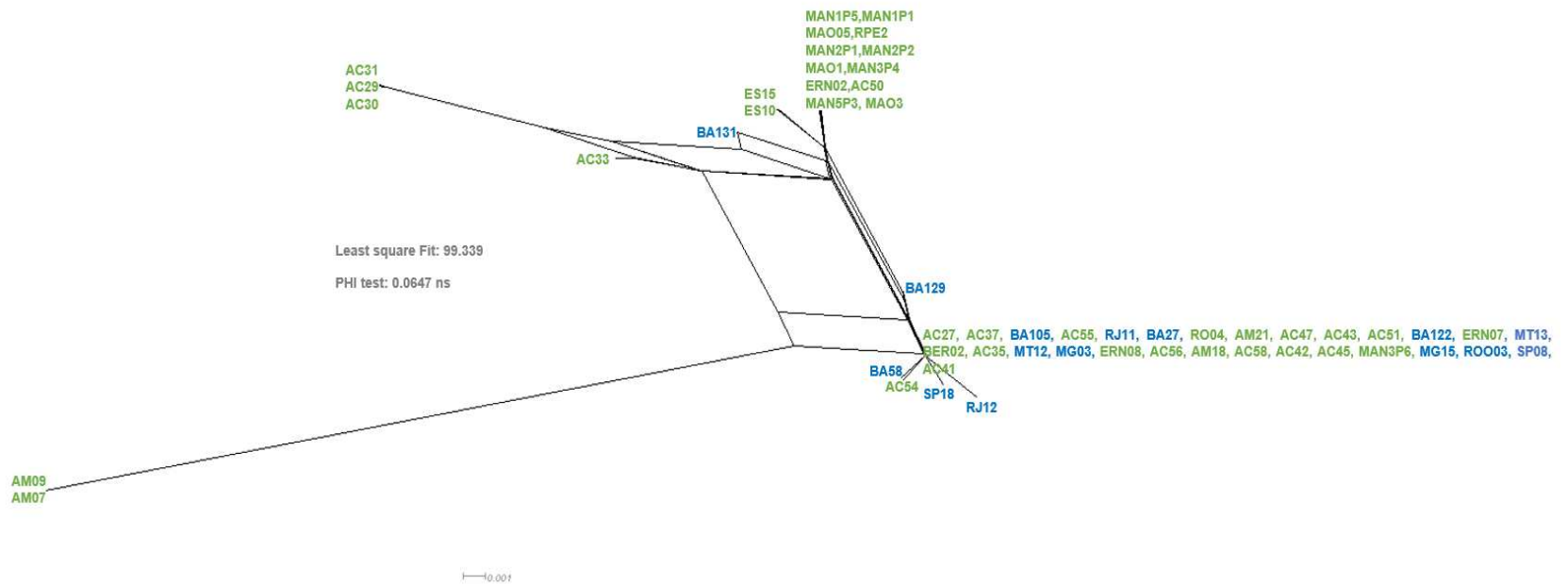


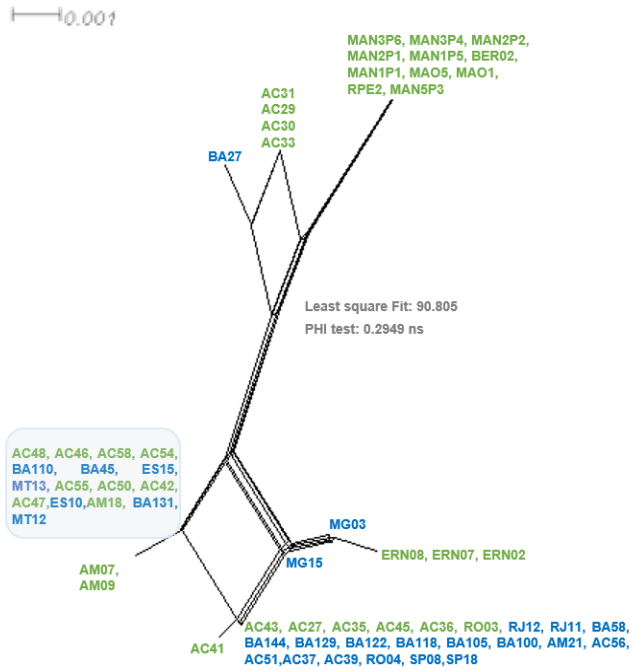
Figure 4. Ferreira et al. 2018

**PuECP2**



**Figure 4. Ferreira et al. 2018**

**PuECP5**



**PuECP6**

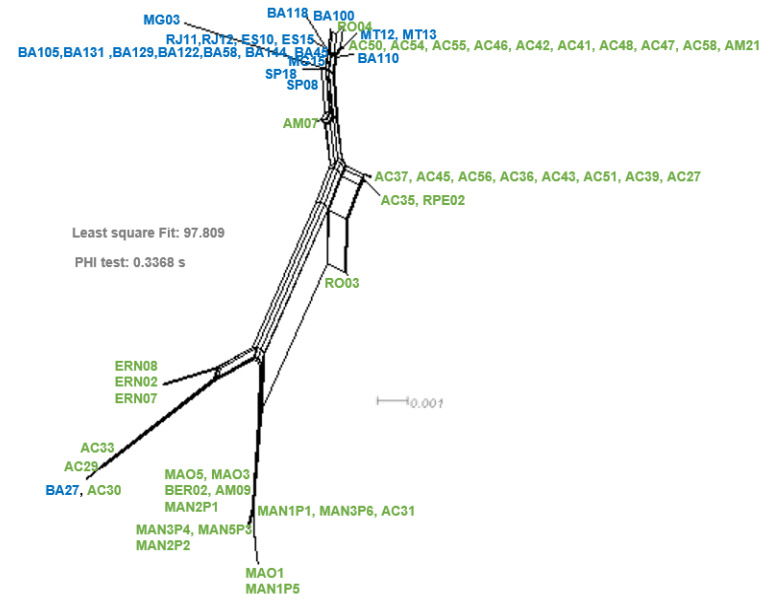


**Figure 4. Ferreira et al. 2018**

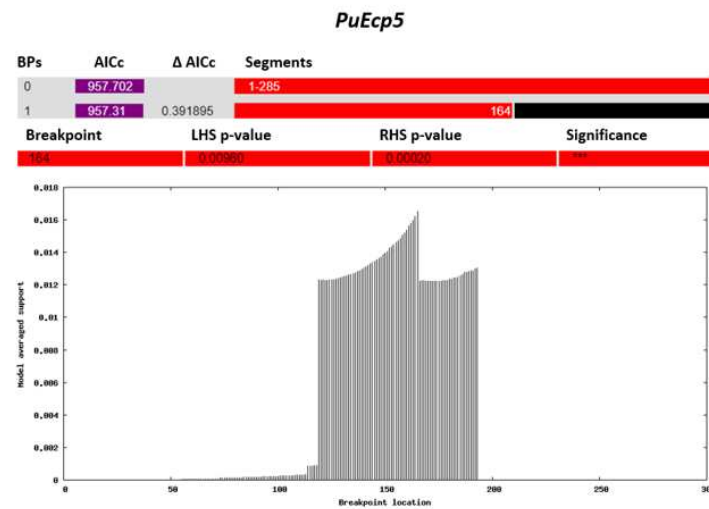
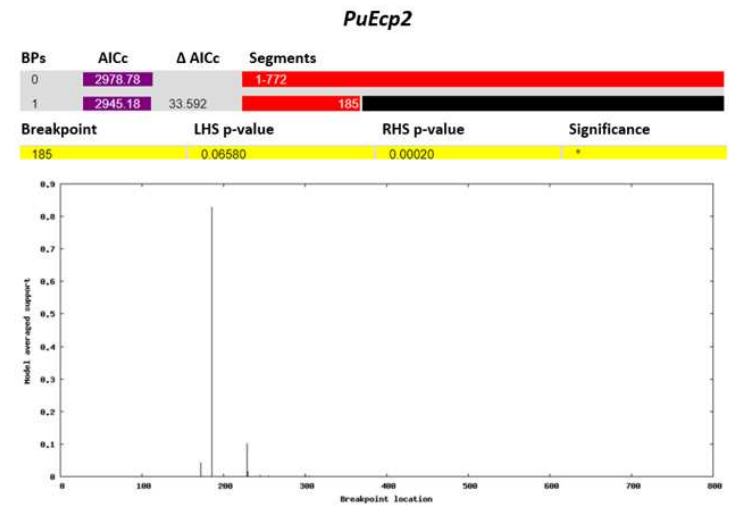
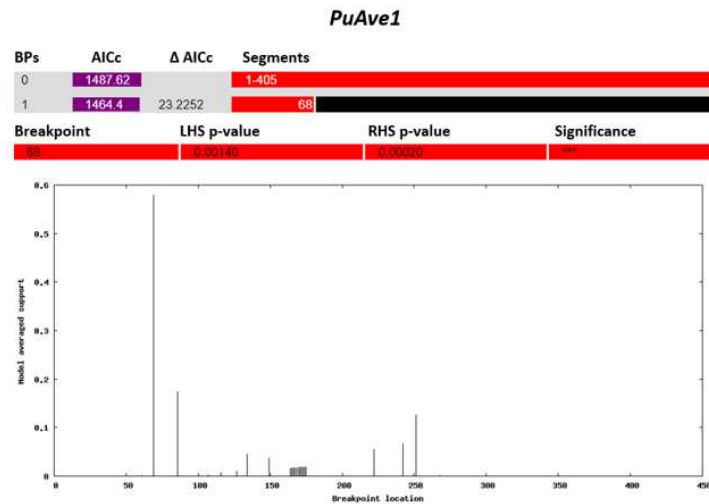


Figure 5. Ferreira et al. 2018.

**Table 1.** List of oligonucleotides using in the study to amplify putative genes effectors of *Pseudocercospora ulei*.

Locus	Primer	Sequence 5' - 3'	Annealing (°C)
AVEL	PuAve1-2F	CATCACTTGGCGTGACTGAT	58
	PuAve1-2R	CATTCTACCGCGAGCTGTG	
AVR4	PuAVR4F	CCGAGCAACGAACTTGATTT	60
	PuAVR4R	GACCATGGCCTCTTCAAAAA	
ECP2	PuECP2F	GCATCAGCGATGATACAGGA	59.4
	PuECP2R	GGAAACAAGAGGGTGGGTTT	
ECP5	PuECP5F	GCCTTTCATGTGCCATAGGT	58
	PuECP5R	ATGACATAACGCGGTTTCAACA	
ECP6	PuECP6F	TCTTCACGCGAATACAGCAC	55
	PuECP6R	GTCTCGAAACATGGCGTCTC	

\*Primer design by Hora-junior, 2014 (unpublished)



**Table 2.** Standard diversity index for five putative effector genes and in the population of *Pseudocercospora ulei* from Amazonian (AM) and Non-Amazonian (N-AM) regions.

Effector Gene	POP	Region	Size (bp)	S	Eta	$\pi$	H	Hd	Gc%
<b><i>PuAve1</i></b>									
AM <i>n</i> =39		Intron	1 - 194	7	8	0.01209	6	0.776	0.657
		Exon I	195 - 518	18	18	0.02232	7	0.803	0.602
		Pseudogene	518 - 1367	7	7	0.00291	4	0.627	0.543
		Exon II	1368 - 1448	2	2	0.00437	3	0.344	0.558
		Total	1 - 1448	27	28	0.01646	8	0.815	0.616
N-AM <i>n</i> =21		Intron	1 - 194	3	3	0.00191	3	0.186	0.654
		Exon I	195 - 518	14	14	0.00647	3	0.186	0.599
		Exon II	1368 - 1448	1	1	0.00118	2	0.095	0.556
Total	1 - 1448	18	18	0.00423	3	0.186	0.612		
<b><i>PuAvr4</i></b>									
AM <i>n</i> =40		Intron I	1 - 96	1	1	0.00875	2	0.508	0.578
		Exon	97 - 447	5	6	0.00217	5	0.531	0.639
		Intron II	448 - 635	1	1	0.00095	2	0.142	0.613
		Total	1 - 635	7	8	0.00253	6	0.615	0.626
N-AM <i>n</i> =16		Intron I	1 - 96	6	7	0.02417	5	0.629	0.564
		Exon	97 - 447	4	4	0.00250	5	0.676	0.637
		Intron II	448 - 635	-	-	-	-	-	-
		Total	1 - 635	10	11	0.00461	7	0.771	0.622
<b><i>PuEcp2</i></b>									
AM <i>n</i> = 39		Intron I	1 - 152	8	8	0.02282	4	0.591	0.515
		Exon	153 - 393	12	12	0.00516	3	0.238	0.617
		Intron II	394 - 447	3	3	0.01180	3	0.505	0.477
		Exon II	448 - 683	19	19	0.01137	4	0.282	0.612
		Intron III	684 - 772	6	6	0.01360	4	0.282	0.589
		Total	1 - 772	48	48	0.01194	6	0.649	0.582
N-AM <i>n</i> = 16		Intron I	1 - 152	10	10	0.01782	6	0.617	0.514
		Exon I	153 - 393	2	2	0.00104	2	0.125	0.617
		Intron II	394 - 447	-	-	-	-	-	-
		Exon II	448 - 683	2	2	0.00177	3	0.342	0.620
		Intron III	684 - 772	-	-	-	-	-	-
Total	1 - 772	14	14	0.00510	7	0.692	0.583		
<b><i>PuEcp5</i></b>									
AM <i>n</i> =31		Intron I	1 - 113	2	2	0.00891	2	0.503	0.513
		Exon	114 - 401	11	11	0.01481	5	0.720	0.634
		Intron II	402 - 641	10	10	0.02174	4	0.695	0.497
		Total	1 - 641	23	23	0.01606	5	0.720	0.567
N-AM <i>n</i> =14		Intron I	1 - 113	2	2	0.00642	2	0.363	0.513
		Exon	114 - 401	8	8	0.00517	3	0.385	0.632
		Intron II	402 - 641	6	6	0.00365	2	0.143	0.527
		Total	1 - 641	16	16	0.00479	3	0.385	0.573
<b><i>PuEcp6</i></b>									
AM <i>n</i> =42		Exon	1 - 849	41	43	0.01701	14	0.86	0.660
N-AM <i>n</i> =21		Exon	1 - 849	40	41	0.00546	10	0.81	0.658

S: number of polymorphic (segregating) sites  
 Eta: total number of mutations  
 $\pi$ : nucleotide diversity  
 h: number of haplotypes  
 Hd: Nei's haplotype GC%:  
 G+C content

**Table 3.** Estimates of recombination ( $\rho$ ), mutation rates ( $\Theta$ ) and the Pairwise Homoplasmy Index test ( $\Phi_w$ ) of putative effector genes in Amazonian and Non-Amazonian populations of *Pseudocercospora ulei*.

Gene	Pop	$\Theta$	$\Theta/\text{site}$	$\rho$	$\rho/\text{site}$	$\rho/\Theta$	Mean $\Phi_w$ (p-value)
<i>PuAve1</i>	AM	7.714	$1.761 \times 10^{-02}$	3.744 (2.306 – 6.493)	$8.548 \times 10^{-03}$ ( $5.266 \times 10^{-03}$ – $1.482 \times 10^{-02}$ )	0.485	0.05 (0.2153)
	N-AM	10	$1.698 \times 10^{-02}$	0.141 (0.005 – 0.524)	$2.4 \times 10^{-4}$ ( $1 \times 10^{-5}$ – $.89 \times 10^{-3}$ )	0.0121	
<i>PuAvr4</i>	AM	1.92	$3.575 \times 10^{-03}$	362.028 (13.444 – 1406.607)	0.6741 ( $2.504 \times 10^{-02}$ – 2.619)	188.556	0.07 (0.9959)
	N-AM	0.96	$2.735 \times 10^{-03}$	327.013 (1.801 – 1366.43)	0.9316 ( $5.131 \times 10^{-03}$ – 3.893)	340.638	
<i>PuEcp2</i>	AM	16.636	$2.998 \times 10^{-02}$	0.9483 ( $1.068 \times 10^{-02}$ – 3.96)	$1.709 \times 10^{-03}$ ( $1.925 \times 10^{-05}$ – $7.134 \times 10^{-03}$ )	$5.7 \times 10^{-02}$	0.03 (0.0647)
	N-AM	2.182	$3.331 \times 10^{-03}$	288.994 (0.3864 – 1529.295)	0.4412 ( $5.9 \times 10^{-04}$ – 2.335)	132.44	
<i>PuEcp5</i>	AM	5.280	$1.517 \times 10^{-02}$	1.496 ( $2.615 \times 10^{-02}$ – 8.767)	$4.3 \times 10^{-03}$ ( $7.514 \times 10^{-05}$ – $2.519 \times 10^{-02}$ )	0.2833	0.3 (0.2949)
	N-AM	5.334	$1.418 \times 10^{-02}$	0.132 ( $7.595 \times 10^{-03}$ – 0.4613)	$3.514 \times 10^{-04}$ ( $2.02 \times 10^{-05}$ – $1.227 \times 10^{-03}$ )	$2.478 \times 10^{-02}$	
<i>PuEcp6</i>	AM	11.99	$1.33 \times 10^{-02}$	3.493 (1.318 – 6.811)	$3.872 \times 10^{-03}$ ( $1.461 \times 10^{-03}$ – $7.551 \times 10^{-3}$ )	0.2912	<b>0.10</b> <b>(0.03368*)</b>
	N-AM	13.786	$1.539 \times 10^{-02}$	$1.283 \times 10^{-02}$ ( $1.042 \times 10^{-02}$ – $3.443 \times 10^{-02}$ )	$1.432 \times 10^{-05}$ ( $1.163 \times 10^{-05}$ – $3.843 \times 10^{-05}$ )	$9.308 \times 10^{-04}$	

**Table 4.** Intragenic recombination events in putative effector genes of *P. ulei* inferred with RDP program.

Event	Recombinant	Parents		Methods	P-value
		Major	Minor		
<b>PuECP2</b>					
1	AM09	AC31	RJ12	RBMC3S	1.078X10 <sup>-02</sup>
	AM07	AC31	RJ12	RBMC3S	
2	BA131	AC31	RJ12	MC	6.564X10 <sup>-03</sup>
<b>PuECP6</b>					
1	RO03	BA118	MAN1P5	MB3S	9.757X10 <sup>-04</sup>
2	MG03	BA118	Unknown	MB3S	

**Table 5.** Neutrality and selection tests for genomic regions of isolates of the Amazonian and Non-Amazonian populations of *Pseudocercospora ulei*.

Gene	Tajima D		Fu and Li D*		Fu and Li F*		dN/dS		SLAC		FEL		REL	
	AM	N-AM	AM	N-AM	AM	N-AM	AM	N-AM	Positive	Negative	Positive	Negative	Positive	Negative
PuAve1	1.505	-1.616	<b>1.458</b>	-0.857	<b>1.647</b>	-1.125	23/2	13/2	0	3	1	1	6	0
PuAvr4	0.590	0.401	0.454	-0.439	-0.428	-0.220	5/2	2/0	0	3	0	2	0	2
PuEcp2	-0.615	-0.831	<b>1.708</b>	-0.497	1.0141	-0.620	22/9	1/3	0	1	0	2	0	2
PuEcp5	1.756	-1.547	0.933	-1.660	1.2938	-1.698	7/4	6/2	0	1	0	3	0	4
PuEcp6	1.381	<b>-2.398</b>	1.264	<b>-3.384</b>	1.4823	<b>-3.300</b>	31/21	19/23	0	3	0	15	6	21

\*Bold numbers were significant

**Table S1.** Sampling site of *Pseudocercospora ulei* in Brazil.

Isolate	Local	Region	POP	Year	Collector
AC27	Bujari	Acre	AM	2010	B. T. Hora Junior
AC29	Bujari	Acre	AM	2010	B. T. Hora Junior
AC30	Bujari	Acre	AM	2010	B. T. Hora Junior
AC31	Bujari	Acre	AM	2010	B. T. Hora Junior
AC33	Bujari	Acre	AM	2010	B. T. Hora Junior
AC35	Rio Branco	Acre	AM	2010	B. T. Hora Junior
AC36	Rio Branco	Acre	AM	2010	B. T. Hora Junior
AC37	Rio Branco	Acre	AM	2010	B. T. Hora Junior
AC39	Rio Branco	Acre	AM	2010	B. T. Hora Junior
AC41	Rio Branco	Acre	AM	2010	B. T. Hora Junior
AC42	Xapuri	Acre	AM	2010	B. T. Hora Junior
AC43	Xapuri	Acre	AM	2010	B. T. Hora Junior
AC45	Xapuri	Acre	AM	2010	B. T. Hora Junior
AC46	Xapuri	Acre	AM	2010	B. T. Hora Junior
AC47	Xapuri	Acre	AM	2010	B. T. Hora Junior
AC48	Xapuri	Acre	AM	2010	B. T. Hora Junior
AC50	Xapuri	Acre	AM	2010	B. T. Hora Junior
AC51	Xapuri	Acre	AM	2010	B. T. Hora Junior
AC54	Xapuri	Acre	AM	2010	B. T. Hora Junior
AC55	Xapuri	Acre	AM	2010	B. T. Hora Junior
AC56	Xapuri	Acre	AM	2010	B. T. Hora Junior
AC58	Xapuri	Acre	AM	2010	B. T. Hora Junior
AM07	Boca do Acre	Amazonas	AM	2014	B. T. Hora Junior
AM09	Boca do Acre	Amazonas	AM	2014	B. T. Hora Junior
AM18	Boca do Acre	Amazonas	AM	2014	B. T. Hora Junior
AM21	Boca do Acre	Amazonas	AM	2014	B. T. Hora Junior
BA100	Bahia	Bahia	N-AM	2008	B. T. Hora Junior
BA105	Bahia	Bahia	N-AM	2008	B. T. Hora Junior
BA110	Bahia	Bahia	N-AM	2008	B. T. Hora Junior
BA118	Bahia	Bahia	N-AM	2008	B. T. Hora Junior
BA122	Bahia	Bahia	N-AM	2008	B. T. Hora Junior
BA129	Bahia	Bahia	N-AM	2008	B. T. Hora Junior
BA131	Bahia	Bahia	N-AM	2008	B. T. Hora Junior
BA144	Bahia	Bahia	N-AM	2008	B. T. Hora Junior
BA27	Bahia	Bahia	N-AM	2008	B. T. Hora Junior
BA45	Bahia	Bahia	N-AM	2008	B. T. Hora Junior
BA58	Bahia	Bahia	N-AM	2008	B. T. Hora Junior
BER2	Beruri	Amazonas	AM	2015	A. F.T.A.F. Ferreira
ERN7	Eirunepé	Amazonas	AM	2015	E.S.G. Mizubuti
ERN8	Eirunepé	Amazonas	AM	2015	E.S.G. Mizubuti
ERN2	Eirunepé	Amazonas	AM	2015	E.S.G. Mizubuti
ES10	Espirito Santo	Espirito Santo	N-AM	2010	B. T. Hora Junior
ES15	Espirito Santo	Espirito Santo	N-AM	2010	B. T. Hora Junior

**Table S1. Continued**

<b>Isolate</b>	<b>Local</b>	<b>Region</b>	<b>POP</b>	<b>Year</b>	<b>Collector</b>
MAN1P1	Manicoré	Amazonas	AM	2016	A.F.T.A.F. Ferreira
MAN1P5	Manicoré	Amazonas	AM	2016	A.F.T.A.F. Ferreira
MAN2P1	Manicoré	Amazonas	AM	2016	A.F.T.A.F. Ferreira
MAN2P2	Manicoré	Amazonas	AM	2016	A.F.T.A.F. Ferreira
MAN3P4	Manicoré	Amazonas	AM	2016	A.F.T.A.F. Ferreira
MAN3P6	Manicoré	Amazonas	AM	2016	A.F.T.A.F. Ferreira
MAN5P3	Manicoré	Amazonas	AM	2016	A.F.T.A.F. Ferreira
MAO1	Manaus	Amazonas	AM	2016	A.F.T.A.F. Ferreira
MAO3	Manaus	Amazonas	AM	2016	A.F.T.A.F. Ferreira
MAO5	Manaus	Amazonas	AM	2016	A.F.T.A.F. Ferreira
MG03	Minas Gerais	Minas Gerais	N-AM	2010	B. T. Hora Junior
MG15	Minas Gerais	Minas Gerais	N-AM	2010	B. T. Hora Junior
MT12	Mato Grosso	Mato Grosso	N-AM	2010	B. T. Hora Junior
MT13	Mato Grosso	Mato Grosso	N-AM	2010	B. T. Hora Junior
RJ11	Rio de Janeiro	Rio de Janeiro	N-AM	2010	B. T. Hora Junior
RJ12	Rio de Janeiro	Rio de Janeiro	N-AM	2010	B. T. Hora Junior
RO03	Rondônia	Rondônia	AM	2010	J. Honorato Junior
RO04	Rondônia	Rondônia	AM	2010	J. Honorato Junior
RPE2	Rio Preto da Eva	Amazonas	AM	2016	A.F.T.A.F. Ferreira
SP08	São Paulo	São Paulo	N-AM	2010	B. T. Hora Junior
SP18	São Paulo	São Paulo	N-AM	2010	B. T. Hora Junior

**Table S2.** Distribution of the isolates of *Pseudocercospora ulei* in haplogroups (HG) for the PuAve1, PuAvr4, PuEcp2, PuEcp5 and PuEcp6 genes.

HG	Effector genes				
	PuAve1	PuAvr4	PuEcp2	PuEcp5	PuEcp6
H1	AM07, AM09, BA100, BA105, BA110, BA118, BA122, BA129, BA131, BA144, BA45, BA58, ES10, ES15, MG15, MG03, MT12, MT13, RJ11, SP08, SP18	BA122	ERN02, MAN1P1, MAN1P5, MAN2P1, MAN2P2, MAN3P4, MAN5P3, MAO1, MAO3, MAO5, RPE2	BER02	MAN1P5
H2	AC29, AC35, AC37, AC39, AC43, AC51, AC56, RO04, RO03	AC27, AC35, AC36, AC37, AC39, AC41, AC42, AC43, AC45, AC46, AC47, AC48, AC50, AC51, AC54, AC55, AC56, AC58, AM07, AM09, AM18, AM21, BA105, BA110, BA129, BA131, BA27, BA45, BA58, ERN07, ERN02, ERN08, ES10, ES15, MG15, MT12, RJ11, RJ12, SP08	ES10, ES15	ERN02, ERN07, ERN08	MAO1
H3	AC45	AC30	AC33	AC29	MAN2P2
H4	BER02, MAN1P1, MAN1P5, MAN2P1, MAN2P2, MAN3P4, MAN3P6, MAN5P3, MAO1, MAO3, MAO5, RPE02	AC33	AC29, AC30, AC31	BA27	AC31, AM09, BER02, MAN1P1, MAN2P1, MAN3P6, MAO3, MAO5
H5	AC41, AC42, AC48, AC50, AC55, AC58, RJ12, AC47, AC54	BER02, MAN1P1, MAN1P5, MAN2P1, MAN2P2, MAN3P4, MAN3P6, MAN5P3, MAO1, MAO3, MAO5, RPE02,	BA131	AC27	MAN3P4, MAN5P3
H6	AC33	AC29	BA129	AC42	ERN02, ERN07, ERN08
H7	AC30, AC31, AM18, BA27	BA118	AC54	AM07	AC29, C33
H8	ERN02, ERN07, ERN08		AC27, AC35, AC37, AC41, AC42, AC43, AC45, AC47, AC51, AC55, AC56, AC58, AM18, AM21, BA105, BA122, BA27, BER02, ENR07, ERN08, MAN3P6, MG03, MG15, MT13, MT12, RJ11, RO03, RO04, SP08		AC30, BA27
H9			BA58		RO02
H10			SP18		AC35
H11			RJ11		AC27, AC37, AC39, AC43, AC45, AC51, AC56, AC36, RPE02

HG	Effector genes				
	PuAve1	PuAvr4	PuEcp2	PuEcp5	PuEcp6
H12			AM07, AM09		AM07
H13					SP18
H14					SP08
H15					MG03, MG15, SP08
H16					BA105, BA122, BA129, BA131, BA144, BA45, BA58, ES10, ES15
H17					BA110
H18					RJ11, RJ12
H19					BA100
H20					RO04
H21					AC41, AC42, AC46, AC47, AC48, AC50, AC54, AC55, AC58, AM21
H22					MT13, MT12
H23					BA118

\*To origin of isolates see the Table S1.



**Figure S1.** Partial alignment of the inferred protein sequences derived from PuAve1 coding region showing the 4 aa (12 bp) insertion typical of isolates from the oriental Amazon (blue arrow) and part of the large insertion of a probably nonfunctional peptide in the middle of the protein sequence. The red arrow highlights the presence of a stop codon early in the inserted sequence.



**Figure S2.** Alignment of the inferred protein sequences derived from PuEcp5 coding region showing the large deletion of 91 aa (273 bp) in the sequence of several strains.



## CHAPTER 3

### The dark side of *Pseudocercospora ulei*

## ABSTRACT

Melanins are dark natural pigments broadly synthesized in all kingdoms of life, formed from the polymerization of phenolic or indole compounds. In many fungi, melanin is related to virulence and protection under unfavorable environmental conditions. *Pseudocercospora ulei* causes South American Leaf Blight, the most destructive disease of the rubber tree (*Hevea brasiliensis*), and pathogen structures formed on the host and in culture media are pigmented. Supposedly, pigments in these structures reduce nucleic acid quality and make difficult other biochemical procedures to be performed with this pathogen. We used Matrix-Assisted Laser Desorption/Ionization Time-of-Flight (MALDI-TOF) mass spectrometry, Fourier Transform Infrared spectroscopy (FT-IR), and histochemical assays to characterize the dark pigment synthesized by *P. ulei*. We also investigated the melanin biosynthesis by cultivating *P. ulei* with tricyclazole, an inhibitor of the 1, 8-DHN pathway in fungi, and searched for the genes involved in this route in a draft genome of the fungus. The MALDI-TOF analysis failed to provide results on the melanin polymer but revealed that data on beta-glucans have apparently been mistakenly assigned to melanin in recent reports in the literature. The FT-IR analysis showed absorption bands characteristic of melanin and polysaccharides, thus confirming the mixture of both components in melanin extract of *P. ulei*. The histochemical analysis of stromata using the periodic-acid-Schiff assay showed the presence of polysaccharides as the most abundant constituent in this structure. The melanization of *P. ulei* was inhibited by the addition of tricyclazole, a specific inhibitor of the 1,8-dihydroxynaphthalene (1, 8-DHN) melanin pathway in fungi. Additionally, the genes encoding the enzymes responsible for the biosynthesis of 1,8DHN were found in the genome of *P. ulei*.

These results demonstrate that 1,8-DHN melanin is synthesized by *P. ulei*. Overall, we found evidence of two major components in the black stromata produced by *P. ulei*, DHN melanin and polysaccharides. We were also able to inhibit the melanization of stromata *in vitro* with tricyclazole, a finding that may be used for developing cultivation protocols aiming at the production of light-colored mycelia amenable to common techniques required in biochemistry and molecular biology studies.

**Key words:** Dark pigments, melanin, *P. ulei*, MALDI-TOF, IR, DHN.

## INTRODUCTION

*Pseudocercospora ulei* (Henn.) Hora Júnior & Mizubuti (Hennings 1904; Hora Júnior et al. 2014) causes South American Leaf Blight of *Hevea* spp., which is the main fungal disease of rubber trees, and the principal reason for the decline of plantations in the Amazon region, and consequently the reduction of natural rubber production in Brazil (Grandin 2009; Lieberei 2007). The fungus infects young stems, fruits and leaves, and the complete life cycle takes place in association with plants of the genus *Hevea*. *P. ulei* produces conidia (asexual spores) that infect leaves at younger stages and are responsible for secondary cycles of SALB. An intermediate spermogonial phase is followed by the formation of sexual structures containing ascospores, and both reproductive phases occur on black stromata formed on the surface of mature infected leaves (Garcia et al. 2011; Gasparotto et al. 1997; Hora Júnior et al. 2014). *P. ulei* does not produce aerial mycelia in culture media. Instead, the fungus grows slowly by producing hard black stromata, and a typical colony containing many small stromata scattered on the agar surface may take months to form (Chee 1978).

The production of hard stromata impregnated with dark pigment and the lack of soft aerial mycelia make the extraction and purification of nucleic acids and proteins from *P. ulei* difficult tasks, hindering the investigations on population biology, gene expression and transcriptomics, and proteomic profiling of the pathogen. In other fungal species, such as *Aspergillus nidulans*, *Rhizoctonia solani* and *Cladosporium* sp., it has been shown that melanin forms a kind of shell on the cell wall, preventing cell lysis (Kuo and Alexander 1967; Bloomfield and Alexander 1967). Melanin is the putative dark pigment present in the reproductive

structures of *P. ulei*, but to date no studies were conducted to characterize this compound.

Melanins are a natural group of pigments broadly synthesized by plants, animals, fungi and bacteria. They are formed by the polymerization of phenolic and indolic monomers, giving rise to macromolecular amorphous structures that are hydrophobic, negatively charged, usually black and brown in color, and insoluble in most solvents (White 1958; Nosanchuk, Stark, and Casadevall 2015; Bell and Wheeler 1986; Belozerskaya, Gessler, and Aver'yanov 2017).

In ascomycetes, two main pathways of melanin synthesis are known, one proceeding with a polyketide route via 1,8-dihydroxynaphthalene (DHN-melanin) and the other via polymerization of L-3,4-dihydroxyphenylalanine catalyzed by phenoloxidases (DOPA-melanin) (Bell and Wheeler 1986). In some cases, the same species can produce both types of melanin, each with different functions, such as in *Aspergillus fumigatus*, which synthesizes DOPA melanin to protect the cell wall of the hyphae and DHN melanin to maintain the structural integrity of conidia and contribute to their adhesion (Pihet et al. 2009). Most melanin producing ascomycetes investigated to date synthesize using the DHN route (Funa et al. 1999).

The biosynthesis of DHN (Figure 1) begins with the reaction of one molecule of acetyl-coenzyme A (acetyl-CoA) and four molecules of malonyl-CoA to form the pentaketide 1,3,6,8-tetrahydroxynaphthalene (1,3,6,8-THN). This reaction is catalyzed by the 1,3,6,8-THN polyketide synthase enzyme (PKS1). Next, 1,3,6,8-THN is reduced by the 1,3,6,8-THN reductase enzyme (4HNR) to scytalone, which is dehydrated to 1,3,8-trihydroxynaphthalene (1,3,8-THN) by the scytalone dehydratase (SCD1). The 1,3,8-THN is reduced to vermelone by the

1,3,8-trihydroxynaphthalene reductase (3HNR). Finally, the SCD1 catalyzes the dehydration of vermeline to 1,8-DHN, which is polymerized by unknown enzymes into melanin (Langfelder et al. 2003; Thompson et al. 2000; Alspaugh, Perfect, and Heitman 1998; Funa et al. 1999).

Some compounds can bind to enzymes involved in the biosynthesis of 1,8-DHN and block melanin production in fungi. The fungicide tricyclazole inhibits the reduction of 1,3,6,8-tetrahydroxynaphthalene to scytalone and the reduction of 1,3,8-trihydroxynaphthalene to vermeline (Figure 1), resulting in the accumulation of intermediates and other shunt products of their transformation, abolishment of 1,8-DHN production and, consequently, loss of melanization (Langfelder et al. 2003).

Melanin plays important roles in the survival and pathogenesis of fungi. In the natural environment, fungal melanin confers protection against numerous physical and chemical stressors, including extreme pH values, UV radiation, desiccation, enzymatic activities and oxidative stresses produced by predators and hosts (Cordero and Casadevall 2017; Gessler, Egorova, and Belozerskaya 2014; Butler and Day 1998). For some plant pathogens, the melanization process is the main factor responsible for the establishment of the disease. *Colletotrichum lagenarium*, *C. lindemuthianum*, *C. kahawae*, and *Pyricularia grisea* require the melanization of appressoria in order to build up enough turgor pressure and penetrate the plant tissues (Bell and Wheeler 1986; Chumley 1990; Chen et al. 2004), and in *Gaeumannomyces graminis* there are reports of albino mutants that are nonpathogenic to barley and wheat (Butler and Day 1998).

Melanin is mostly associated with the fungal cell wall, and present in various structures, such as hyphae, conidia, stromata, appressoria,



chlamydospores and sclerotia. The fungal cell wall is composed mainly of branches of polysaccharides, mostly  $\beta$ -glucans and chitin, with small proteins in the inner layer and mannoproteins in the outer layer. Melanin may be present in the inner or outer layer and in different amounts, depending on the fungal species, but always as an integral component of the fungal cell wall (Latgé 2007; Yarden and Osherov 2010).

Due to its high molecular weight and marked insolubility in most solvents, the melanin molecular structure remains undefined (Bell and Wheeler 1986). One way of studying melanin is through its physical properties detected by infrared (IR) and electron paramagnetic resonance (EPR) spectroscopy (Enochs, Nilges, and Swartz 1993; Pal, Gajjar, and Vasavada 2013). The use of specific biosynthesis inhibitors such as kojic acid (DOPA) and tricyclazole (DHN) provides indirect evidence of the type of melanin produced by a fungal species (Thines et al. 1995). This can also be achieved through phenotypic and genetic analyses of melanin-deficient or albino mutants (Bell and Wheeler 1986). More recently, some studies have reported the rapid and direct characterization of melanin by matrix-assisted laser desorption/ionization time-of-flight mass spectrometry (MALDI-TOF MS) (Beltrán-García et al. 2014; Varga et al. 2016).

We investigated the composition and biosynthesis of melanin in *P. ulei*. Specifically, we characterized melanin-containing extracts by MALDI-TOF MS and IR, tested the effects of tricyclazole on melanization *in vitro*, and investigated the presence of genes encoding enzymes involved in DHN melanin biosynthesis in a draft genome of *P. ulei*.

## MATERIAL AND METHODS

### Selection of isolate and cultivation

The experiments of characterization of dark pigments present in *P. ulei* were conducted using the isolate ERN8, collected from a rubber tree in the municipality of Eirunepé, Amazonas state (S 06°39'16.9" - W 69°54'23.8"). The same isolate was subjected to whole genome sequencing (unpublished). The strain was cultivated in 125 mL Erlenmeyer flasks (Figure 2) containing 30 mL of modified M3 medium at pH 5.0 (sucrose - 10 g, neopeptone - 6 g, potato 250 g, KH<sub>2</sub>PO<sub>4</sub> - 2 g, MgSO<sub>4</sub>.7H<sub>2</sub>O - 1 g, lysine hydrochloride - 10 mg, threonine – 0.25 mg, tryptophan - 0.25 mg, chloramphenicol - 50 mg, distilled water - 1 L) (Junqueira et al. 1984) incubated at 25 °C during 30 days under agitation in orbital shaker (125 rpm). The fungal mass was filtered, dried, and stored at -80 °C until analysis.

### Melanin extraction

The melanin present in *P. ulei* was extracted following the protocol described for *Mycosphaerella fijiensis* (Beltrán-García et al. 2014). Initially, one gram of fungal stromata was ground with a mortar and pestle in 5 mL of a NaOH 2M solution. After maceration, samples were collected in a flat bottom flask with additional 45 mL of NaOH 2M and digested at 100 °C for 3 h under reflux. After centrifugation at 2218 x g for 10 min, the supernatant was decanted into new flasks and precipitated by lowering the pH to 2.0 with concentrated HCl. Precipitates were collected by centrifugation, transferred to flat bottom flasks with 50 mL of HCl 6N and digested at 100 °C under reflux for 2 h for degradation of proteins and other macromolecules. The insoluble residues were concentrated by centrifugation, washed twice with methanol and chloroform for elimination of

lipids and dried at room temperature. The solids were re-dissolved in NaOH 2M and centrifuged for 20 min. The supernatant was precipitated with HCl, concentrated by centrifugation, washed 5 times with ultra-pure water, dried and stored at -20 °C.

### **Mass spectrometry**

Due to the marked insolubility of melanin in most solvent systems, mass spectrometric analyses were done on solid melanin extract samples using the matrix-assisted desorption-ionization technique coupled to a time-of-flight mass analyzer (MALDI-TOF). Samples were spotted on a 384/600 µm AnchorChip™ MALDI sample support (Bruker Daltonics, Germany), overlaid with 1.2 µL of the matrix solution composed of 2,5-dihydroxybenzene (DHB, 20 mg/L) in acetonitrile - 0,1% trifluoroacetic acid (1:1), and dried at room temperature.

A Ultraflex III MALDI-TOF-TOF spectrometer (Bruker Daltonics) was used. Manual shooting of spots with N<sub>2</sub> laser pulses (337 nm wavelength) was used to generate ions analyzed in the positive linear mode, in the mass-to-charge ratio range of  $m/z$  800 to 2500. Target peaks detected in the linear mode were chosen for MS/MS fragmentation using the LIFT device of the spectrometer. The Peptide Calibration Standard II (Bruker, Daltonics) was used and analyses were done with the FlexControl 3.3 software (Bruker Daltonics). Data visualization and analyses were done in FlexAnalysis 1.3 (Bruker Daltonics).

### **FT-IR spectroscopy**

To determine the presence of diagnostic functional groups in the melanin extract of *P. ulei*, aliquots of the same samples used for MALDI-TOF analysis were subject to Fourier Transform Infrared spectroscopy (FT-IR) on a Varian 660-IR FT-IR spectrometer equipped with a Pike GladiATR accessory. Spectra were

obtained in the medium infrared region from 4000 to 400  $\text{cm}^{-1}$  at 4  $\text{cm}^{-1}$  of optical resolution and by acquisition of 256 scans.

### **Histochemical assay of carbohydrates on *P. ulei* stromata**

Single stromata of isolate ERN8 cultivated on M3 medium for one month were fixed in the Zamboni's solution (0.1 M phosphate buffer, pH 7.3, containing 2% paraformaldehyde and 0.2% picric acid) (Stefanini, Martino, and Zamboni 1967) during two hours. After a dehydration sequence in ethanol (70, 80, 90 and 99%), the samples were imbibed in glycol methacrylate resin (Leica Histoiresin, Germany) and dried. Sample blocks were cut in transversal sections (3  $\mu\text{m}$ ) on an automated Leica RM2255 rotary microtome (Leica, Germany) followed by staining with the periodic acid-Schiff (PAS) (Mantle and Allen 1978), for detection of polysaccharides in the cell wall of *P. ulei* stromata. The sections were visualized in a Zeiss EM 109® optical microscope (Zeiss, Germany).

### **Inhibition of melanization**

The Bim® 750 BR (Dow AgroSciences, EUA) systemic fungicide, recommended for the control of rice blast fungus *Pyricularia oryzae* (Zhang et al. 2016), was used in the assays. Bim® 750 BR contains 75% of tricyclazole (5-methyl-1,2,4-triazolo[3,4-b] [1,3] benzothiazole), which acts as an inhibitor of the reductase enzymes in the 1,8 DHN pathway. The fungicide was dissolved in distilled water, filtered through 0.22  $\mu\text{m}$  membrane, and added to unsolidified M3 medium (Junqueira et al. 1984) in the following concentrations: 0, 30, 50 and 100  $\mu\text{g}/\text{mL}$  of tricyclazole. One-month-old colonies of isolate ERN8 grown on M3 solid medium were transferred to M3 medium amended with tricyclazole in two ways: by directly transferring of single stromata to the plates or by applying 100  $\mu\text{L}$  of a conidial suspension in distilled water ( $1 \times 10^{-5}$  mL) on the tricyclazole-medium

surface. The colonies were incubated at room temperature in the dark and evaluated weekly for 30 days.

### **Genes involved with 1,8-DHN biosynthesis in *P. ulei***

Coding sequences (CDS) of the genes for 1,3,6,8-tetrahydroxynaphthalene polyketide synthase (PKS1) in *Ascochyta rabiei* (Akamatsu et al. 2010), 1,3,6,8-tetrahydroxynaphthalene reductase (4HNR) in *Pyricularia oryzae* (Thompson et al. 2000), scytalone dehydratase (SCD1) in *C. lagenarium* (Kubo et al. 1996), and 1,3,8-trihydroxynaphthalene reductase (3HNR) in *P. oryzae* (Vidal-Cros et al. 1994) were used to query the GenBank using BLAST. Annotated and non-annotated CDS from other plant pathogenic fungi were downloaded and used to query the draft genome sequence of *P. ulei* isolate MG15 (unpublished) using the standalone blast-suite version 2.7.1+ (<ftp://ftp.ncbi.nlm.nih.gov/blast/executables/blast+/LATEST/>). A multiple alignment was built for each target gene using the 'Align Codons' option of MUSCLE software (Edgar 2004), as implemented in the MEGA 7 program (Kumar, Stecher, and Tamura 2016). The alignments were translated to amino acid sequences and subjected to Neighbor-Joining phylogenetic analyses using the Poisson model of amino-acid evolution and pairwise deletion of missing data. Clade support was inferred by making 1000 bootstrap pseudoreplicates. Functional annotation of the putative PKS1 of *P. ulei* was done using the PKS/NRPS Analysis Web-site (Bachmann and Ravel 2009) and by comparison with the PKS1 of *Zymoseptoria tritici* (Lendenmann et al. 2014).

## RESULTS

### MALDI-TOF spectrometry

MALDI-TOF spectra of the melanin extract from isolate ERN8 cultivated on liquid M3 medium showed a series of peaks equally spaced by  $m/z$  162.1 in the range of  $m/z$  851 to 1824 (Figure 3). Each of those peaks was followed by another peak 18 mass units smaller, representing a dehydration step. The regular series of peaks is typical of a polymeric structure, and the mass difference of  $m/z$  162.1 between sequential oligomers conformed to the MALDI-TOF MS data attributed to melanin isolated from the plant pathogen *Pseudocercospora fijiensis* (Beltrán-García et al. 2014) and from *Avena strigosa* (Varga et al. 2016). However, the observed mass difference between consecutive peaks does not fit the expected value of  $m/z$  158, corresponding to the 'in-chain' mass of 1,8-DHN monomers in an unbranched melanin chain (Cecchini et al. 2017) (Figure 4A).

Further examination of MALDI-TOF spectra from the melanin extract of isolate ERN8 and comparisons with MS data of other natural polymers revealed that the observed peaks correspond to an oligomer of hexose sugar molecules (Hung et al. 2008; Yamada et al. 2012), most probably belonging to polysaccharides contained in the cell walls of stromata. A closer inspection of the peaks showed that they are composed by sodium adducts  $(M+Na^+)^+$  of hexose oligomers (López-García et al. 2016). The actual masses of the oligomers can be calculated by the formula  $162.1 \times n + 22.99 + 18.01$ , where  $n$  is the number of hexose molecules, 22.99 the monoisotopic mass of  $Na^+$  and 18.01 the mass of the ending residues (Figure 4B) (López-García et al. 2016; Hung et al. 2008).

Target fragmentation of peaks at  $m/z$  851, 1013, and 1175 (Figure 5) yielded a series of daughter peaks equally spaced by  $m/z$  162.1, followed by

dehydration peaks. The smallest oligomer detected in the spectrum is that of the dimer of hexoses, represented by the peak at  $m/z$  365 ( $162 \times 2 + 22.99 + 18.01$ ) and its dehydration at  $m/z$  347 (Figure 5). A comparison between the MALDI-TOF spectrum of *P. ulei* melanin extract and the spectra attributed to melanin in black oat (*A. strigosa*) (Varga et al. 2016) and to glucans produced by the fungus *Ganoderma lucidum* (Hung et al. 2008) shows that they share the same peaks spaced by  $m/z$  162 (Figure 6).

### **FT-IR spectroscopy**

The FT-IR spectrum of the melanin extract of *P. ulei* showed three main regions of absorption (Figure 7). The broad band centered at  $3362\text{ cm}^{-1}$  is due to stretch absorptions of hydroxyl groups (O—H) involved in hydrogen bonding (Pavia et al. 2014). This absorption is found in phenolic compounds and aliphatic alcohols and may either refer to 1,8-DHN melanin or to a polysaccharide (Drewnowska et al. 2015; Chen et al. 2008).

The absorption at  $1615\text{ cm}^{-1}$  and remaining weaker absorptions in the range  $1730$  to  $1417\text{ cm}^{-1}$  can be attributed to C=C / C=O stretching vibrations of aromatic nature (Pavia et al. 2014), characteristic of aromatic melanin unities (Kumar et al. 2011; Drewnowska et al. 2015). Bands adjacent to this region ( $\sim 1640\text{ cm}^{-1}$ ) contain CO symmetrical and asymmetrical stretching vibrations of carbonyl containing carboxylic acids and amides (Chen et al. 2008), as well as bending vibrations of O—H groups (Chen et al. 2016). The presence of these bands in spectra of natural polysaccharides isolated from fungi are generally attributed to residues of sugar-associated proteins (Chen et al. 2008) or water (Deng et al. 2012; Chen et al. 2016), respectively.

The strongest absorption centered at 1061 cm<sup>-1</sup> in the FT-IR spectrum is attributed to C—O—C ether stretching vibrations, especially those involved in glycosidic bonds of polysaccharides (Deng et al. 2012; Chen et al. 2008, 2016). Phenolic compounds also exhibit C—O absorption in this region (Pavia et al. 2014). However, synthetic melanin shows only weak absorption at this region (Kumar et al. 2011; Drewnowska et al. 2015), in contrast to strong bonds found in natural polysaccharides.

The FT-IR results support the presence of hydroxylated aromatic rings in the sample, an indicative of the presence of melanin. However, they also point to the presence of polysaccharides in the samples. By comparing the obtained IR spectrum with those of synthetic melanin and fungal polysaccharides, it is possible to infer the prevalence of the latter over the former in melanin extracts of *P. ulei* (Figure 8).

### **Histochemical assay**

The micrographs of transversal sections obtained from stromata of *P. ulei* stained with the periodic acid-Schiff (PAS) are shown in Figure 9. All cellular structures were stained with the periodic acid-Schiff, indicating the predominance of polysaccharides in the cell walls of the stromatic tissues, conidiophores and conidia.

### **Inhibition of melanization by tricyclazole**

Tests with tricyclazole showed the inhibition of melanization, supporting that the melanin present in *P. ulei* is derived from 1,8-DHN. The first change in pigmentation of the colony occurred after 10 days, when a completely hyaline mycelial growth was observed (Figure 10). After 15 days of incubation, the colonies assumed a pale reddish-brown color (Figure 11B and C) but did not return to the natural black phenotype (Figure 11A) until the last day of the



evaluation. Normal growth of the colonies was observed in plates containing up to 30 µg of tricyclazole/ mL of medium. At 50 µg/mL a rather slow growth of the fungus was observed and at the concentration of 100 µg/mL there was no fungal growth, probably due to a fungitoxic effect of the fungicide (Figure 11D and H).

### **Genes involved with 1, 8-DHN biosynthesis in *P. ulei***

Putative homologs of the genes encoding for the main enzymes involved in the 1, 8-DHN melanin biosynthesis in ascomycetes were found in a draft genome of *P. ulei* isolate MG15. Only one copy of each queried gene was found in the draft genome. Local Blast searches with the 1,3,6,8-tetrahydroxynaphthalene polyketide synthase (PKS1) gene sequence from different fungal species identified a fragment of 4866 base pairs (bp) spanning through six contigs (contig numbers 03455, 31897, 40311, 50100, 35221, 09965). The multiple alignment showed that around 1650 bp of the PKS1 gene could not be found in the genome contig assembly. Analysis of the 1626 amino-acids (aa) of the putative PKS1 using the enzyme prediction tool identified motifs corresponding to fragments of the beta-ketoacyl synthase and acyl transferase domains, as well as to the entire span of the dehydratase, acyl-carrier protein (2 motifs) and the thioesterase domains (Figure 12).

The putative PKS1 of *P. ulei* formed a monophyletic group with a hypothetical protein from *P. fijiensis* in the phylogenetic tree (Figure 13). This group was placed in a larger clade containing sequences of PKS1 and other proteins involved in pigmentation from various plant pathogenic species belonging to the Dothideomycetes class. Homologous sequences of the genes coding for the two related reductase enzymes active in the biosynthesis of 1,8-DHN melanin were found in the contigs 04199 (4HNR) and 09217 (3HNR) of the

*P. ulei* genome. The multiple sequence alignment contained 892 bp, corresponding to 295 aa (including gaps). The fragments of the putative 1,3,6,8-tetrahydroxynaphthalene reductase (4HNR) and 1,3,8-trihydroxynaphthalene reductase (3HNR) proteins of *P. ulei* contained 274 and 255 aa, respectively. The phylogenetic analysis placed the putative 4HNR and 3HNR proteins of *P. ulei* in well-supported clades with homologous proteins from other Dothideomycetes taxa (Figure 14).

A single fragment of 216 bp (72 aa) belonging to contig 07297 was found when the genome of *P. ulei* was queried with DNA sequences coding for the scytalone dehydratase (SCD1) gene. The sizes of the SCD1 gene sequences retrieved from GenBank varied from 465 bp (155 aa) to 900 bp (300 aa). The phylogenetic tree constructed with data of 72 aa, covering the homologous fragment retrieved from the genome, placed the putative SCD1 from *P. ulei* in a clade with other SCD1 proteins from plant pathogenic Dothideomycetes, despite low overall support for most clades (Figure 14).

## DISCUSSION

The melanization process has evolutionary significance in the kingdoms of life, playing an important role in the adaptation of many species of fungi to extreme environments of radiation, salinity, water stress, pH, temperature and resistance to antifungal agents (Belozerskaya, Gessler, and Aver'yanov 2017; Gessler, Egorova, and Belozerskaya 2014), and directly contributes to the virulence in pathogenic fungi (Cordero and Casadevall 2017; Casadevall 2018). Melanin was supposedly abundantly present in different structures of *P. ulei*, but it had not been characterized. Thus, we combined a series of techniques to study this compound produced by *P. ulei*.

MALDI-TOF analysis was employed to characterize the black pigmented extract of *P. ulei*, after modifications of the protocol used for *M. fijiensis* (Beltrán-García et al. 2014). This method can identify and characterize biomolecules, organic molecules and microorganisms (bacteria and fungi) present in samples in the ionized gaseous state, providing the mass/charge ratio according to the time of flight (Wieser et al. 2012; Nielen 1999). In this perspective, large and insoluble molecules such as melanin can be analyzed. Instead, a series of peaks characteristic of polysaccharides (glucan) was detected in the spectra (Hung et al. 2008). The same pattern of polymer structure with mass differences of  $m/z$  162.1 occurred in the MALDI-TOF spectra of dark pigmented extracts from the fungus *P. fijiensis* and the plant *A. strigosa* (Beltrán-García et al. 2014; Varga et al. 2016). On the other hand, mass spectrometric analysis of a synthetic polymer of 1,8-DHN obtained by enzymatic polymerization revealed a series of peaks having a mass difference of  $m/z$  158, as predicted for a linear chain of this monomer (Cecchini et al. 2017). These evidences indicate that MALDI-TOF MS

data of polysaccharides have incorrectly been attributed to melanin polymers. This conclusion is supported the findings of Buskirk and colleagues that demonstrated the effects of melanin from *Aspergillus niger* in suppressing the ionization, and consequent generation of suitable MALDI-TOF spectra (Buskirk et al. 2011).

Corroborating with the misinterpretation of the spectra, the methodology used for melanin extraction involves a hot treatment with NaOH followed by another with HCl (Beltrán-García et al. 2014). Curiously, a very similar methodology can be used for the extraction of beta glucans from fungi (Kao et al. 2012; Hung et al. 2008). In addition to the examples discussed in the results section, we observed the same peaks found in the MALDI-TOF spectra of the melanin extract from *P. ulei* in surveys of polysaccharides produced by *A. fumigatus* (Fontaine et al. 2000), *G. lucidum* (Hung et al. 2008), and *Daedalea quercina* (Barrientos, Clerigo, and Paano 2016). The link between melanin and polysaccharides in the cell wall was demonstrated in a study with *Cryptococcus neoformans*, where NMR analysis showed that melanin was covalently cross-linked with polysaccharide components derived from mannose monomers present in the cell wall (Zhong et al. 2008), being difficult to dissociate.

FT-IR analysis of *P. ulei* melanin extract was done with the same samples used for MALDI-TOF MS and absorption bands from melanin and polysaccharide nature were expected. The O—H stretching band observed resembles more that of synthetic melanin, although it is not as broad, and ends at around 3000  $\text{cm}^{-1}$ . Synthetic melanin is based on L-DOPA and contains carboxylic acid groups that give rise to very broad bands in this region (Pavia et al. 2014). The stretching absorption of aromatic double bonds at 1615  $\text{cm}^{-1}$  is supportive of the presence

of melanin in the sample, although bands around this region are often found in the IR spectra of natural fungal polysaccharides and considered as contamination by proteins or water. On the other hand, the strong absorption around  $1050\text{ cm}^{-1}$  is not present in the spectra of synthetic melanins but is characteristic of C—O—C ether stretching vibrations of carbohydrates. These data support the interpretation of a mixture of melanin and carbohydrates present in the dark extract of *P. ulei*. The co-occurrence of melanin pigments and polysaccharide appears to be commonplace in studies of naturally extracted melanins, where the C—O—C strong stretching absorption of polysaccharide nature is often detected in the IR spectra of supposed purified melanins (Drewnowska et al. 2015; Suryanarayanan et al. 2004; Raman and Ramasamy 2017).

The histochemical tests support the results obtained in MALDI-TOF and FT-IR analyses. Stromata structures stained positive with the periodic acid-Schiff (PAS), thus showing the abundant presence of polysaccharides as the main component of these structures. Periodic acid Schiff (PAS) is a method commonly used in histochemical analysis to detect polysaccharides and glycoproteins in diverse tissues. In this reaction, the periodic acid is responsible for oxidizing glucose residues (glycols), producing two aldehyde molecules, which will react with Schiff's reagent producing the magenta coloration (Bangle and Alford 1954). Structures of stromata have a large amount of carbohydrates and are usually poor in proteins on the cell walls. Stromata of *Cordyceps scarabaecola* showed large quantities of the carbohydrates glucose (46.6%), mannose (35.4%) and galactose (18.0%) (Yu, Kim, and Suh 2003).

After spectroscopy and histochemical methods confirmed the predominant presence of polysaccharides, we used the fungicide tricyclazole to study the route

of melanin biosynthesis in *P. ulei*. Tricyclazole as well pyroquilon and phthalide are known as specific inhibitors of the 1,8-DHN melanin pathway but are not capable of inhibiting the synthesis of other types of melanin, such as the L-DOPA melanin (Elliott 1995). Addition of tricyclazole to culture medium drastically inhibited the production of melanin in *P. ulei* in the first days in all concentrations without affecting the growth, thus providing indirect evidences that melanin is synthesized via 1,8-DHN in *P. ulei* (Cunha et al. 2005).

The effect of tricyclazole (5-methyl-1,2,4-triazolo [3,4-b] benzothiazole) has been demonstrated in several fungi, generally related to a decrease in virulence, through the reduction of conidial germination, growth and development of the mycelium due to inhibition of mitochondrial respiration (Kong et al. 2018; Kumar et al. 2015). In 1,8-DHN melanin pathway, tricyclazole inhibits two reductases, 1,3,6,8-tetrahydroxynaphthalene to scytalone and 1,3,8-trihydroxynaphthalene to vermelone (Langfelder et al. 2003), resulting in the accumulation of intermediates such as flaviolin, 3-Hydroxyjuglone and 2-Hydroxyjuglone, and other shunt products of their transformation (Beltrán-García et al. 2014). Future adjustments in tricyclazole concentration and incubation conditions of *P. ulei* will be done to optimize the production of light-colored mycelia and melanin-free nucleic acid extracts suitable for molecular biological investigations.

To further support the conclusions reached with the tricyclazole assay, we searched a draft genome sequence of *P. ulei* strain MG15 for putative homologous sequences of the genes coding for the main enzymes active in the biosynthesis of 1,8-DHN. We found only one version of each gene in the genome sequence, indicating that these are orthologues of the known biosynthetic genes

found in other ascomycetes. Phylogenetic analyses conducted with the inferred amino acid sequences of four putative enzymes involved in the melanin biosynthesis in *P. ulii* (PKS1, 4HNR, SCD1, 3HNR) placed them in clades containing homologous protein sequences from related plant pathogens of the Dothideomycetes class. The incompleteness of sequences coding for the putative PKS1 and SCD1 found in the genome is most probably a result of the sequencing process and not real gene deletion events.

The genes involved in the melanization process are usually organized in biosynthetic gene cluster (BGC) (Ebert et al. 2018; Keller, Turner, and Bennett 2015). Among the four main genes that encode the enzymes responsible for the biosynthesis of 1,8 DHN, the PKS1 gene that encodes the enzyme polyketide synthase is the most important, being the target of several studies ranging from attenuation in the conidia pigmentation to the Quantitative Trait Loci (Loppnau, Tanguay, and Breuil 2004; Lendenmann et al. 2014). The fungal PKS1 is composed of functional domains: beta-ketoacyl synthase (KS), acyl transferase (AT), and acyl-carrier protein (ACP), and optional thioesterase (TE) and dehydratase (DH) domains (Keller, Turner, and Bennett 2005). In orchestrated way PKS domains join head to tail into a linear chain and cyclization of acetate molecules (Butler and Day 1998). After complete assembly of *P. ulii* genome, all these domains can be better studied, and their functions elucidated.

We investigated the nature of the compounds present in the black stromata typically formed by *P. ulii* on the host surfaces and on culture media and found evidences for two major components: polysaccharides and 1,8-DHN melanin. Our results also suggest that mass spectrometric data on abundant polysaccharides have incorrectly been attributed to melanin in recent literature

reports. Besides probing the nature of the melanin produced by *P. ulei*, the results obtained with the tricyclazole assay provide a strategy for the development of a cultivation protocol that will facilitate the extraction of nucleic acids and proteins from this important but difficult plant pathogen.



## ACKNOWLEDGMENTS

We are grateful to the Núcleo de Análise de Biomoléculas of the Universidade Federal de Viçosa for providing the facilities for the conduction of the experiments. The authors also acknowledge the financial support by the following Brazilian agencies: Fundação de Amparo à Pesquisa do Estado de Minas Gerais (Fapemig), Coordenação de Aperfeiçoamento de Pessoal de Nível Superior (CAPES), Conselho Nacional de Desenvolvimento Científico e Tecnológico (CNPq), Financiadora de Estudos e Projetos (Finep) and Sistema Nacional de Laboratórios em Nanotecnologias (SisNANO)/Ministério da Ciência, Tecnologia e Informação (MCTI). Dr Humberto Josué de Oliveira Ramos and Edvaldo Barros for the help with MALDI-TOF analysis and friendship. We thank Dr. José Eduardo Serrão and Wagner Gonçalves of the Laboratório de Ultraestrutura Celular/UFV for helping with the histochemistry analysis. Felipe Moura of the Central Analítica UFAM/AM for helping with the interpretation of spectra from Maldi-tof Analysis. Ricardo Oliveira for providing the BIM fungicide. This study was financed in part by the Coordenação de Aperfeiçoamento de Pessoal de Nível Superior - Brasil (CAPES) - Finance Code 001.

## REFERENCES

- Akamatsu, H. O., Chilvers, M. I., Stewart, J. E., and Peever, T. L. 2010. Identification and function of a polyketide synthase gene responsible for 1,8-dihydroxynaphthalene-melanin pigment biosynthesis in *Ascochyta rabiei*. **Current Genetics**. 56:349–360.
- Alspaugh, J. A., Perfect, J. R., and Heitman, J. 1998. Signal transduction pathways regulating differentiation and pathogenicity of *Cryptococcus neoformans*. **Fungal Genetics and Biology**. 25:1–14.
- Bachmann, B. O., and Ravel, J. 2009. Methods for *in silico* prediction of microbial polyketide and nonribosomal peptide biosynthetic pathways from dna sequence data. **Methods in enzymology**. 458,181–217.
- Bangle, R., and Alford, W. C. 1954. The chemical basis of the periodic acid Schiff reaction of collagen fibers with reference to periodate consumption by collagen and by insulin. **The journal of Histochemistry and Cytochemistry**. 2:62–76.
- Barrientos, R. C., Clerigo, M. M., and Paano, A. M. C. 2016. Extraction, isolation and MALDI-QTOF MS/MS analysis of  $\beta$ - d -glucan from the fruiting bodies of *Daedalea quercina*. **International Journal of Biological Macromolecules**. 93:226–234.
- Bell, A. A., and Wheeler, M. H. 1986. Biosynthesis and functions of fungal melanins. **Annual Review of Phytopathology**. 24:411–451.
- Belozerskaya, T. A., Gessler, N. N., and Aver'yanov, A. A. 2017. Melanin pigments of fungi. **Fungal Metabolites**. 263–291.
- Beltrán-García, M. J., Prado, F. M., Oliveira, M. S., Ortiz-Mendoza, D., Scalfio, A. C., Pessoa, A., et al. 2014. Singlet molecular oxygen generation by light-activated dhn-melanin of the fungal pathogen *Mycosphaerella fijiensis* in Black Sigatoka disease of bananas. **PLoS one**. 9:e91616.
- Bloomfield, B. J., and Alexander, M. 1967. Melanins and resistance of fungi to lysis. **Journal of Bacteriology**. 93:1276–80.
- Buskirk, A. D., Hettick, J. M., Chipinda, I., Law, B. F., Siegel, P. D., Slaven, J. E., Green, B. J., and Beezhold, D. H. 2011. Fungal pigments inhibit the matrix-assisted laser desorption/ionization time-of-flight mass spectrometry analysis of darkly pigmented fungi. **Analytical Biochemistry**. 411:122–128.
- Butler, M. J., and Day, A. W. 1998. Fungal melanins: a review. **Canadian Journal of Microbiology**. 44:1115–1136.

- Casadevall, A. 2018. Melanin triggers antifungal defences. **Nature**. 555:319–320.
- Cecchini, M. M., Reale, S., Manini, P., d'Ischia, M., and De Angelis, F. 2017. Modeling fungal melanin buildup: biomimetic polymerization of 1,8-dihydroxynaphthalene mapped by mass spectrometry. **Chemistry - A European Journal**. 23:8092–8098.
- Chee, K. H. 1978. South American Leaf Blight of *Hevea brasiliensis*: culture of *Microcyclus ulei*. **Transactions of the British Mycological Society**. 70:341–344.
- Chen, F., Ren, C.-G., Zhou, T., Wei, Y.-J., and Dai, C.-C. 2016. A novel exopolysaccharide elicitor from endophytic fungus *Gilmaniella* sp. AL12 on volatile oils accumulation in *Atractylodes lancea*. **Scientific Reports**. 6:34735.
- Chen, Y., Xie, M.-Y., Nie, S.-P., Li, C., and Wang, Y.-X. 2008. Purification, composition analysis and antioxidant activity of a polysaccharide from the fruiting bodies of *Ganoderma atrum*. **Food Chemistry**. 107:231–241.
- Chen, Z., Nunes, M. A., Silva, M. C., and Rodrigues, C. J. 2004. Appressorium turgor pressure of *Colletotrichum kahawae* might have a role in coffee cuticle penetration. **Mycologia**. 96:1199–208.
- Chumley, F. G. 1990. Genetic analysis of melanin-deficient, nonpathogenic mutants of *Magnaporthe grisea*. **Molecular Plant-Microbe Interactions**. 3:135.
- Cordero, R. J. B., and Casadevall, A. 2017. Functions of fungal melanin beyond virulence. **Fungal Biology Reviews**. 31:99–112.
- Cunha, M. M. L., Franzen, A. J., Alviano, D. S., Zanardi, E., Alviano, C. S., De Souza, W., and Rozental, S. 2005. Inhibition of melanin synthesis pathway by tricyclazole increases susceptibility of *Fonsecaea pedrosoi* against mouse macrophages. **Microscopy Research and Technique**. 68:377–384.
- Deng, C., Hu, Z., Fu, H., Hu, M., Xu, X., and Chen, J. 2012. Chemical analysis and antioxidant activity in vitro of a  $\beta$ -d-glucan isolated from *Dictyophora indusiata*. **International Journal of Biological Macromolecules**. 51:70–75.
- Drewnowska, J. M., Zambrzycka, M., Kalska-Szostko, B., Fiedoruk, K., and Swiecicka, I. 2015. Melanin-like pigment synthesis by soil *Bacillus weihenstephanensis* isolates from northeastern Poland. **PloS one**. 10:e0125428.
- Ebert, M., Spanner, R., Jonge, R. de, Smith, D., Holthusen, J., Secor, G., Thomma, B., and Bolton, M. 2018. Gene cluster conservation identifies melanin and perylenequinone biosynthesis pathways in multiple plant pathogenic fungi.

bioRxiv. :379305.

Edgar, R. C. 2004. MUSCLE: multiple sequence alignment with high accuracy and high throughput. **Nucleic Acids Research**. 32:1792–1797.

Elliott, M. L. 1995. Effect of melanin biosynthesis inhibiting compounds on *Gaeumannomyces* species. **Mycologia**. 87:370.

Enochs, W. S., Nilges, M. J., and Swartz, H. M. 1993. A standardized test for the identification and characterization of melanins using electron paramagnetic resonance (EPR) spectroscopy. **Pigment Cell Research**. 6:91–9.

Fontaine, T., Simenel, C., Dubreucq, G., Adam, O., Delepierre, M., Lemoine, J., Vorgias, C. E., Diaquin, M., and Latgé, J-P. 2000. Molecular organization of the alkali-insoluble fraction of *Aspergillus fumigatus* cell wall. **Journal of Biological Chemistry**. 275:27594–607.

Funa, N., Ohnishi, Y., Fujii, I., Shibuya, M., Ebizuka, Y., and Horinouchi, S. 1999. A new pathway for polyketide synthesis in microorganisms. **Nature**. 400:897–899.

Garcia, D., Carels, N., Koop, D. M., de Sousa, L. A., Andrade Junior, S. J. de, Pujade-Renaud, V., Mattos, C. R. R., and Cascardo, J. C. M. 2011. EST profiling of resistant and susceptible *Hevea* infected by *Microcyclus ulei*. **Physiological and Molecular Plant Pathology**. 76:126–136.

Gasparotto, L., Santos, A. D., Pereira, J. C. R., and Ferreira, F. V. 1997. Doenças da seringueira no Brasil. EMBRAPA-SPI/Manaus: EMBRAPA-CPAA.

Gessler, N. N., Egorova, A. S., and Belozerskaya, T. A. 2014. Melanin pigments of fungi under extreme environmental conditions. **Applied Biochemistry and Microbiology**. 50:105–113.

Grandin, G. 2009. Fordlandia: the rise and fall of Henry Ford's forgotten jungle city. **New York: Metropolitan**. 398.

Mantle, M., and Allen, A. 1978. A colorimetric assay for glycoproteins based on the periodic acid/Schiff stain [proceedings]. **Biochemical Society transactions**. 6:607–9.

Hennings, P. 1904. Über die auf Hevea-arten bisher beobachteten parasitischen pilze. **Notizblatt des Königl. botanischen Gartens und Museums zu Berlin**. 4:133.

Hora Júnior, B. T. da, de Macedo, D. M., Barreto, R. W., Evans, H. C., Mattos, C.

R. R., Maffia, L. A., and Mizubuti, E. S. G. 2014. Erasing the past: a new identity for the damoclean pathogen causing South American leaf blight of rubber. **PloS one**. 9:e104750.

Hung, W.-T., Wang, S.-H., Chen, C.-H., and Yang, W.-B. 2008. Structure determination of  $\beta$ -glucans from *Ganoderma lucidum* with Matrix-assisted Laser Desorption/ionization (MALDI) Mass Spectrometry. **Molecules**. 13:1538–1550.

Junqueira, N. T. V., Chavees, G. M., Zambolim, L., Romeiro, R. da S., and Gasparotto, L. 1984. Isolamento, cultivo e esporulação de *Microcyclus ulei*, agente etiológico do mal-das-folhas da seringueira. **Revista Ceres**. 31:322–331.

Kao, P.-F., Wang, S.-H., Hung, W.-T., Liao, Y.-H., Lin, C.-M., and Yang, W.-B. 2012. Structural characterization and antioxidative activity of low-molecular-weights beta-1,3-glucan from the residue of extracted *Ganoderma lucidum* fruiting bodies. **Journal of Biomedicine & Biotechnology**. 2012:673764.

Keller, N. P., Turner, G., and Bennett, J. W. 2005. Fungal secondary metabolism - from biochemistry to genomics. **Nature Reviews Microbiology**. 3:937–947.

Keller, N. P., Turner, G., and Bennett, J. W. 2015. Translating biosynthetic gene clusters into fungal armor and weaponry. **Nature Chemical Biology**. 11:671–677.

Kong, Q., Yu, X., Song, D., and Ren, X. 2018. Effect of tricyclazole on morphology, virulence and gene expression of *Aspergillus aculeatus* for management of soft rot disease in peach. **Journal of Applied Microbiology**.

Kubo, Y., Takano, Y., Endo, N., Yasuda, N., Tajima, S., and Furusawa, I. 1996. Cloning and structural analysis of the melanin biosynthesis gene SCD1 encoding scytalone dehydratase in *Colletotrichum lagenarium*. **Applied and Environmental Microbiology**. 62:4340–4.

Kumar, C. G., Mongolla, P., Pombala, S., Kamle, A., and Joseph, J. 2011. Physicochemical characterization and antioxidant activity of melanin from a novel strain of *Aspergillus bridgeri* ICTF-201. **Letters in Applied Microbiology**. 53:350–358.

Kumar, M., Chand, R., Dubey, R. S., and Shah, K. 2015. Effect of tricyclazole on morphology, virulence and enzymatic alterations in pathogenic fungi *Bipolaris sorokiniana* for management of Spot Blotch disease in barley. **World Journal of Microbiology and Biotechnology**. 31:23–35.

Kumar, S., Stecher, G., and Tamura, K. 2016. MEGA7: Molecular evolutionary genetics analysis version 7.0 for bigger datasets. **Molecular Biology and**

**Evolution.** 33:1870–1874.

Kuo, M. J., and Alexander, M. 1967. Inhibition of the lysis of fungi by melanins. **Journal of Bacteriology.** 94:624–9.

Langfelder, K., Streibel, M., Jahn, B., Haase, G., and Brakhage, A. A. 2003. Biosynthesis of fungal melanins and their importance for human pathogenic fungi. **Fungal Genetics and Biology.** 38:143–58.

Latgé, J.-P. 2007. The cell wall: a carbohydrate armour for the fungal cell. **Molecular Microbiology.** 66:279–290.

Lendenmann, M. H., Croll, D., Stewart, E. L., and McDonald, B. A. 2014. Quantitative trait locus mapping of melanization in the plant pathogenic fungus *Zymoseptoria tritici*. **G3: Genes, Genomes, Genetics.** 4:2519–2533.

Lieberei, R. 2007. South American leaf blight of the rubber tree (*Hevea* spp.): new steps in plant domestication using physiological features and molecular markers. **Annals of botany.** 100:1125–42.

López-García, M., García, M. S. D., Vilariño, J. M. L., and Rodríguez, M. V. G. 2016. MALDI-TOF to compare polysaccharide profiles from commercial health supplements of different mushroom species. **Food Chemistry.** 199:597–604.

Loppnau, P., Tanguay, P., and Breuil, C. 2004. Isolation and disruption of the melanin pathway polyketide synthase gene of the softwood deep stain fungus *Ceratocystis resinifera*. **Fungal Genetics and Biology.** 41:33–41.

Mantle, M., and Allen, A. 1978. A colorimetric assay for glycoproteins based on the periodic acid/Schiff stain [proceedings]. **Biochemical Society transactions.** 6:607–9

Nielen, M. W. F. 1999. Maldi time-of-flight mass spectrometry of synthetic polymers. **Mass Spectrometry Reviews.** 18:309–344.

Nosanchuk, J. D., Stark, R. E., and Casadevall, A. 2015. Fungal melanin: what do we know about structure? **Frontiers in Microbiology.** 6:1463.

Pal, A. K., Gajjar, D. U., and Vasavada, A. R. 2013. DOPA and DHN pathway orchestrate melanin synthesis in *Aspergillus* species. **Medical Mycology.** 52:1–9.

Pavia, D. L., Lampman, G. M., Kriz, G. S., and Vyvyan, J. R. 2014. Introduction to spectroscopy. **Cengage Learning.**

Pihet, M., Vandeputte, P., Tronchin, G., Renier, G., Saulnier, P., Georgeault, S.,

Mallet, R., Chabasse, D., Symoens, F., and Bouchara, J-P. 2009. Melanin is an essential component for the integrity of the cell wall of *Aspergillus fumigatus* conidia. **BMC Microbiology**. 9:177.

Raman, N. M., and Ramasamy, S. 2017. Genetic validation and spectroscopic detailing of DHN-melanin extracted from an environmental fungus. **Biochemistry and Biophysics Reports**. 12:98–107.

Stefanini, M., Martino, C. De, and Zamboni, L. 1967. Fixation of ejaculated spermatozoa for electron microscopy. **Nature**. 216:173–174.

Suryanarayanan, T. S., Ravishankar, J. P., Venkatesan, G., and Murali, T. S. 2004. Characterization of the melanin pigment of a cosmopolitan fungal endophyte. **Mycological Research**. 108:974–8.

Thines, E., Daußmann, T., Sterner, O., Semar, M., and Anke, H. 1995. Fungal melanin biosynthesis inhibitors: introduction of a test system based on the production of dihydroxynaphthalene (DHN) melanin in agar cultures. **Zeitschrift für Naturforschung**. 50:813–819.

Thompson, J. E., Fahnestock, S., Farrall, L., Liao, D.-I., Valent, B., and Jordan, D. B. 2000. The second naphthol reductase of fungal melanin biosynthesis in *Magnaporthe grisea*. **Journal of Biological Chemistry**. 275:34867–34872.

Varga, M., Berkesi, O., Darula, Z., May, N. V., and Palágyi, A. 2016. Structural characterization of allomelanin from black oat. **Phytochemistry**. 130:313–320.

Vidal-Cros, A., Viviani, F., Labesse, G., Boccara, M., and Gaudry, M. 1994. Polyhydroxynaphthalene reductase involved in melanin biosynthesis in *Magnaporthe grisea*. **The FEBS Journal**. 219:985–92.

White, L. P. 1958. Melanin: a naturally occurring cation exchange material. **Nature**. 182:1427–1428.

Wieser, A., Schneider, L., Jung, J., and Schubert, S. 2012. MALDI-TOF MS in microbiological diagnostics - identification of microorganisms and beyond (mini review). **Applied Microbiology and Biotechnology**. 93:965–974.

Yamada, M., Yao, I., Hayasaka, T., Ushijima, M., Matsuura, M., Takada, H., Shikata, N., Setou, M., Kwon, A-H., and Ito, S. 2012. Identification of oligosaccharides from histopathological sections by MALDI imaging mass spectrometry. **Analytical and Bioanalytical Chemistry**. 402:1921–1930.

Yarden, O., and Osherov, N. 2010. The cell wall of filamentous fungi. In: Cellular and molecular biology of filamentous fungi. **American Society of Microbiology**.

224–237.

Yu, K. W., Kim, K. M., and Suh, H. J. 2003. Pharmacological activities of stromata of *Cordyceps scarabaecola*. **Phytotherapy Research**. 17:244–249.

Zhang, N., Luo, J., Rossman, A. Y., Aoki, T., Chuma, I., Crous, P. W., Dean, R.; de Vries, R. P., Donofrio, N.; Hyde, K. D., Lebrun, M-H., Talbot, N. J., Tharreau, D., Tosa, Y., Valent, B., Wang, Z., and Xu, J-R. 2016. Generic names in Magnaporthales. **IMA Fungus**. 7:155–159.

Zhong, J., Frases, S., Wang, H., Casadevall, A., and Stark, R. E. 2008. Following fungal melanin biosynthesis with solid-state NMR: biopolymer molecular structures and possible connections to cell-wall polysaccharides. **Biochemistry**. 47:4701–4710.



## FIGURE LEGENDS

**Figure 1.** Schematic representation of DHN-melanin biosynthesis in fungi. Arrows indicate each step of the biosynthetic pathway and red bars represent the inhibition points by the fungicide tricyclazole. Enzymes involved in biosynthesis are shown in bold, dehydration (-H<sub>2</sub>O) and reduction (+H<sup>+</sup>) reactions involved are indicated. The full descriptions about enzymes and reactions are described in the text. Adapted from Bell and Wheeler (1986).

**Figure 2.** Dark pigments present in *Pseudocercospora ulei*. **A:** Fungus growing in M3 liquid medium. **B:** Fungus growing and sporulating on solid M3 medium in a Petri's dish. **C:** Fungus preserved in slanted BSA medium in test tube.

**Figure 3.** MALDI-TOF spectrum of the melanin extract of the *P. ulei* isolate ERN8 in the positive mode, in the range of *m/z* 800 to 2500. The regular spacing of *m/z* 162.1 between sequential peaks of the putative melanin polymer is annotated in the spectrum

**Figure 4.** Graphical representation of the polymerization of 1,8-DHN and glucose. **A:** The polymerization of 1,8-DHN to form melanin occurs by oxidative coupling of aromatic rings, generating C–C bonds between naphthalene unities, with the consecutive loss of two hydrides (2H<sup>-</sup>) (Dewick, 2002). The formula to calculate the mass of oligomers in a series of peaks spaced by *m/z* 158 of a MALDI-TOF spectrum is  $158 \times n + 2.02 + 1.01$  (in the positive mode) or  $158 \times n + 2.02 - 1.01$  (in the negative mode, Cecchini et al. 2017), where *n* is the number of 1,8-DHN unities, 2.02 the mass of end H atoms highlighted in blue in the polymer, and 1.01 the mass of the proton gained (M+H<sup>+</sup>)<sup>+</sup> or lost (M-H<sup>+</sup>)<sup>+</sup> during the ionization; **B:** The polymerization of glucose and other pyranose monosaccharides occurs via glycosidic bonds between the carbonyl of the anomeric carbon 1 and hydroxyl groups of other glucose molecules, with the consecutive loss of one water molecule. The figure shows the 1,3 bonding of a polysaccharide resulting in the 'in chain' differences of *m/z* 162 between oligomers. The mass of the oligomers in a MALDI-TOF spectrum can be calculated by the formula described in the main text.

**Figure 5.** Fragmentation of the peak at *m/z* 1175.5 observed in the MALDI-TOF spectrum of the melanin extract from isolate ENR78 of *Pseudocercospora ulei*.

**Figure 6.** MALDI-TOF mass spectra of **A:** spectrum obtained in this study of *Pseudocercospora ulei*; **B:** 'p-coumaric acid melanin' of black oat (Varga et al. 2016). **C:** glucan of *Ganoderma lucidum* (Hung et al. 2008); Spectra B and C were adapted from the respective publications.

**Figure 7.** FT-IR spectrum of dark pigments present in stromata from isolate ERN8 of *Pseudocercospora ulei*.

**Figure 8.** FT-IR spectra of **A:** melanin extract obtained in this study from *Pseudocercospora ulei*; **B:** Polysaccharides of *Ganoderma atrum* (Chen et al. 2008); **C:** Synthetic melanin (Kumar et al. 2011). Spectra B and C were adapted from the respective publications.

**Figure 9.** Micrographs of sections of stromata (A, B, C), conidiophores and conidia (D) of *Pseudocercospora ulei* stained with the periodic acid-Schiff (PAS) reagent for specific detection of polysaccharides.

**Figure 10.** Mycelial growth and sporulation of *Pseudocercospora ulei* in M3 medium. **A:** Sporulation of *P. ulei* at 30 days in M3 medium (Control); **B:** Sporulation of *P. ulei* at 30 days in M3 medium supplemented with 30 µg/ mL of Tricyclazole; **C:** Hyaline mycelial growth of *P. ulei* at 10 days in M3 medium supplemented with 30 µg/ mL of Tricyclazole.

**Figure 11.** Inhibition of the pathway of melanin synthesis present in *Pseudocercospora ulei* cultured in M3 medium supplied with different concentrations of Tricyclazole. **A-E:** growth of *P. ulei* without tricyclazole; **B-F:** growth of *P. ulei* with 30 µg/ mL of Tricyclazole; **C-G:** growth of *P. ulei* with 50 µg/ mL of Tricyclazole; **D-H:** growth of *P. ulei* with 100 µg/ mL of Tricyclazole.

**Figure 12.** Schematic representation of the PKS1 protein of *Zymoseptoria tritici* (Lendenmann et al. 2014) and the putative homolog of *Pseudocercospora ulei*. The whole protein contains 1275 amino acids and the following functional domains are highlighted: beta-ketoacyl synthase (KS), acyl transferase (AT), dehydratase (DH), acyl-carrier protein (ACP) and thioesterase (TE) domains. Opaque regions in the KS and AT domains of *P. ulei* PKS1 correspond to missing data.

**Figure 13.** Neighbor-Joining phylogenetic tree of PKS1 and related proteins involved in the melanization of fungi.

**Figure 14.** Neighbor-Joining phylogenetic tree of 4HNR and 3HNR proteins involved in the melanization of fungi.

**Figure 15.** Neighbor-Joining phylogenetic tree of SCD1 proteins involved in the melanization of fungi.

## FIGURES AND TABLES

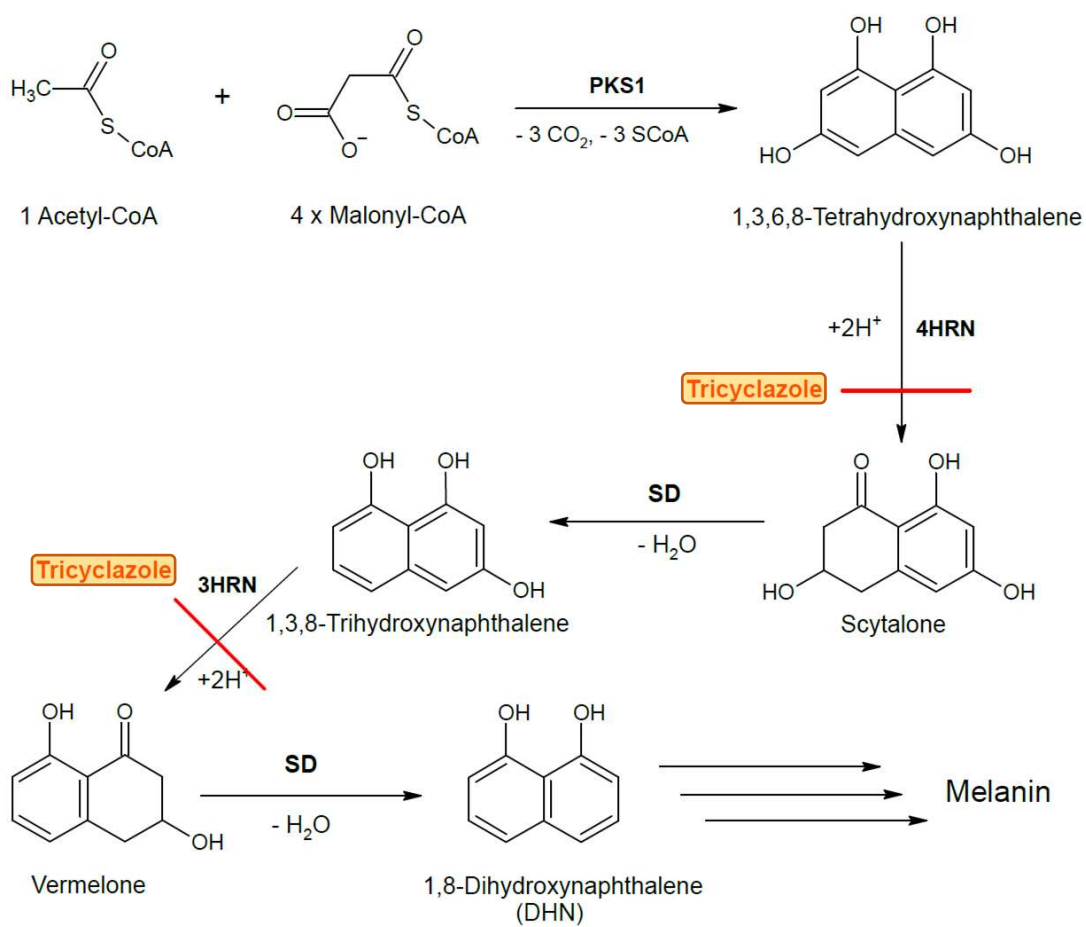


Figure 1. Ferreira et al. 2018.

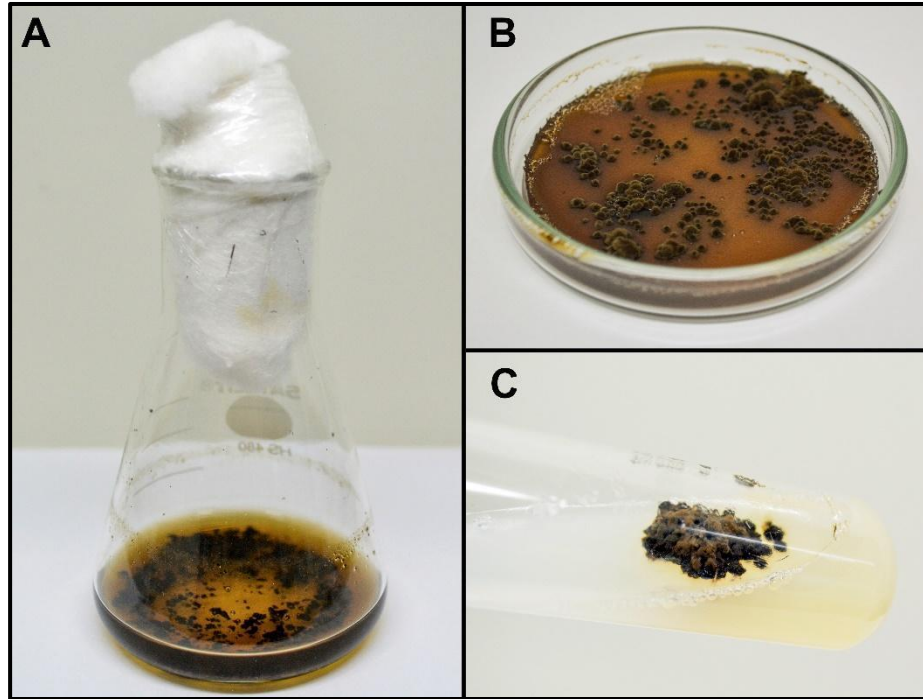


Figure 2. Ferreira et al. 2018.

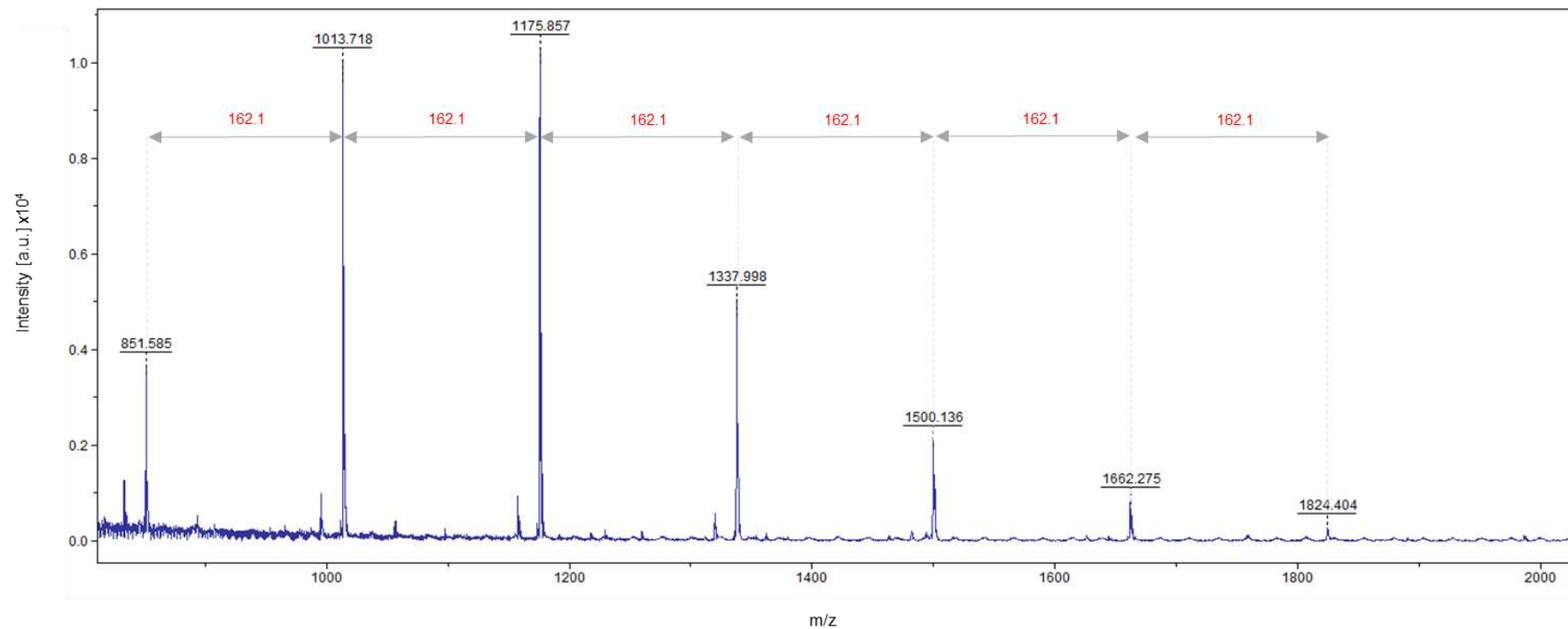
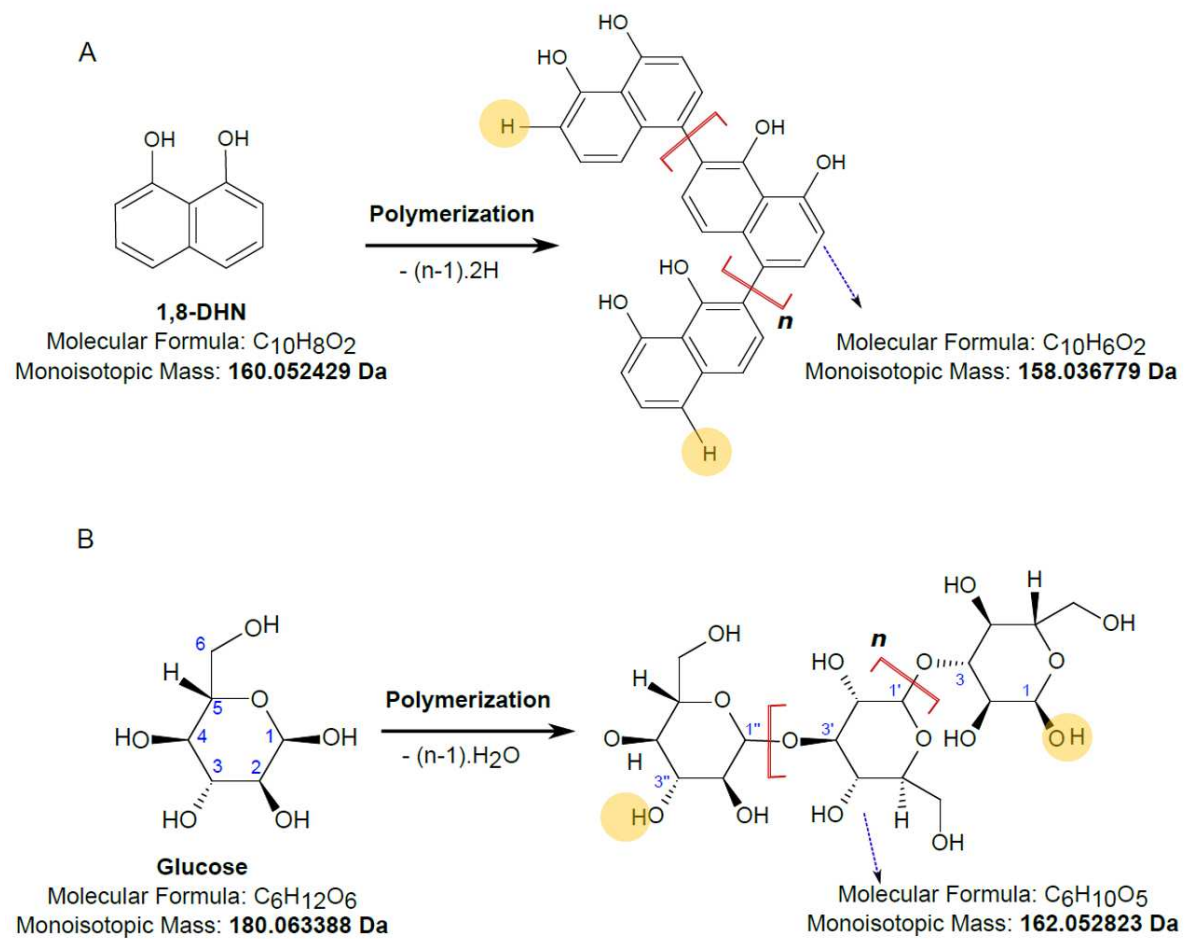


Figure 3. Ferreira et al. 2018.



**Figure 4. Ferreira et al. 2018.**

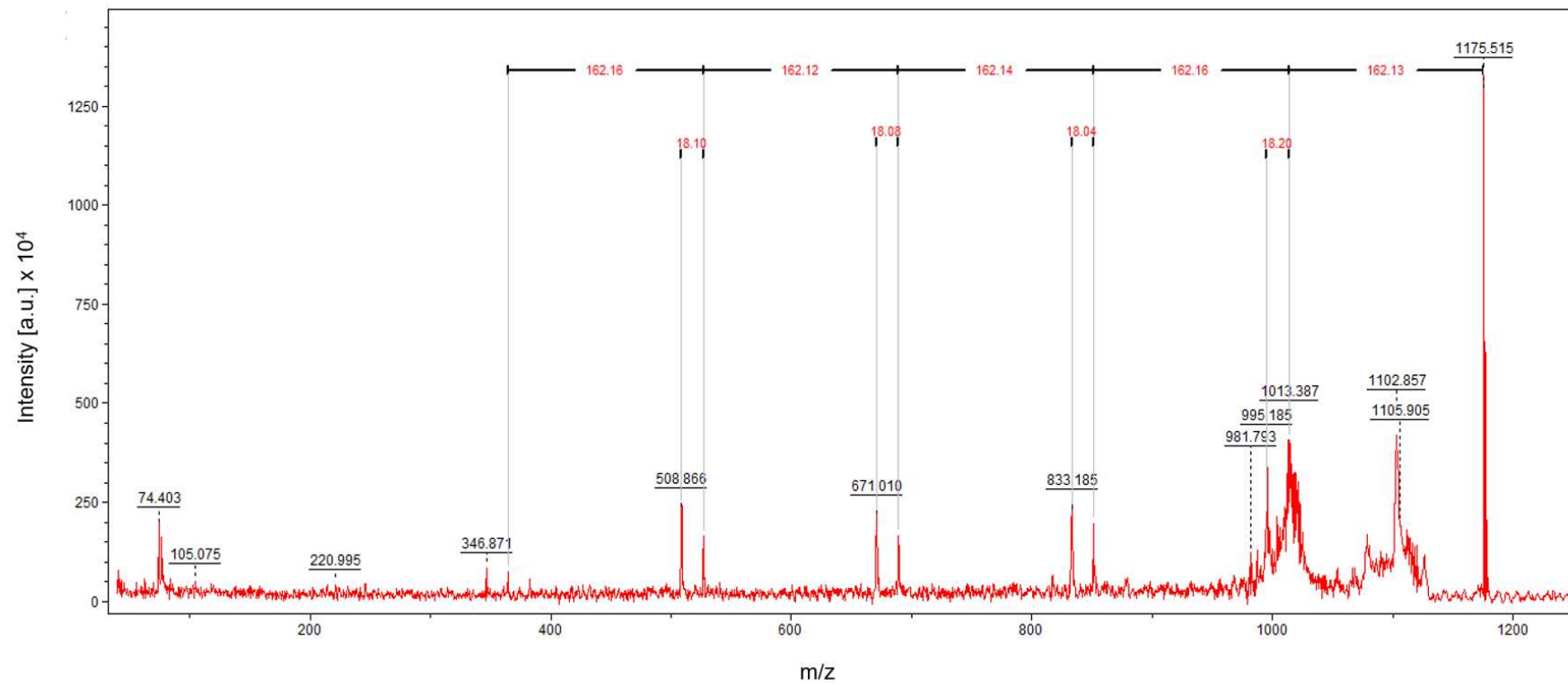


Figure 5. Ferreira et al. 2018.



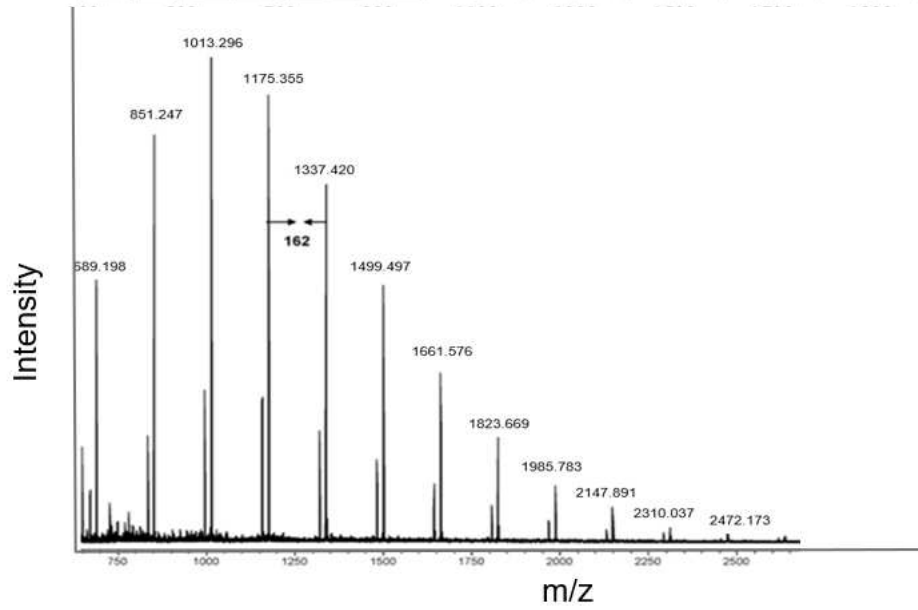
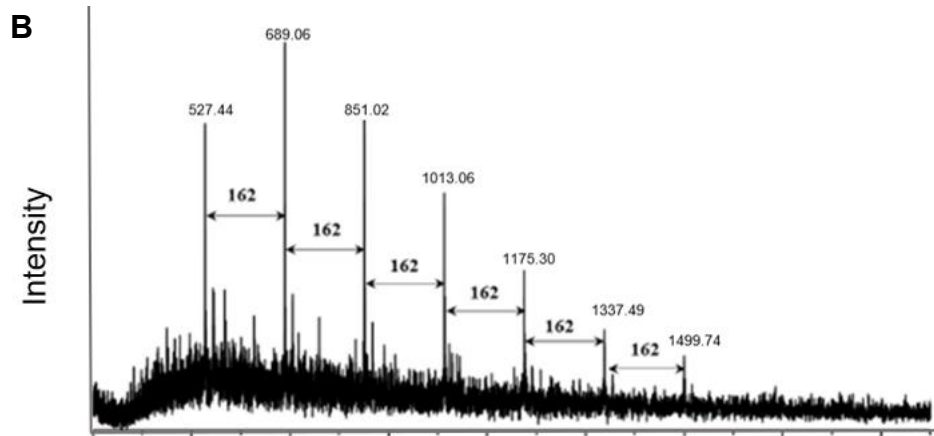
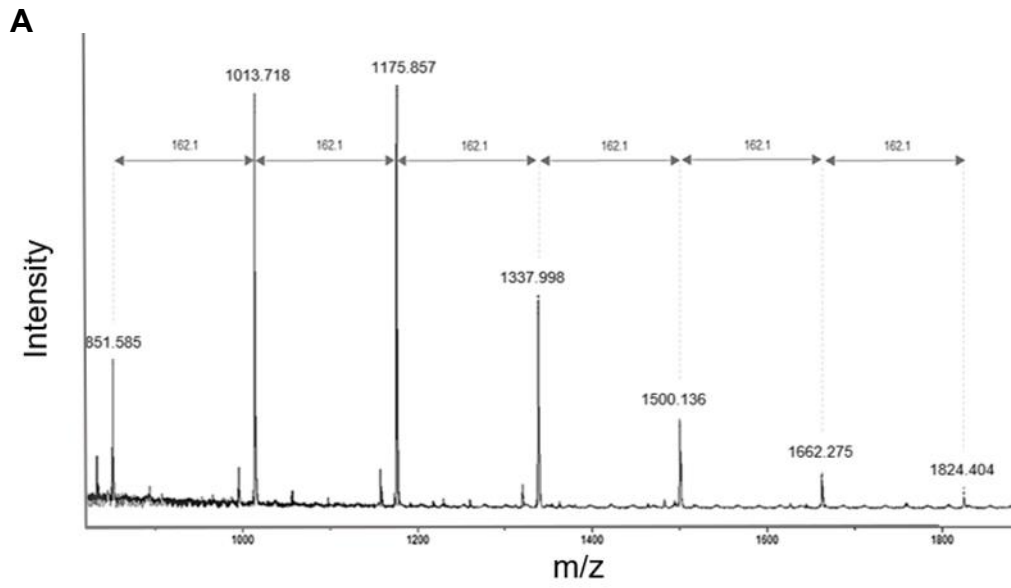


Figure 6. Ferreira et al. 2018.

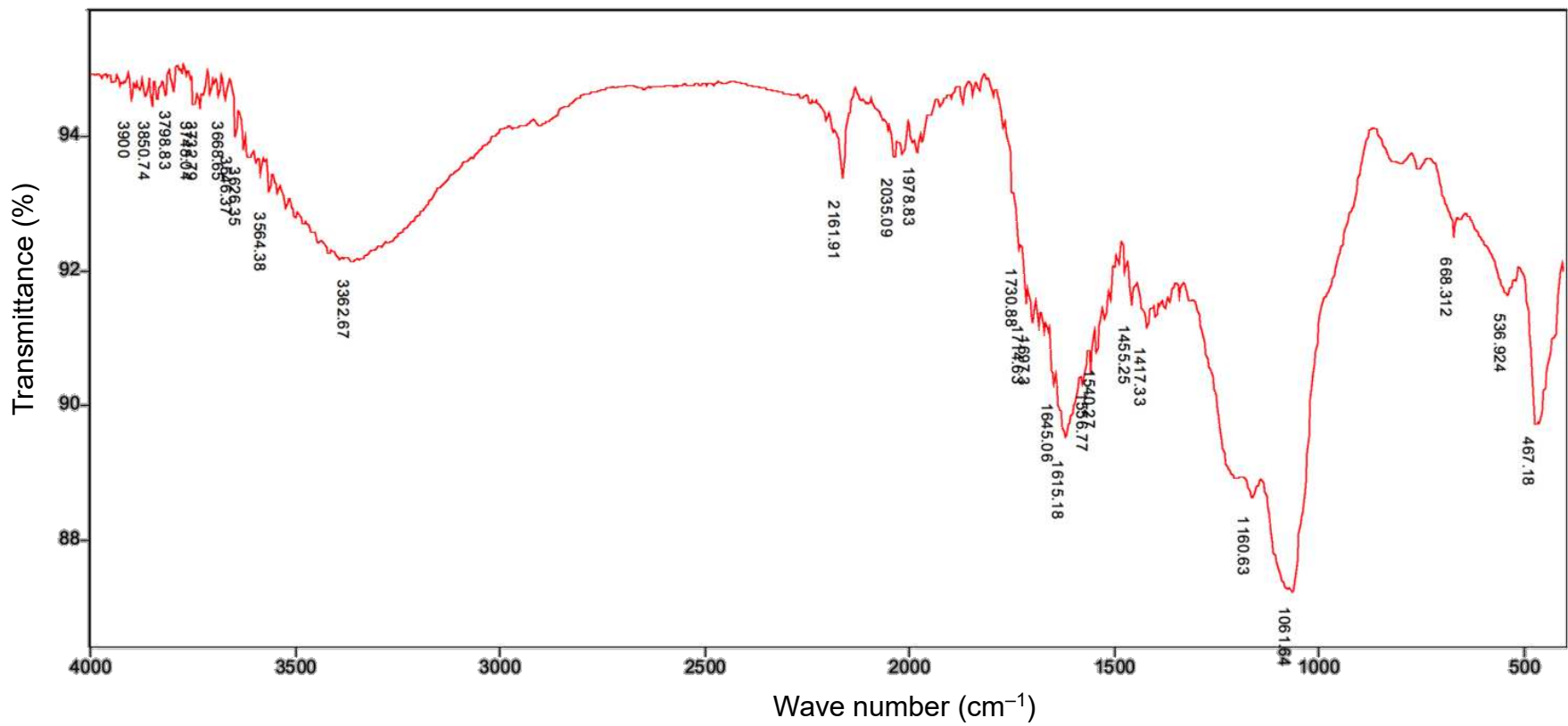


Figure 7. Ferreira et al. 2018.

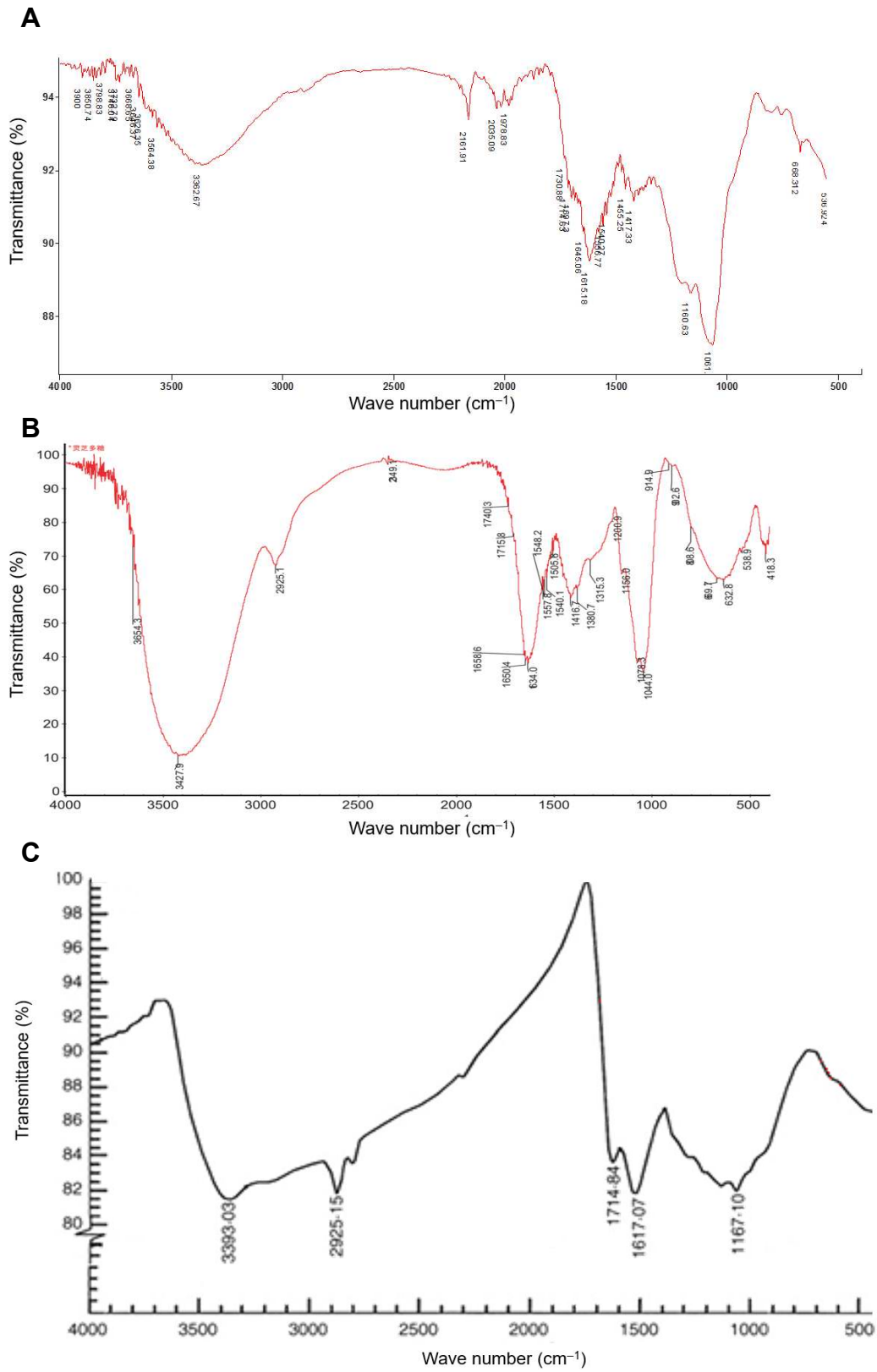


Figure 8. Ferreira et al. 2018.

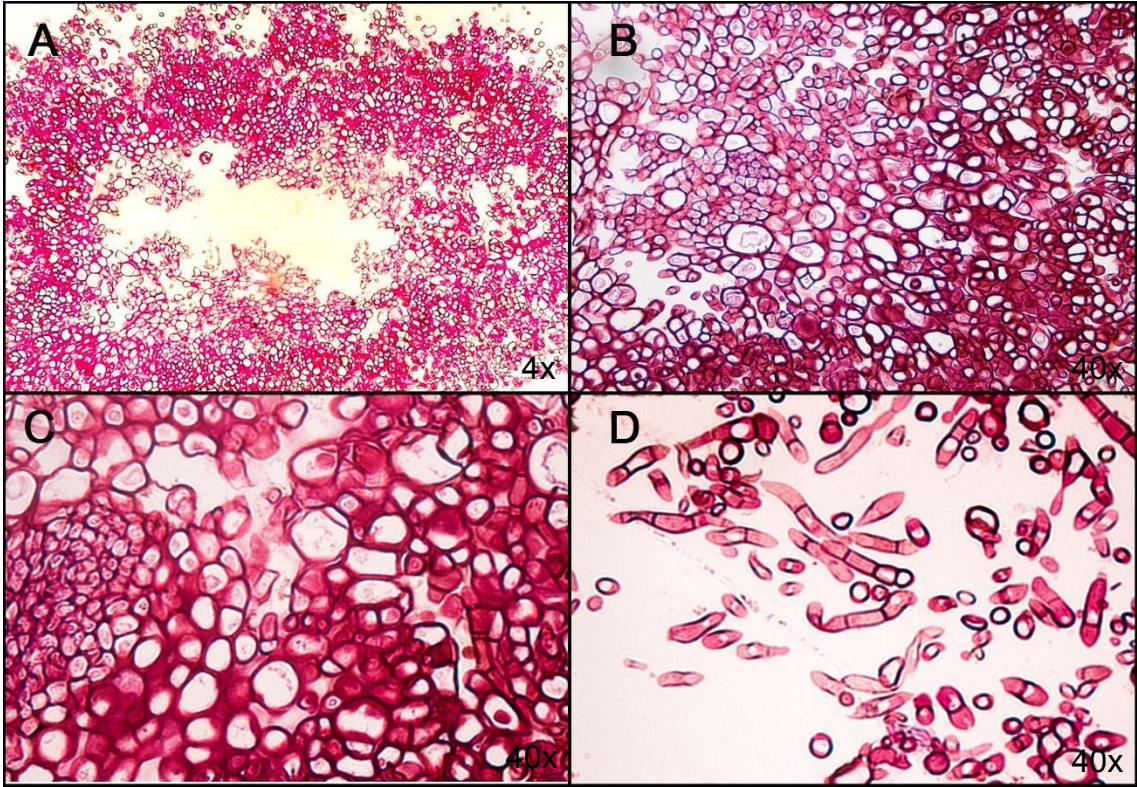


Figure 9. Ferreira et al. 2018.

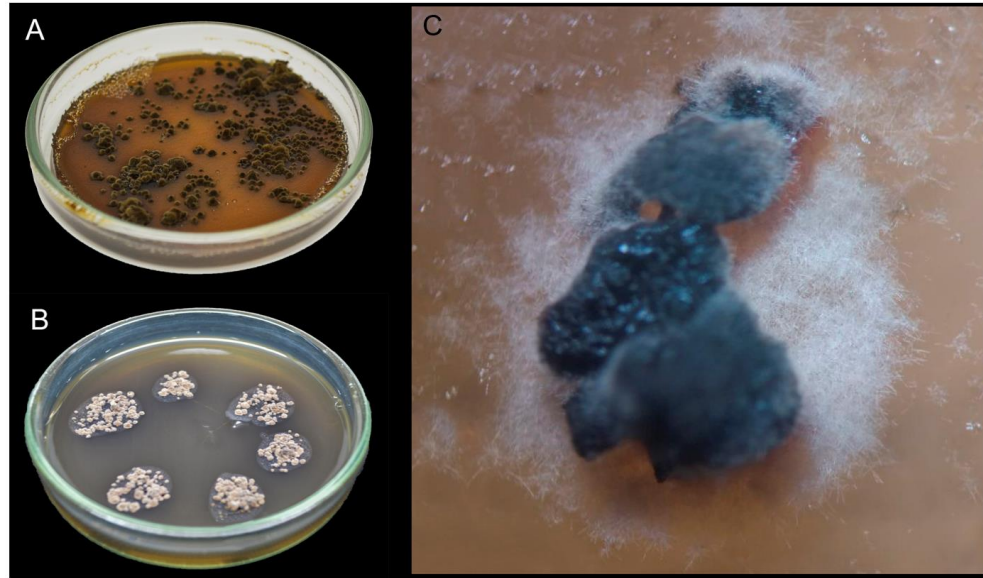


Figure 10. Ferreira et al. 2018.

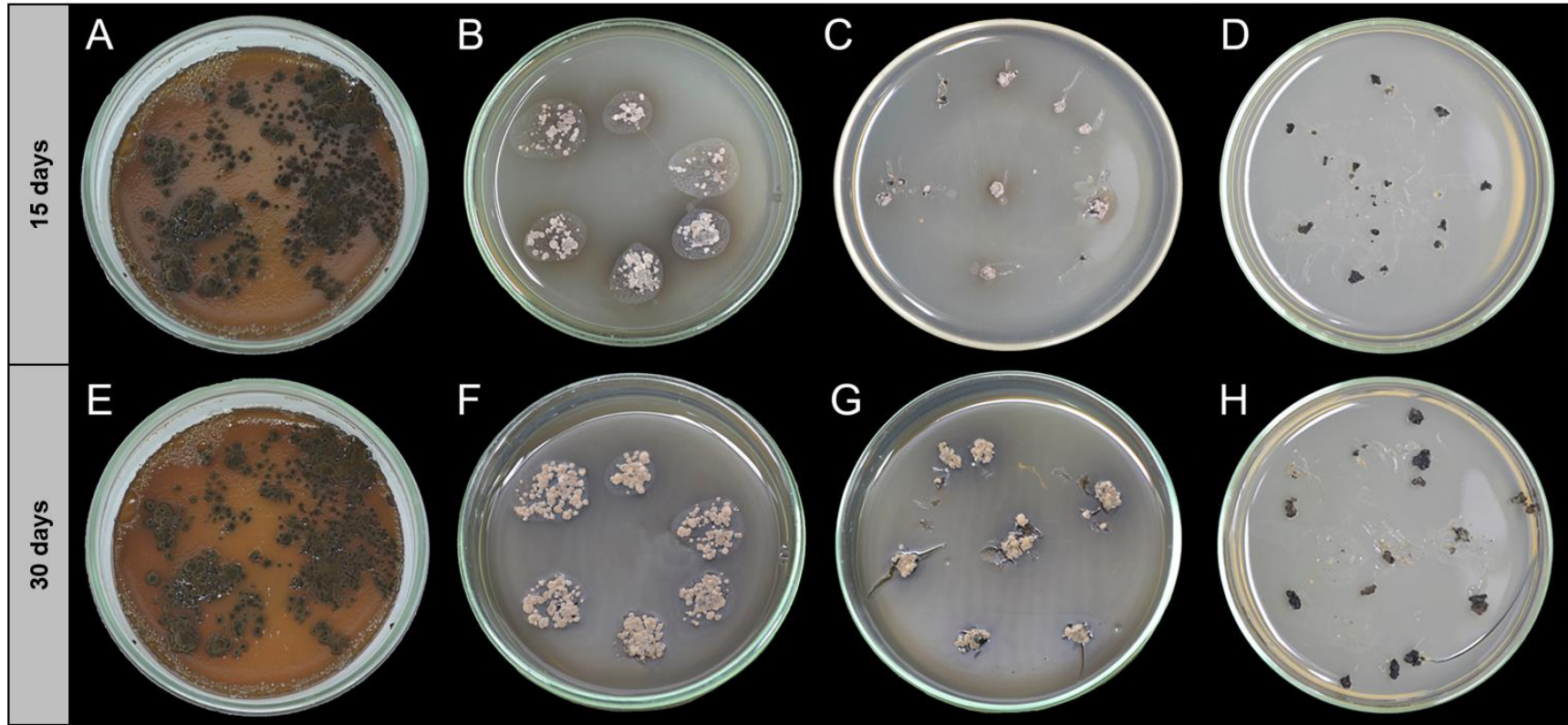


Figure 11. Ferreira et al. 2018.

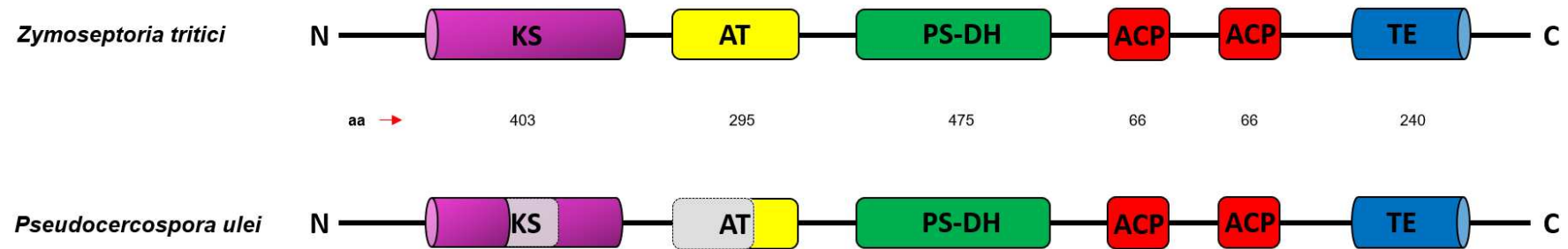


Figure 12. Ferreira et al. 2018.

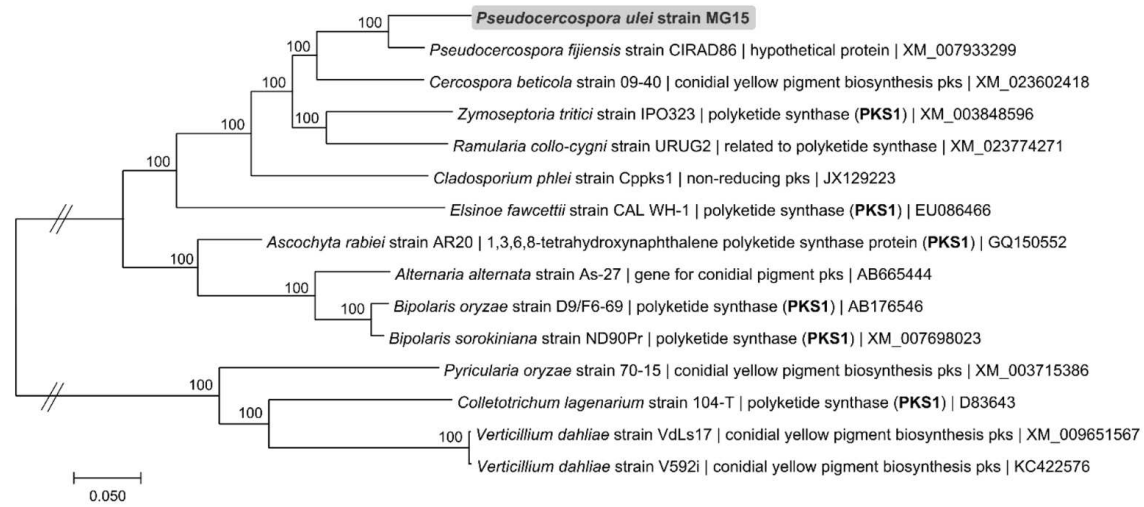


Figure 13. Ferreira et al. 2018.



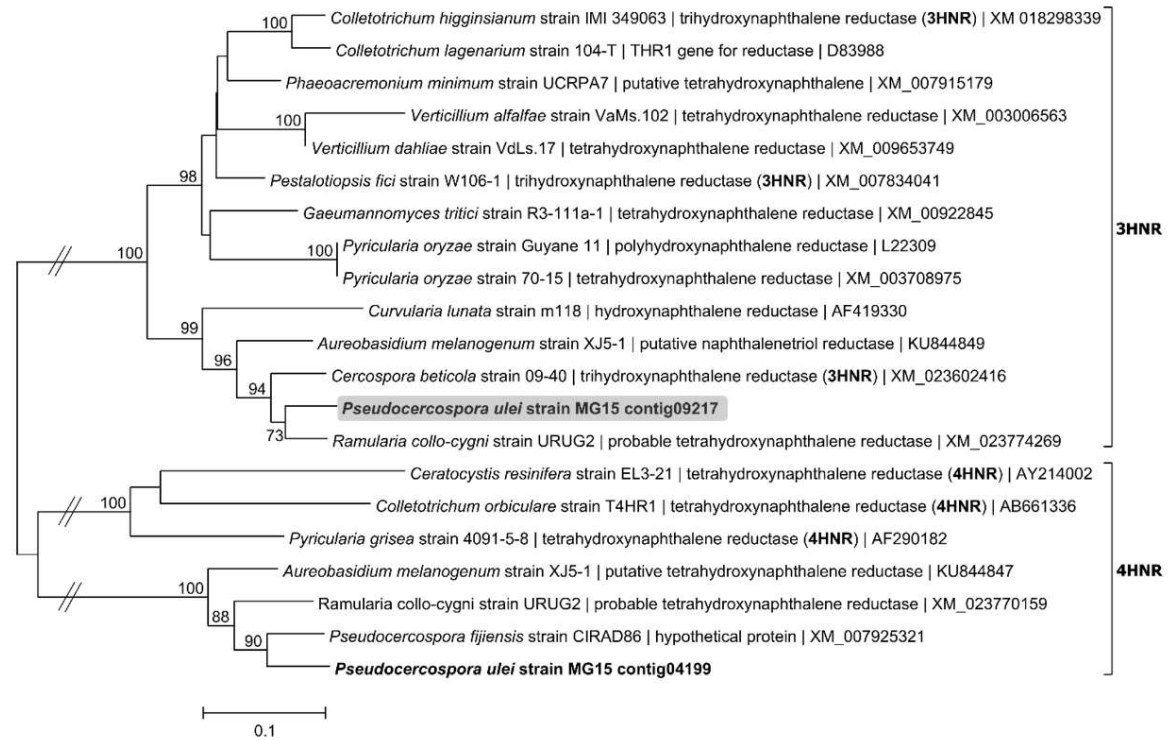
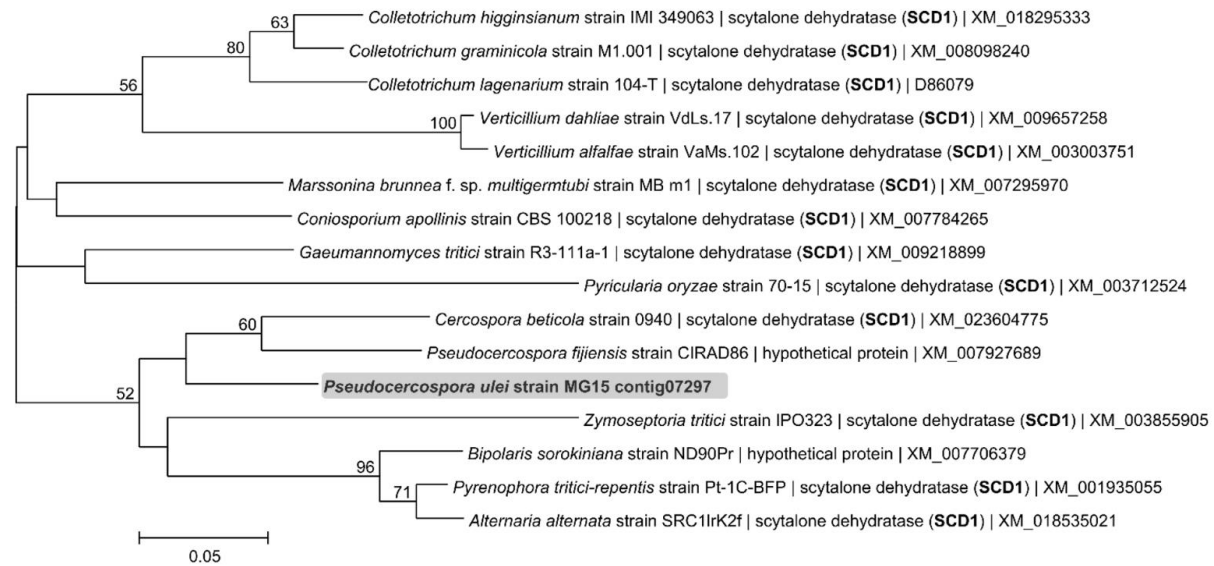


Figure 14. Ferreira et al. 2018.



**Figure 15. Ferreira et al. 2018.**

## GENERAL CONCLUSIONS

1. The diversity of fungal and prokaryotic endophyte in *H. brasiliensis* was shaped by organ (leaf and sapwood) and there is strong evidence that microbial community shifts as a function of geographic distance.
2. Functional prediction revealed important roles of microorganisms that can help plant establishment and disease suppressiveness, but also *P. ulei* and other plant pathogens.
3. The MALDI-TOF and FT-IR analysis was unable to detect melanin, but detected a B-glucans, and we found that B-glucans has been mistakenly assigned to melanin in several studies.
4. Tricyclazole assay inhibited the melanization process in *P. ulei*, thus proving that the melanin synthesized by the fungus is 1,8 DHN.
5. The putative effector genes revealed high polymorphism levels in the populations of *P. ulei*, and intragenic recombination and positive selection were detected.